AD-E951 858

②

TECHNICAL REPORT RD-WS-92-4

DIFFUSION IN THE FORMATION OF PHOTOPOLYMER HOLOGRAMS

David John Lanteigne
Weapons Sciences Directorate
Research, Development, and Engineering Center

S DTIC
ELECTE
JUL 13 1992
A D

APRIL 1992

U.S. ARMY MISSILE COMMAND

Redstone Arsenal, Alabama 35898-5000

Approved for public release; distribution is unlimited.

92

92-18136

REPORT DOCUMENTATION PAGE

Form Approved
OMB No. 0704-0188

1a. REPORT SECURITY CLASSIFICATION	1b. RESTRICTIVE MARKINGS
Unclassified	

2a. SECURITY CLASSIFICATION AUTHORITY	3. DISTRIBUTION/AVAILABILITY OF REPORT
2b. DECLASSIFICATION/DOWNGRADING SCHEDULE	Approved for public release; distribution is unlimited.

4. PERFORMING ORGANIZATION REPORT NUMBER(S)	5. MONITORING ORGANIZATION REPORT NUMBER(S)
Technical Report-RD-WS-92-4	

6a. NAME OF PERFORMING ORGANIZATION	6b. OFFICE SYMBOL (If applicable)	7a. NAME OF MONITORING ORGANIZATION
Weapons Sciences Directorate RD&E Center	AMSMI-RD-WS-PO	

6c. ADDRESS (City, State, and ZIP Code)	7b. ADDRESS (City, State, and ZIP Code)
Commander, U.S. Army Missile Command ATTN: AMSMI-RD-WS-PO Redstone Arsenal, AL 35898-5248	

8a. NAME OF FUNDING/SPONSORING ORGANIZATION	8b. OFFICE SYMBOL (If applicable)	9. PROCUREMENT INSTRUMENT IDENTIFICATION NUMBER

8c. ADDRESS (City, State, and ZIP Code)	10. SOURCE OF FUNDING NUMBERS			
	PROGRAM ELEMENT NO.	PROJECT NO.	TASK NO.	WORK UNIT ACCESSION NO.

11. TITLE (Include Security Classification)

DIFFUSION IN THE FORMATION OF PHOTOPOLYMER HOLOGRAMS

12. PERSONAL AUTHOR(S)
David J. Lanteigne

13a. TYPE OF REPORT	13b. TIME COVERED	14. DATE OF REPORT (Year, Month, Day)	15. PAGE COUNT
Final	FROM Sep 87 TO Nov 91	April 1992	162

16. SUPPLEMENTARY NOTATION

17. COSATI CODES			18. SUBJECT TERMS (Continue on reverse if necessary and identify by block number)
FIELD	GROUP	SUB-GROUP	Polymer; photopolymer; film; hologram; diffusion; monomer; gratings

19. ABSTRACT (Continue on reverse if necessary and identify by block number)

The research presented in this report shows that the formation of holographic gratings in the Polaroid DMP-128 photopolymer medium is largely a result of the diffusion of lithium acrylate monomer within the medium. DMP-128 and other similar holographic photopolymers are capable of recording volume phase gratings by means of the physical and chemical changes that occur in the media when they are exposed to an optical interference pattern. In the presence of light, the absorption of photons by a sensitizing dye leads to the formation of free radicals. The free radicals, in turn, catalyze the linkage of simple monomer molecules into long-chain polymer molecules. The chemical reaction alters the molar refraction, and thus the index of refraction of the medium.

If the illumination is spatially periodic, as when due to the interference of two plane waves, the chemical reaction also induces periodic variations in the concentration of monomer. The result is the diffusion of monomer from dark fringes, where little polymerization occurred, to bright fringes, where monomer was depleted by the photochemical reaction. This diffusion causes a periodic modulation of the mass density, (continued on page ii)

20. DISTRIBUTION/AVAILABILITY OF ABSTRACT	21. ABSTRACT SECURITY CLASSIFICATION
☐ UNCLASSIFIED/UNLIMITED ☒ SAME AS RPT. ☐ DTIC USERS	Unclassified

22a. NAME OF RESPONSIBLE INDIVIDUAL	22b. TELEPHONE (Include Area Code)	22c. OFFICE SYMBOL
David J. Lanteigne	(205) 876-6418	AMSMI-RD-WS-PO

DD Form 1473, JUN 86 Previous editions are obsolete.

Block # 19 (continued):

which also modulates the index of refraction of the medium, according to the Lorentz-Lorenz relationship. A mathematical model developed in this research predicts that the amplitude of the periodic concentration decays exponentially with time; the time constant varies quadratically with the period of the grating.

A detectable grating is formed in DMP-128 immediately upon holographic exposure. Experiment revealed that when the grating period was 25 microns or more, the effect of diffusion was insignificant, and the diffraction efficiency continued to increase long after exposure ended, due to residual free radical in the system. Shorter grating periods led to progressively more rapid decay of diffraction efficiency after exposure. The decay can be explained by assuming that the index modulation of the medium was varying as the sum of two decaying exponentials, indicating that both monomer and the sensitizing dye were diffusing within the medium. The total amplitude of the decay indicates that less than 10% of available monomer is free to diffuse within the photopolymer medium.

ACKNOWLEDGEMENTS

Accesion For	
NTIS CRA&I	✓
DTIC TAB	☐
Unannounced	☐
Justification	
By	
Distribution /	
Availability Codes	
Dist	Avail and / or Special
A-1	

TABLE OF CONTENTS

LIST OF FIGURES

LIST OF SYMBOLS

c_R, c_S	Volume grating obliquity factors
CT	Computerized tomography
d	Thickness of grating
D	Diffusion coefficient, also film density in Chapter 1
D	Electric field displacement
DCG	Dichromated gelatin
e	Electron charge
E	Time integrated optical energy per unit area
E_d	Molecular activation energy of diffusion
E	Applied electric field
f_i	Initiation efficiency
f_k	Strength of kth oscillator mode
f_0	Spatial frequency of grating
h	Planck's constant
HRLF	Holographic reciprocity law failure
k_L	Rate constant of monomer loss
$\mathbf{k}_n$	Wave vector of nth plane wave
$\mathbf{k}_p$	Propagation rate constant
k_t	Termination rate constant
K	Grating vector
HOE	Holographic optical element
I	Light intensity

I_a	Absorbed light intensity
I_s	Sinusoidal component of holographic intensity pattern
I_0	Average value of holographic intensity pattern
J	Diffusive flux
J_n	Bessel function of the nth order and the first kind
L	Monomer loss function
m	Fringe visibility
mJ	Millijoules
mW	Milliwatts
M	Molecular weight, or monomer
MMA	Methyl methacrylate
MTF	Modulation transfer function
n	Index of refraction
n_D	Index of material at sodium D line
nm	Nanometers
n_0	Base index
n_1	Amplitude of sinusoidal index modulation
N	Number of molecules per unit volume
N_A	Avogadro's number
p	Molecular dipole moment
P	Bulk polarization
PMMA	Poly(methyl methacrylate)
r	Free radical concentration

LIST OF SYMBOLS (cont'd)

r	Reference wavevector
R	Molar refraction, or amplitude of reference wave
s	Signal wavevector
S	Amplitude of signal wave
T	Intensity transmission of developed film
T_a	Amplitude transmission
T_g	Glass transition temperature
u	Monomer concentration function
v_i	Initiation rate
v_p	Propagation rate
v_t	Termination rate
α	Real part of complex absorption, or molecular polarizability
β	Wave vector magnitude, or slope of linear part of silver halide T_a-E curve in Chapter 1
Δn, δn	Index modulation
ε	Permittivity
Γ	Particle jump frequency in diffusion
η	Diffraction efficiency
ϑ	Volume hologram dephasing factor
κ	Grating coupling constant
λ	Wavelength of light in vacuum
Λ	Spatial period of holographic grating

LIST OF SYMBOLS (cont'd)

μm	Micron
μW	Microwatt
ν	Modulation parameter of a volume hologram
ρ	Mass density
σ	Standard deviation of noise
τ_D	Characteristic diffusion time
ϕ, Φ	Electric potential functions
ϕ_i	Quantum efficiency
χ	Dielectric susceptibility
χ^2	Chi-squared error estimate
Ω	Spatial frequency

I. INTRODUCTION

A. Classical Reciprocity Failure and Image Formation

This research is directed towards a general understanding of holographic image formation in photopolymers, of which Polaroid's DMP-128 holographic photopolymer is an example. However, it is useful to first look at the development of the theories of both classical reciprocity failure and holographic reciprocity failure in conventional silver halide films. The reciprocity failure is the name given to the fact that for silver halide films, the exposure energy necessary to produce a certain effect in the film depends upon the intensity of the exposure. Earlier research by others into the reciprocity failure led to an understanding of the physical basis of image formation in silver halide films.

Conventional films and photopolymer recording media form images quite differently. The chemistry and physics of image formation in the two types of medium are quite distinct, but they have at least two things in common. Both types of media amplify the effects of incident photons, and both are subject to time-dependent processes which form the basis for reciprocity failure. This thesis will show that for photopolymers, the critical time-dependent process is the diffusion of monomer and other photopolymer components, with the characteristic diffusion time controlled by the diffusion constants of the medium and the spatial periodicity of the hologram.

A conventional photographic medium consists of small silver halide crystals dispersed in a gelatin film, along with sensitizing dyes and other agents. When the film is exposed to a pattern of varying light intensity, an invisible, or latent, image is formed. Development maps the invisible latent image into a visible pattern of varying absorption. Figure 1-1 shows a characteristic plot of T, the intensity transmission of the developed film, versus E, the time-integrated optical energy per unit area that was used to expose the film. The slope of the linear portion of the T vs. E curve is important in holography and will be discussed later. A more commonly used measure of the response of the film to exposure is the optical density D, defined as [1]:

$$D = \log \left(\frac{1}{T}\right) \tag{1-1}$$

In the nineteenth century, early photographic researchers believed that the density of an exposed photographic emulsion depended only on the total light energy per unit area that exposed the film, not on the intensity or duration of the exposure. The formulation of this belief was called the reciprocity law; that is, a decrease in intensity could be compensated for by a reciprocal increase in exposure time to achieve the same final optical density. The reciprocity law was experimentally confirmed for various photo-chemical reactions. However, astronomical exposures made at extremely low intensities revealed a failure of the reciprocity law [2]. It was established that at both very high [3] and very low intensities, a greater amount of light energy per unit area is required to produce a given density than that required at intermediate intensity levels. Reciprocity law failure is illustrated in Figure 1-2. Intensity is assumed to be constant, so that the exposure E (whose log is plotted on the vertical axis) is the product of intensity I and time t. The curve is a contour of constant optical density D.
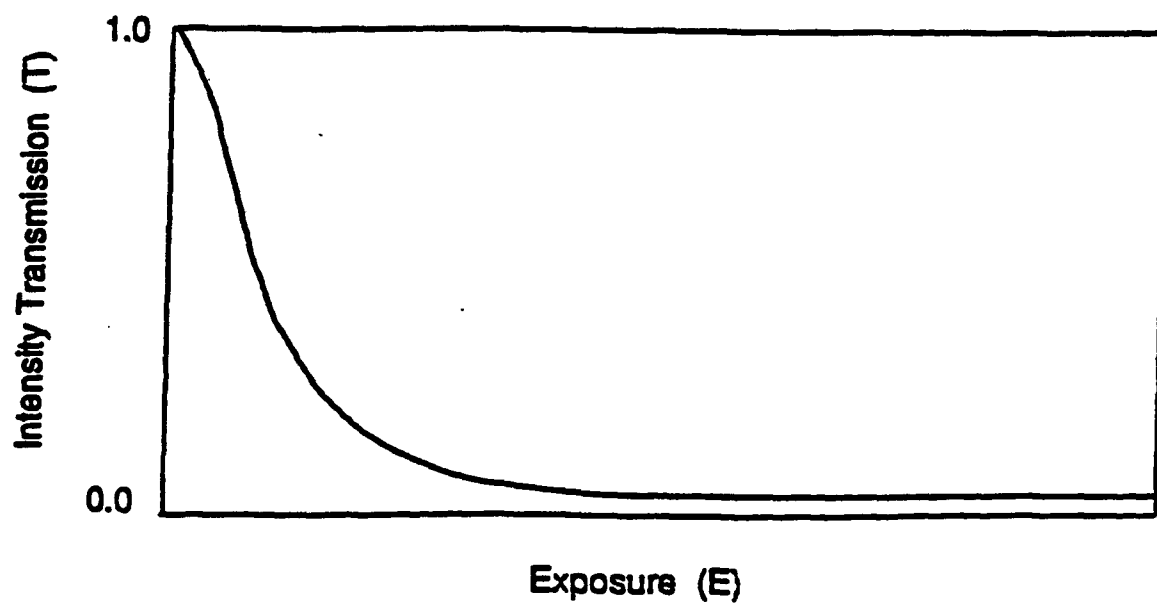
Figure 1-1: Transmission versus exposure for a typical silver halide film.
[Figure adapted from Reference 1, p.163]
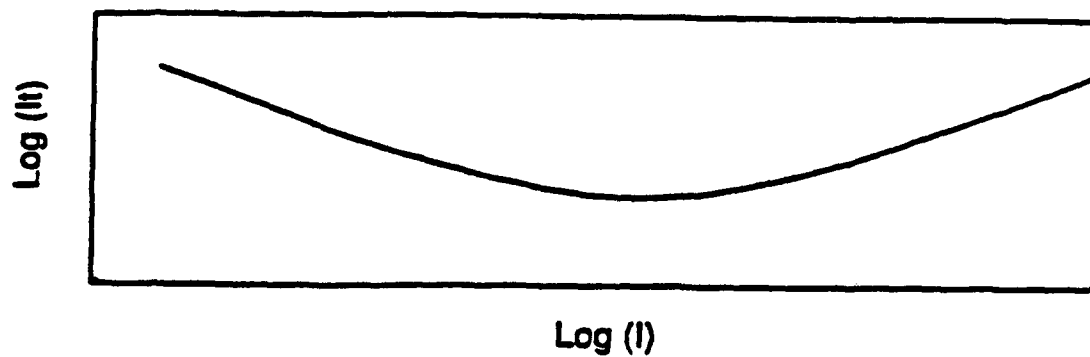
Figure 1-2: Contour of constant density D for time integrated exposure (It) vs. intensity (I).
[Figure adapted from Reference 1, p.200]

It shows that at both low and high intensities, exposure time must be increased over "normal" values to obtain a given optical density.

Understanding of the reciprocity failure had to await the development of a theory of latent image formation. The first comprehensive theory, still accepted for the most part today, was laid out by Ronald W. Gurney and Nevill F. Mott [4]. In their model, the absorption of a photon in a silver halide (usually AgBr) grain liberates an electron-hole pair in the grain. The electron becomes trapped in a "sensitivity site." There the electron may attract and neutralize an interstitial silver ion. If as few as four to six neutral silver atoms collect at the sensitivity site, the developer will be able to reduce the entire grain into a speck of metallic silver, which will contribute to the optical density of the film, while the undeveloped AgBr grains are washed out of the emulsion by the fixing bath. Further insights into the formation of the latent image were provided by Mitchell [5], who observed that the sensitivity sites were often crystal defects, such as dislocations.

The Gurney-Mott framework explained the great sensitivity of silver-halide emulsions in terms of a gain mechanism. The action of a few photons was sufficient to form a latent pre-speck of silver atoms which could catalyze the reduction of the entire grain. In his recent review article, Tani [6] estimates that a 1 micron grain contains approximately 20 billion silver ions; therefore the gain of a typical emulsion is on the order of a billion reduced silver atoms per absorbed photon. An increase in grain size will reduce the resolution of a photographic film, but also increase the sensitivity, by providing a larger cross-section for photon interaction, and a larger quantity of material to be reduced by the same four to six atom pre-speck.

The high-intensity reciprocity failure was explicable in the Gurney-Mott model in terms of the low mobility of the interstitial silver ions [7]. At a sufficiently high light intensity, photoelectrons are generated and accumulate at the sensitivity sites so rapidly that the relatively slow-moving silver ions cannot neutralize them immediately. A net negative charge builds up at the sensitivity sites, preventing the accumulation of further photoelectrons until the sites can be neutralized by the migration of ions. Therefore, the effect of high intensity is to decrease the quantum efficiency of the latent image formation process, and to increase the amount of energy necessary to produce a given optical density.

Another necessary insight into the reciprocity failure came from the work of J.H. Webb of Kodak, who in 1933 linked low-intensity reciprocity failure to the so-called intermittency effect [8]. It had been observed that a rapidly flashing light produced an exposure that depended only on the integrated energy. However, if the flashing fell below a certain critical frequency, an increase in exposure was necessary to produce the same optical density. The critical frequency was different for various types of films and plates. Webb realized that "from the standpoint of discrete light quanta incident upon a photographic grain, all exposures may be viewed as intermittent exposures. Further it is known that reciprocity law failure is governed in some manner, yet undetermined, by the time distribution of reception of quanta by some portion or all of a photographic grain."

More than a decade later Webb developed the currently accepted explanation of the low-intensity reciprocity failure in terms of the thermally induced dissociation of silver pre-specks [9]. The explanation rested on the observation that the reciprocity failure curve for a given emulsion, as shown in Figure 1-2, shifts to the left as the temperature is lowered. In other words, a latent image in the beginning of its formation is less likely to decay if the temperature is low. It seemed that a latent image pre-speck had to contain a minimum number of silver atoms to survive. If not, its binding energy would be so low that thermal fluctuations would cause the pre-speck to disintegrate before enough photons were absorbed to produce a stable, developable cluster.

Webb modeled the absorption of photons and the generation of photoelectrons at a grain sensitivity site as a Poisson process. This was appropriate for a theory of low-intensity reciprocity failure, since the Poisson model gives the distribution of photon arrival time intervals when the photon arrivals are so infrequent as to be discrete and countable. As the pre-speck forms by the combination of photoelectrons and silver ions, its electrons are bound to the sensitivity site with a binding energy ε, and they oscillate at a frequency ν. The probability per unit time P of an electron being ejected is given by the product of the frequency and the probability of electron ejection per oscillation, given by the Boltzmann factor:

$$P = \nu \exp\left[-\frac{\varepsilon}{kT}\right] \cdot \qquad (1-2)$$

Comparison of the model with low-intensity exposure data at various temperatures led to the conclusion that reciprocity failure occurs when a sensitivity site does not accumulate at least two neutral silver atoms within a critical time τ. A single silver atom at a site has an estimated dissociation energy of the order of 0.7 ev, and a corresponding lifetime, at room temperature, of only a few seconds. The silver dimer is, however, effectively stable at room temperature, but unless the second atom is added to the site before the first one dissociates, the pre-speck disappears. Note that the formation of a stable silver dimer is only a necessary but not sufficient condition for the formation of a developable pre-speck. It is thought that at least four to six silver atoms must cluster to make development of the grain possible.

In summary, the early stages of formation of the silver halide latent image are affected by a time-dependent decay process. It is this thermally induced decay that causes the failure of the reciprocity law at low light intensities, since a photographic grain may start to form a latent pre-speck, lose it by thermal ejection of an electron, and repeat this process until a stable silver dimer is formed. Only then is it even possible for the grain to integrate the effect of more photons and become capable of development.

B. The Holographic Reciprocity Failure

The holographic reciprocity failure was identified as a distinct phenomenon during dissertation work by Kristina Johnson at Stanford University [10]. The motivation for the work was to develop a means to display the output of medical computerized tomography (CT) scanners as a three-dimensional holographic display. CT scanners produce cross-sectional image slices of the human body by digital processing of X-ray absorption data, but they lack true three-dimensional display capability. Johnson's approach was to record the image slices as multiple exposure holograms on a single recording plate. Each single exposure hologram was of the Leith-Upatnieks type [11], a recording of the interference between separate object and reference waves, as shown in Figure 1-3. However, the initial results were unsatisfactory, since for equal exposure energies, each successively recorded hologram had a smaller diffraction efficiency than the one that came before. This effect was labeled the HRLF (holographic reciprocity law failure).

Johnson's analysis of the HRLF began with Biederman's empirical expression for the diffraction efficiency η of a single exposure hologram [12]:

$$\eta = \left(\frac{\beta \cdot E_b \cdot m \cdot MTF(\Omega)}{2} \right)^2 \qquad (1\text{-}3)$$

where E_b is the bias exposure energy, m is the exposure fringe visibility, and the MTF (modulation transfer function) of the recording medium is a function of Ω, the spatial frequency. β is a film-dependent characteristic based on the so-called amplitude transmission, T_a. The amplitude transmission is the square root of the previously discussed intensity transmission, shown in Figure 1-1. In the Biederman approximation, holographic exposures occur on the linear part of the T_a - E curve, and β is the slope of the linear region. In these terms, it appeared that the reduced diffraction efficiency of multiple exposure holograms was due to some mechanism that reduced the slope of the T_a-E characteristic curve after the first exposure.

The T_a - E characteristic curve for multiple exposures was simulated using Monte Carlo techniques. The grains of the holographic film were simulated as a checkerboard array, each element subject to the random arrival of photons, which form neutral silver atoms at a sensitivity site, in accordance with the Gurney-Mott theory. Between exposures, the array elements that have accumulated two or more silver atoms remain unchanged. Those with exactly one silver atom are subject to decay back to zero accumulated atoms, with a half-life of about two seconds. After all the multiple exposures are simulated, those cells with four or more atoms represent a developed grain. The fraction of developed grains gives the intensity transmittance, and the square root of this quantity is T_a, the amplitude transmittance.

Object Wave

Hologram

θ

Reference Wave

Recording geometry

Conjugate Image

Virtual Image

θ

θ

Viewer
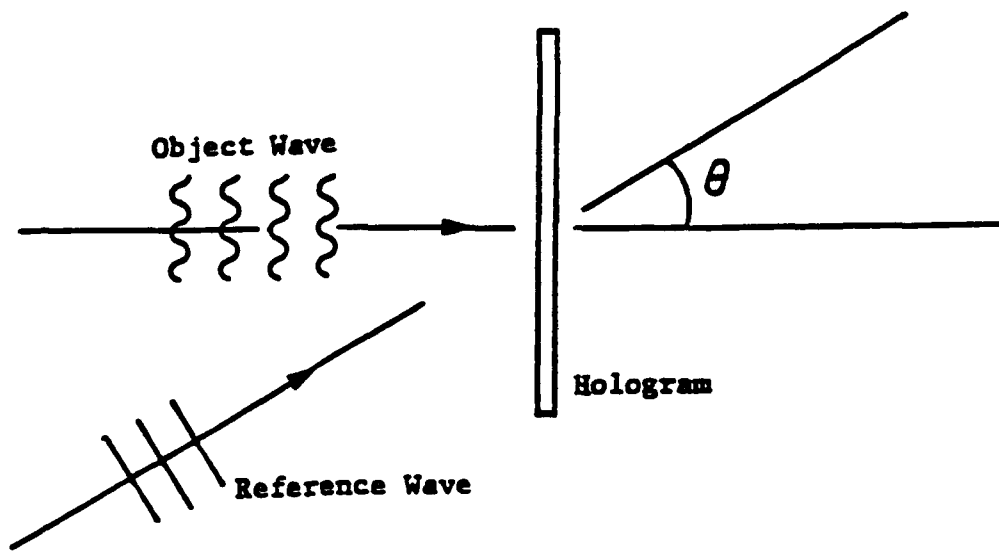
Hologram
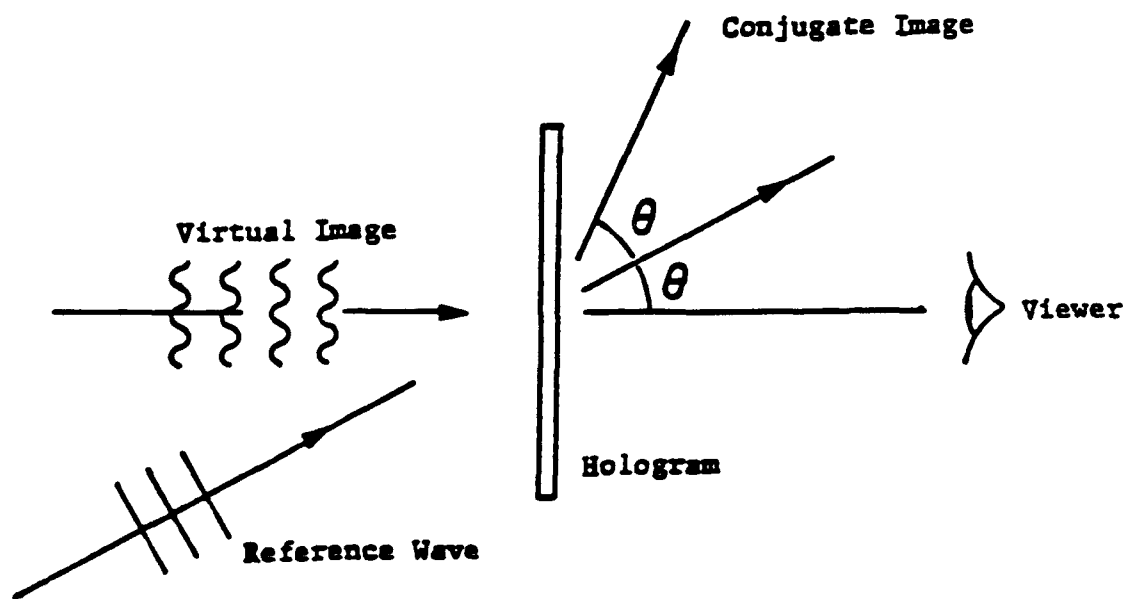
Reference Wave

Reconstruction Geometry

Figure 1-3: Leith-Upatnieks hologram geometry.
[Figure adapted from Reference 10]

6

The Monte Carlo calculations indicated that, as expected, the value of β decreased with increasing number of multiple exposures when the delay between exposures was on the order of or greater than two seconds. The Monte Carlo calculations were confirmed by analytical techniques that treated silver atom formation and dissociation as stochastic Poisson birth and death processes. The agreement between the numerical and analytical techniques was good. Finally, the theoretical results were verified by experiments in which multiple exposures with various time intervals between the exposures were used to determine β. Experimental and theoretical T_a-E curves are shown in Figure 1-4.

The crucial mechanism responsible for the HRLF was the dissociation of single atom pre-specks at sensitivity sites during the intervals between holographic exposures. Johnson presented an intuitive argument for this. Consider the case of two holographic exposures on the same plate, several seconds apart, and assume that four silver atoms are necessary to develop a grain. Some grains will accumulate three atoms in the first exposure, and one atom in the second exposure. These grains will tend to be located where the first exposure was bright, and the second dark, and thus they will contribute to the signal from the first hologram, and to the noise of the second. An equal number of grains will accumulate one atom in the first exposure, which will dissociate, and three more in the second exposure. Of course these grains will not develop, and being situated where the first hologram is dim and the second one is bright, their failure to develop will diminish the density of the second hologram.

The complete treatment of HRLF in Johnson's thesis also involved Monte Carlo simulation of multiple exposure hologram formation, an analytical model, and experiments. Figure 1-5 shows the calculated and observed decrease in diffraction efficiency for a second holographic exposure made at various time intervals after the first.

The practical result of this exhaustive analysis was the development of techniques to compensate for the holographic reciprocity law failure. The first technique was to give the holographic plate a uniform pre-exposure, too small to really expose the plate but sufficient to give most grains stable silver dimers at their sensitivity sites, thus reducing the problems associated with the decay of single atom sites. The second technique was to increase the exposure of later multiple exposures inversely to their theoretically calculated decline in efficiency. Though both techniques were successfully used to compensate for the HRLF, the latter yielded a better signal to noise ratio, and was used to generate three-dimensional displays of CT data.

The investigation of the holographic reciprocity failure brings together, in one theory, the time-dependent processes responsible for latent image formation, and the holographic recording properties of silver halide emulsions. This suggests that other holographic recording media whose exposure process is more complicated than the simple integration of incident photons, may also be better understood by an analysis of the image formation mechanism.
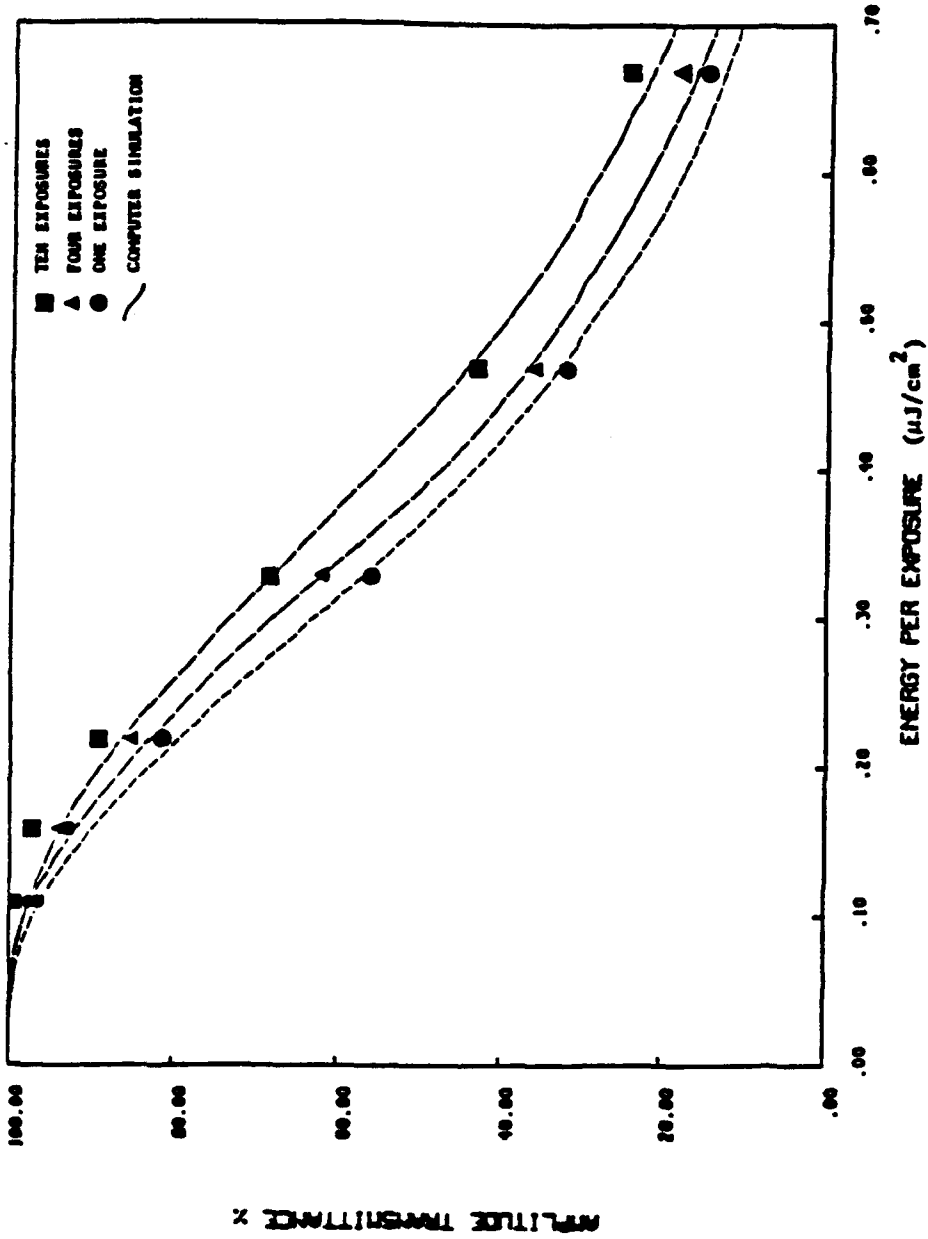
Figure 1-4: Multiple exposure T_a-E curves with $\Delta T = 0.5$ seconds.

[Adapted from Reference 10]

8
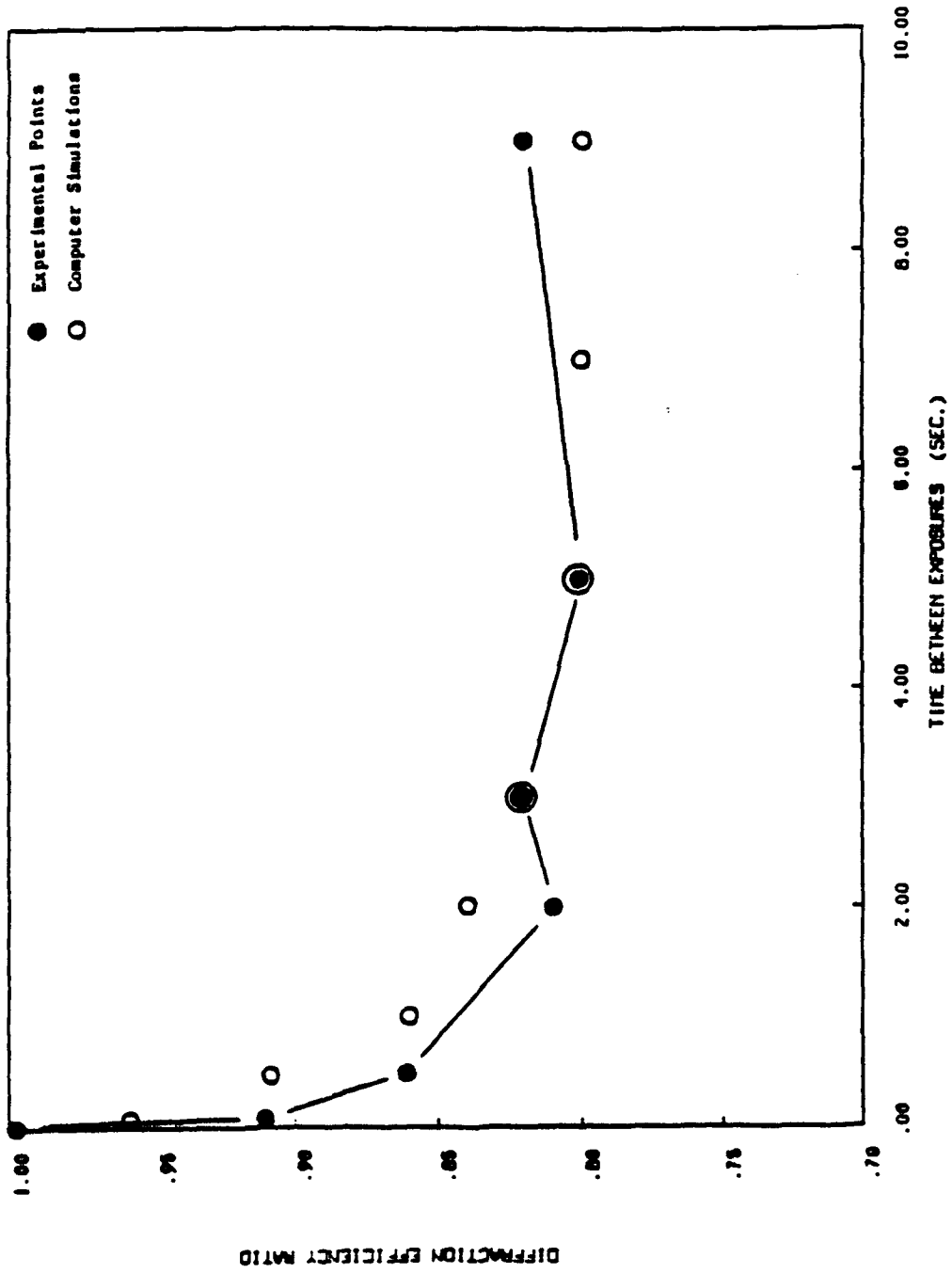
Figure 1-5: Ratio between double exposure diffraction efficiencies, vs. time between exposures.

[Adapted from Reference 10]

9

C. Holographic Photopolymers

The word photopolymer is generally used to refer to light sensitive compositions that record images by photochemically effecting permanent changes in a polymeric material, or by forming polymers by the action of light on monomers. Photopolymers of various types have found applications in holography [13,14], printing, and electronic circuit fabrication [15]. The polymerized material may differ from its original form in its solubility, adhesion, or index of refraction.

The current work presented here uses the Polaroid photopolymer composition known as DMP-128 as an example of a currently available and well-known photopolymer. Initial reports [16,17] indicated that volume phase holograms recorded in this material are similar in quality and have the high diffraction efficiency of those recorded in dichromated gelatin (DCG), while requiring less exposure energy and less stringent environmental controls during processing. In contrast to DCG and earlier photopolymer systems, DMP-128 need not be coated on glass plates immediately before exposure, but can be prepared months in advance. Researchers have exploited this material in fabricating matched spatial filters and multi-focus holographic optical elements (HOE's) with high diffraction efficiencies [18,19,20,21]. Users of DMP-128 have accumulated a body of empirical knowledge relating holographic diffraction efficiency to total exposure, reference to object beam intensity ratio, and the spatial frequency of the holographic grating [22]. However, there is little understanding of these properties in terms of the underlying mechanism of image formation.

The formation of holograms in DMP-128 is similar to that in other photopolymers. The holographic medium is available on glass plates or plastic backing, with emulsion thicknesses ranging from 3 to 20 microns. By a suitable choice of sensitizing dye, it can be made sensitive to the major Argon-ion and Helium-neon laser lines in the visible. The plates are stored over a dessicant, and made sensitive to light by exposing them to air of 51% relative humidity for several minutes. Moisture absorbed by the film makes light-induced polymerization possible; this report will show that the absorbed water has a role in both the photochemistry of the polymerization and the diffusion of monomer necessary for the formation of a high quality grating. Humidity is held constant while the holographic exposure is made. When the reference beam and signal beam are of equal intensity, about 5 mj/cm^2 is required to produce a highly efficient holographic transmission grating. After exposure, a uniform flood of white light serves to uniformly polymerize some of the remaining monomer, and thus fix the image formed by exposure. The final developing stage is an alcohol developing bath, which removes dye and unreacted monomer from the plate, followed by drying of the emulsion.

Image formation in photopolymer materials has little in common with silver halide recording, except that both processes employ a chemical gain mechanism to amplify the effect of incident light. Holographic photopolymers almost always form phase-modulated images, rather than amplitude modulated images [23]. Apart from the sensitizing dye, the entire system must be fundamentally transparent in order to form a phase-only hologram. Therefore, only a small fraction of the incident photons will be absorbed during exposure, so it is important that the system be able to amplify the effects of a single photon. The gain in the process occurs because a single photon can form a radical that will catalyze the combination of thousands of monomer units into a long-chain polymer molecule.

10

A typical photopolymer consists of a sensitizing dye, an initiator capable of forming free radicals, a monomer in solution, and a gel or polymer binder. When a photon is absorbed by the sensitizing dye, the dye molecule enters an excited state. If the dye molecule transfers its excess energy to the initiator, the initiator will dissociate into one or more free radicals. The radical can attach itself to a monomer molecule and catalyze a chain reaction in which monomer molecules are added one at a time to form a long-chain polymer. The polymerization will continue until the free-radical is terminated by combination with another free radical, or quenched by some other reaction. This radical-catalyzed addition of monomers is called vinyl polymerization.

Photopolymerization can form a holographic grating in two ways. First, photopolymerization is capable of mapping the holographic exposure into a modulation of the medium's bulk refractive index, forming a volume phase hologram [24]. Second, some photopolymers form a surface relief grating after an exposure [25]. Whichever effect predominates, the medium still remains transparent, with no appreciable change in the optical density. Both effects have been observed in the DMP-128 photopolymer, and are probably due to an internal mass transport process initiated by photopolymerization [23]. Figure 1-6 depicts a photopolymer film exposed to plane wave object and reference beams at equal and opposite angles with respect to normal incidence. The sinusoidal intensity pattern caused by the interference of the two beams initiates polymerization. The fringe pattern, with a spatial period of Λ, is indicated by dark and light shading in the figure. Polymerization proceeds more rapidly in the bright fringes than in the dark fringes. As the reaction proceeds, the monomer is consumed at a rate dependent upon the intensity, and the resulting concentration gradient causes diffusion of monomer from the dark fringes into the bright fringes. The direction of this diffusive mass flow is indicated by arrows. This diffusion results in a periodic modulation of the mass density of the film. A final high-intensity uniform exposure completes the polymerization of any remaining monomer within the medium and fixes the recording.

The spatial variation of mass density resulting from the photopolymerization reaction is probably responsible for the formation of both a surface relief hologram and a volume phase hologram in the DMP-128 emulsion. Simple subsidence or sagging of the monomer-depleted regions of the emulsion could account for the relief pattern formed on the surface. The existence of a volume phase hologram is inferred from the fact that the material can be used to record transmission gratings with nearly 100% diffraction efficiency; a thin phase grating is not capable of that efficiency [26].

The volume phase hologram is a direct result of the mass density modulation. The Lorentz-Lorenz equation [27] relates refractive index n and mass density ρ of a material by

$$\frac{n^2 - 1}{n^2 + 2} = \frac{4\pi \rho N \alpha}{3M} \tag{1-4}$$

where N is Avogadro's number, M is the molecular weight of the material, and α is the polarizability of a single molecule. It is reasonable to assume in a polymerization reaction that α/M is constant, or nearly so, which is to say that the dipole moment of a large polymer
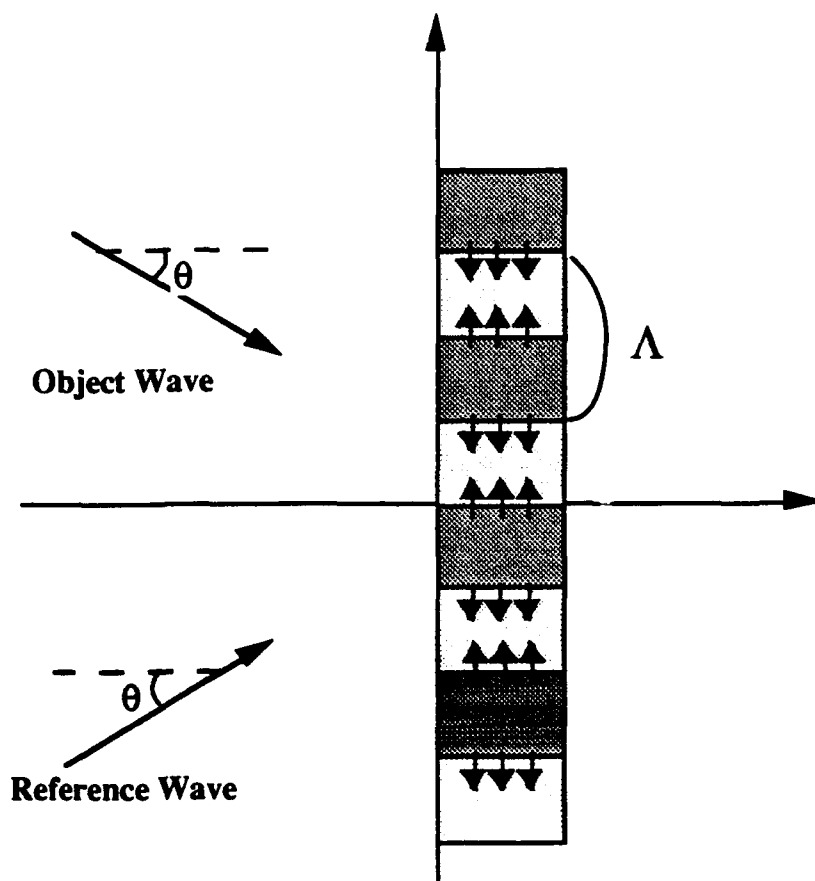
Figure 1-6: Monomer diffusion in a holographic photopolymer.

molecule is approximately equal to the sum of the dipole moments of the constituent monomers. Even when this assumption is violated, Δn due to $\Delta \rho$ dominates [23]. Implicit differentiation of Eq. 1-4 yields the relation of Δn and $\Delta \rho$, to first order, where n is the index of the unpolymerized material:

$$\Delta n = \frac{(n^2 + 2)(n^2 - 1)}{6n} \frac{\Delta \rho}{\rho} \tag{1-5}$$

Although other mechanisms could contribute to the refractive index modulation in DMP-128, only density or composition changes could yield the values of Δn inferred from the diffraction efficiency [28], which are as high as 0.2. However, small changes in molar refractivity due to the breaking of double bonds that occurs in vinyl polymerization could also contribute to Δn. Other interesting optical properties have been observed in polymeric materials, including photoconductivity and second and third order nonlinear responses [29], but none of these properties have been reported in the literature relevant to the commonly used holographic photopolymers.

12

The interest in developing a theory of holographic reciprocity failure in photopolymers stems from two observations. First, it has been shown that an understanding of the classical and holographic reciprocity failure in silver halide materials depends upon an understanding of the process of latent image formation, in particular the exponential decay of the critical first step of image formation. Secondly, image formation in photopolymers is governed by several time-dependent processes such as initiation, polymerization, and diffusion. The practical use of photopolymers may benefit from a theory that can determine the effect of exposure for various intensities and exposure times.

More than a century went by between the first observation of reciprocity law failure and the theoretical explanation of the holographic reciprocity law failure. The prospect for a research program in holographic photopolymers is less daunting. The reason is that the latent images formed in silver halide media are invisible, and almost undetectable, except by the use of extremely sophisticated diagnostics [6]. Holographic photopolymers, on the other hand, may begin to form volume phase gratings almost immediately upon exposure, though chemical baths and other processing techniques may be necessary to complete the formation of a high-efficiency grating.

The means of measuring grating formation are well documented in the photochemical literature [30,31,32]. If the initial stages of a photochemical reaction cause optical absorption or index of refraction changes, a hologram can be recorded. Indeed, most photochemical reactions produce absorption or index changes; the undetectable latent image of silver halide films is the anomaly.

When a photochemical system is exposed to the sinusoidal intensity pattern formed by the interference of two coherent wavefronts, the spatial distribution of index or amplitude modulation will map the interference pattern, forming a holographic grating. The hologram may be weak, and it may disappear quickly, but it will be present. If the chemical system has a narrow spectral responsivity, it may be simultaneously probed with another wavelength which will not activate the chemical reaction. The diffraction efficiency of the probe beam will give a measure of the photochemical reaction. Alternatively, a single light source can be used to form the grating and probe it by chopping the reference beam, as shown in Figure 1-7. The intensity of the conjugate wave, recreated by diffraction of the object wave, gives the efficiency of the grating. In either case, very small diffraction efficiencies may be measured, since the background level of scattered light can be made very small.

Real-time probing of the formation of photopolymer gratings was demonstrated in the early 1970's by researchers developing a holographic photopolymer at DuPont [24]. The photopolymer was exposed with a wavelength of 364 nm, and was probed with a 633 nm He-Ne beam, which did not affect the polymerization. The results of these experiments supported the hypothesis that volume phase holograms are formed in part by diffusion of material within the emulsion.

13
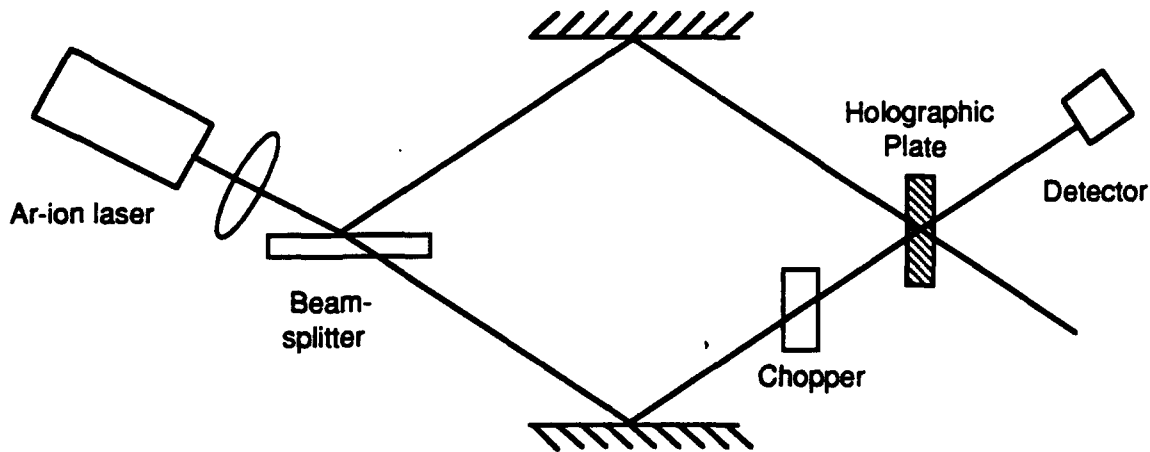
Figure 1-7: Single-beam measurement of transient grating efficiency.

The goal of the present investigation is to apply the techniques of real-time grating measurement to characterize the process of image formation in the DMP-128 photopolymer system, and to determine the implications of this process for hologram fabrication. Chapter Two of this report will summarize the state of the art in the field of holographic photopolymers, and discuss the fundamental photochemistry of this class of materials. A model of latent image formation in holographic photopolymers will be the subject of Chapter Three. Chapter Four will be devoted to the theory of diffusion in photopolymers, and Chapter Five will detail the experimental results of this investigation in light of the imaging model. Finally, Chapter Six will present the overall conclusions of this project, and indicate its relevance to future research and utilitarian applications.

II. PHOTOPOLYMERS FOR HOLOGRAPHY

A. The Development of Photosensitive Polymers

The appearance of commercially available photopolymer films for holography is not a wholly recent innovation, nor is it a sudden departure from the mainstream development of light sensitive materials. The first photograph, created by Nicephore Niepce in 1826, utilized a natural photosensitive resin called bitumen of Judea, which is a light asphalt from Syria. The bitumen was coated on a pewter plate and exposed to a sunny outdoor scene for several hours in a primitive camera. The exposed resin hardened, while the unexposed resin remained soluble and was washed away with mineral oils, leaving a faint image [33]. The hydrocarbon molecules in asphalt are a special type of polymer, large molecules built on a chain of carbon atoms. The very existence of polymers was not widely accepted until a century after Niepce's photograph, but it is now known that the impurities in the asphalt catalyzed a crosslinking reaction that bound the linear polymer molecules together into a dense network, immobilizing the material and making it resistant to solvents.

Niepce and his partner Daguerre (of daguerrotype fame) developed this process further, not for photography, but for printing. The bitumen was coated onto a copper engraver's plate and exposed through a black ink line drawing. The bitumen under the black lines remained soluble and was washed away, exposing the bare copper to the action of an etching solution. When all the bitumen was finally stripped away, the line drawings had become grooves etched into the plate, ready to accept ink. The exposed bitumen resisted the action of the etchant; thus it became known as a resist. In modern terminology it was a negative photoresist, a resist which becomes insoluble on exposure to light by the light activated crosslinking of existing polymer molecules. Negative photoresists are widely used today in various printing techniques, including printed circuit board fabrication.

Within a few years of Niepce's invention, numerous experimenters discovered that dichromate salts converted common organic substances into negative resist imaging layers. Paper, egg albumen, starch, and gelatin could be sensitized by dichromate. Dichromated gelatin became a mainstay of printing technology for over a century. Only in the twentieth century was it understood that the proteins in gelatins are macromolecules, polymers built up from amino acid units, and that photoreduced trivalent chromium ions promote crosslinking of the protein molecules and insolubilization of the exposed areas [23]. The mechanism of dichromated gelatin crosslinking is illustrated in Figure 2-1. The two molecular fragments shown represent simplified amino acids. The amino acids themselves are polymerized amides; the repeated amide group is the carbon atom, doubly-bonded to an oxygen and singly-bonded to a nitrogen. The Cr(III) ion serves as a coordination center, linking together the amide groups from different molecules. As a general rule, crosslinking of a polymer causes a decrease in solubility, though if the crosslinking is sparse, solvent can still penetrate the polymer network and cause swelling.

The development of polymer chemistry led to the creation of synthetic crosslinkable polymers which found wide application in printing technology, and have largely supplanted the use of dichromated gelatin (DCG) as a negative resist. However, this natural polymer system is still widely thought to be the best holographic medium for many applications.
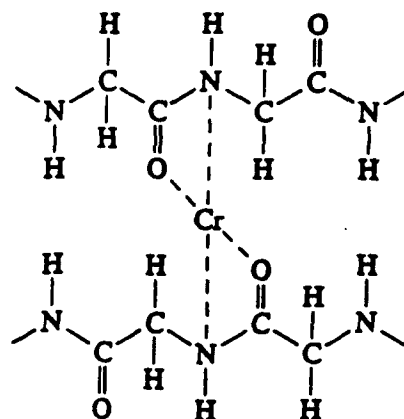
Figure 2-1: Cr(III) co-ordination crosslinking in dichromated gelatin.

[Adapted from Reference 33]

B. Photopolymerization

Unlike the photosensitive polymer resists, which exploit the photo-induced crosslinking of an existing polymer, photopolymerization systems use light to initiate the chemical reaction that creates a polymer from its monomer building blocks. A survey of the literature will show that almost all holographic polymer systems are based on photopolymerization reactions, and that almost always this reaction is of the type known as radical chain polymerization or vinyl polymerization. Furthermore, the holographic polymers in widespread use are almost all based on the reactions of acrylic acid and related compounds that can be dye-sensitized to polymerize under the influence of visible light.

1. Acrylic Acid

As a basis for understanding radical polymerization, it is best to first look at the structure of the acrylic acid molecule shown in Figure 2-2. Acrylic acid is one of numerous carboxylic acids, which owe their acidity to the characteristic carboxylic (COOH) group. Acrylic acid is the simplest of the unsaturated carboxylic acids; unsaturated means that it contains a double carbon bond. This carbon-carbon double bond is a prerequisite for radical chain polymerization [34]. The acrylic monomer in Figure 2-2 is converted to the repeating sub-unit of poly(acrylic acid) shown in Figure 2-3 by "opening" the carbon double bond for linking with the next acrylic monomer [35]. Although reaction kinetics will determine the length of the polyacrylic chain, there is no theoretical maximum to the length that the molecule can reach.

16
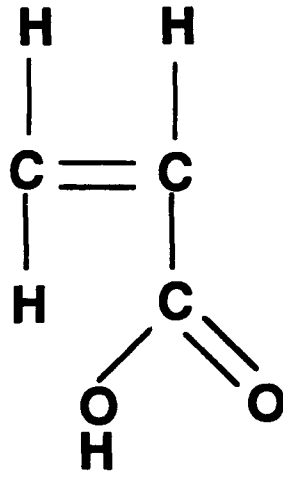
Figure 2-2: Structure of acrylic acid.
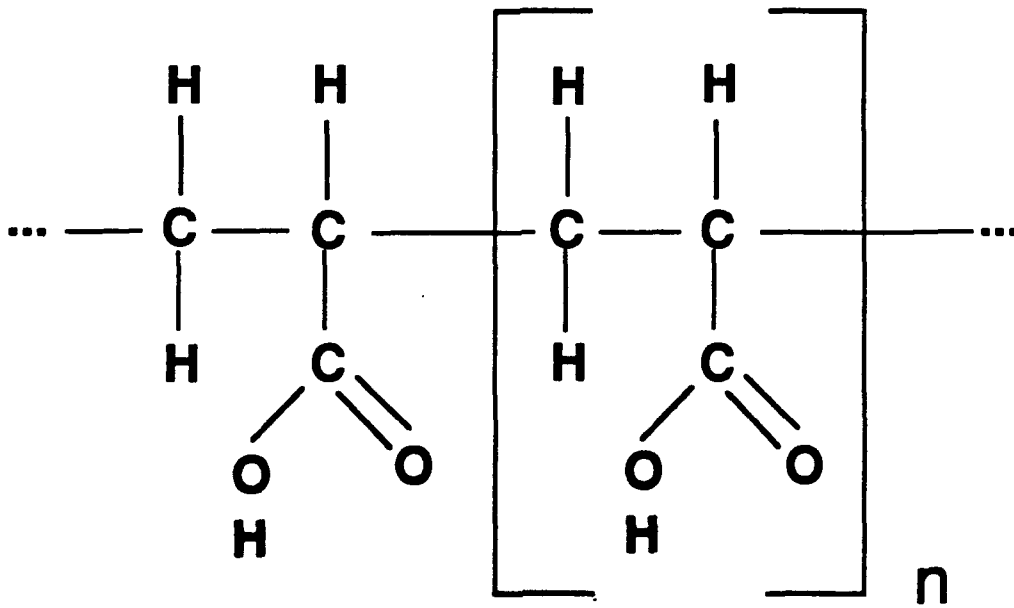
Figure 2-3: Structure of poly(acrylic acid).

In this research, acrylic acid is more than an academic example; almost all of the known holographic photopolymerization systems employ monomers that are salts or esters derived from acrylic acid. Esters are formed by the reaction of alcohols with the carboxylic acid group; likewise, salts form in the normal manner, with a positive metallic ion replacing the hydrogen in the carboxylic group. In either case, the formation of the long-chain carbon backbone from the unsaturated monomers is much the same. The esters of acrylic acid are widely used in industry to form polymers, especially poly(methyl methacrylate), which is better known as Plexiglass. Poly(acrylic acid) itself seems to be used mainly in floor polishes.

2. Radical Chain (Vinyl) Polymerization

Radical chain polymerization is a multi-step chain reaction in which free radicals promote the growth of long polymer chains from monomers [36]. Free radicals are molecular fragments with an unpaired electron capable of forming a covalent bond. The reaction begins with the initiation step, in which a free radical is formed (usually by the thermal or photochemical decomposition of a molecule called the initiator) and bonds itself to a monomer molecule. This radicalized monomer is now itself a radical, and it begins the step of propagation, in which it reacts one-by-one with more monomer molecules to form an ever-larger radicalized macromolecule. Finally, in the termination step, the radical is neutralized by reaction with oxygen or another radical, and the growth of the molecule stops.

The initiation step can be illustrated by the polymerization of acrylic acid as initiated by benzoyl peroxide. This reaction was one of the first radical polymerization processes to be discovered, partly because the peroxide is a commonly occurring impurity in the monomer. The reaction can proceed spontaneously in acrylic acid exposed to light or heat; the polymerization is exothermic, and can be quite violent, even explosive [37]. Benzoyl peroxide is a bilaterally symmetric molecule that can dissociate into two equal halves when excited by thermal excitation or a UV photon. The two halves undergo a further decomposition, yielding free radicals, as shown below:

$$(C_6H_5COO)_2 \rightarrow 2C_6H_5COO \cdot \rightarrow 2C_6H_5 \cdot + 2CO_2$$

(The dot after a chemical formula indicates a free radical.) The following short-hand notation is often used for the formation of a radical $R\cdot$, such as benzoyl peroxide from an initiator, I:

$$I \rightarrow 2R \cdot$$

However, note that in dye-sensitized photopolymerization, to be discussed later, usually only one active free radical is formed from each initiator molecule.

Once a free radical is formed, it is effective in initiating polymerization only if it bonds to a monomer and regenerates the radical. The initiation of an acrylic acid molecule by a generic radical is shown in Figure 2-4. The carbon-carbon double bond is opened to form a bond with the radical fragment, and one carbon is left with an unpaired electron, ready to bond with the next monomer it encounters. This propagation stage can continue for as long as the growing polymer maintains its radical character.

18
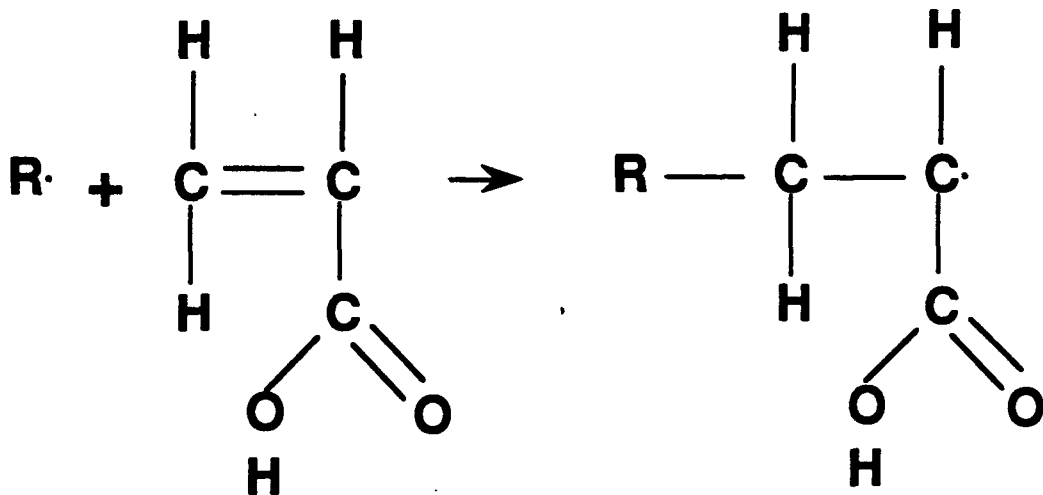
Figure 2-4: Radical initiation of acrylic acid.

The termination of the polymer molecule growth is generally due not to total consumption of all monomer present, but rather to reactions between radicals. When two radicals meet, they react either by combination, in which the two polymer chains are joined head to head by a carbon bond, or by disproportionation, in which a hydrogen is transferred from one chain to another. In disproportionation, the two chains remain separate; one terminates in a single bond, the other in a double bond. Termination of a chain can also occur when a radical is "poisoned" by reaction with atmospheric oxygen.

3. Dye-Sensitized Photopolymerization

The fission of benzoyl peroxide and other "classical" initiators into free radicals can be stimulated by UV photons, but not by visible light. The formation of free radicals by visible light requires a sensitizing dye which engages in reactions with one or more intermediate steps. Some of the first polymerization systems of this type were found by Oster [38]. He found that some dyes initiated polymerization of common monomers (acrylates, styrene, etc.) in the presence of atmospheric oxygen and a reducing agent. When excited by the absorption of a photon, the dye molecule abstracts one or more protons from the reducing agent. Oster hypothesized that the reduced dye molecule then reacted with atmospheric oxygen to yield polymerization-initiating hydroxyl radicals (OH·).

In a recent review of dye-sensitized photopolymerization, [39] one finds that there has been a re-evaluation of Oster's proposed mechanisms; in particular, the reactions that required oxygen may have been due primarily to the formation of atomic oxygen by reaction with excited dye molecules, with the subsequent formation of radical peroxides. Nonetheless, a number of visible light initiating systems are known in which an excited dye molecule abstracts hydrogens from the reducing agent, transforming one molecule of the reducing agent into a potent radical [23]. A reaction of this type is the initiator in Polaroid's DMP-128 holographic photopolymer.

19

The discovery of dye-sensitized polymerization excited considerable interest in the photographic community. It was thought that the sensitivity might match or exceed that of silver halide materials, since the free radical produced by a single photon could polymerize a large number of monomers, just as the reduction of a few silver atoms can catalyze the reduction of an entire photographic grain. In one of Oster's systems [38], acrylamide monomer served as both monomer and reducing agent, with the vitamin riboflavin serving as the sensitizing dye. In the resulting polymerization, over 4,000 monomer molecules were converted to polymer for each photon absorbed by the system. This gain mechanism is important in determining the sensitivity of holographic photopolymers.

4. Photopolymerization Kinetics

As noted before, a propagating polymer chain continues to grow until terminated by combination or disproportionation. The length of the chain, and thus the gain of the light-sensitive system, is determined by the relative rates of initiation, propagation, and termination. Though the reaction kinetics of photopolymerization systems can be quite complex, there are realistic simplifying assumptions that lead to useful models of photopolymerization rates. The most important assumption is the steady-state, or stationary-state condition [40]. This condition exists when the radical concentration during polymerization remains constant, with the loss rate due to termination exactly balanced by radical formation. Also, it is usually assumed that the rates of propagation and termination are independent of the polymer chain length, which has been shown experimentally to be a good approximation in many cases [41].

To derive the steady state kinetics, one starts with initiation. A typical dye-sensitized initiation yields no more than one radical R· from an initiator molecule I that absorbs a photon.

$$I + h\nu \rightarrow R\cdot \tag{2-1}$$

From basic principles of photochemistry [42] one would expect that the rate of free radical formation would be proportional to the number of photons absorbed by the initiator dye. One can write the following expression for the rate of initiation,

$$v_i \equiv \left(\frac{d[M\cdot]}{dt}\right)_i = f_i \, \phi_i \, I_a \tag{2-2}$$

where v_i is the rate of initiation and $[M\cdot]$ is the concentration of radicalized monomer or polymer chains. (Henceforth, square brackets will denote "the concentration of" some substance.) I_a is the absorbed light intensity, ϕ_i is the quantum efficiency of radical creation, and f_i represents the fraction of radicals that succeed in initiating polymerization.

The propagation reaction involves the addition of monomer molecules, one at a time, to a radical polymer chain already n units long.

20

$$M_n\cdot + M \rightarrow M_{n+1}\cdot \qquad (2\text{-}3)$$

The rate of propagation depends jointly on the concentration of the two reactants, monomer M and active radical chains M·,

$$v_p \equiv -\left(\frac{d[M]}{dt}\right)_p = k_p[M][M\cdot] \qquad (2\text{-}4)$$

where k_p is known as the rate of propagation.

Termination can occur either by combination

$$M_n\cdot + M_x\cdot \rightarrow M_{n+x} \qquad (2\text{-}5)$$

or by disproportionation

$$M_n\cdot + M_x\cdot \rightarrow M_n + M_x \qquad (2\text{-}6)$$

but in either case the reaction occurs between two macroradicals, so the termination rate v_t is quadratic with respect to radical concentration

$$v_t \equiv -\left(\frac{d[M\cdot]}{dt}\right)_t = k_t[M\cdot]^2 \qquad (2\text{-}7)$$

and k_t is the termination rate constant. The steady-state radical concentration is found by setting the loss rate of radical due to termination in Eq. 2-7 equal to the radical formation rate in Eq. 2-2. The result is

$$[M\cdot] = \left(\frac{f_i\,\phi_i\,I_a}{k_t}\right)^{1/2} \qquad (2\text{-}8)$$

Given the steady-state radical concentration, the overall rate of polymerization can be found by substituting Eq. 2-8 into the propagation rate, Eq. 2-4:

$$v_p \equiv -\left(\frac{d[M]}{dt}\right) = \frac{k_p}{\sqrt{k_t}}\left(f_i\,\phi_i\,I_a\right)^{1/2}[M] \qquad (2\text{-}9)$$

In the steady state, the rate of polymerization, which is also the rate of monomer loss, is proportional to the square root of the light intensity, and directly proportional to the monomer concentration. This relationship has been experimentally validated, and is exploited to determine polymerization reaction rates in what is known as the sector method [36]. The photopolymerizable system is exposed to light of intensity I through a 50% duty cycle rotating chopper (also known as a sector wheel). The reaction rate

21

is monitored by means of calorimetry or sensitive volume measurements. When chopped slowly, compared to the free radical lifetime, the radical concentration and thus the reaction rate rises to its equilibrium value during the light and falls to zero during the dark. When chopped at a very high speed, the radical concentration cannot follow the intensity fluctuations. The radical concentration and reaction rate act as though the intensity level were cut in half, which means that they decrease by a factor of $\sqrt{2}$. The chopping period at which the reaction rate drops is a good estimate for the mean free radical lifetime.

Inspection of Eq. 2-9 also reveals that the steady-state loss rate of monomer is a first order decay, i.e. the amount of monomer lost per unit time is proportional to the amount remaining, similar to the decay of radioactive elements. However, it is not safe to assume that the decrease of monomer concentration with polymerization follows an exponential decay with a well-defined half-life. The steady-state kinetics are not a good approximation when the "conversion" (fraction of monomer converted to polymer) is large.

The most important deviation from steady-state kinetics is the "auto-acceleration," or "gel" effect [43]. Auto-acceleration is seen when the the rate of polymerization suddenly increases at a certain conversion level. Eventually the accelerated reaction stops when the monomer is nearly depleted. The chain lengths of the polymer molecules tend to be longer than usual after the accelerated reaction. This type of behavior is normally seen when a bulk sample of the nearly pure monomer is used. The accepted explanation is that the increased viscosity of the polymerized material slows the diffusion of active macroradicals, making it more difficult for them to find each other and combine in a termination reaction [44]. Without termination, the macroradical grows until it can no longer find monomer molecules to add to its chain. The onset of auto-acceleration can be delayed by conducting the reaction in a solvent with a low concentration of monomer, so that polymerization does not change the viscosity so dramatically.

Radical termination reactions are usually diffusion controlled, not just in the gel effect. In experiments, systematic variation of the viscosity over a wide range caused a corresponding change in the termination rate. The actual bimolecular termination reaction occurs very rapidly once two radicals meet; the termination rate is set by how often radicals collide. In a review of the subject [45] North identifies two diffusion processes that set the termination rate; the first is the translational diffusion of the macroradicals that brings them into contact, and the second is the conformational twisting of the polymer chain that allows the active ends of the two radicals to meet.

Kloosterboer [46,47,48] has done considerable experimental work on the problem of radical trapping in the polymerization of acrylates. By identifying the electron spin resonance (e.s.r) signals of the free radical, he has shown that active free radical can survive in a polymer at room temperature, under vacuum, for more than seventy days. The shrinkage that occurs during polymerization decreases the free volume of the material and promotes radical trapping. Rapid photopolymerization with an intense light source leads to a large conversion, since the shrinkage tends to lag behind the actual polymerization reaction. However, even at very low conversions, radicals can be trapped. This suggests that even when the overall viscosity of a photopolymer system is low, local areas of high viscosity are formed. Kloosterboer attributes this local viscosity enhancement to polymer molecules that grow in irregular patterns by a random walk growth process.

C. Holographic Photopolymers

1. The Hughes Holographic Photopolymer

In the late 1960's, researchers at the Hughes Aircraft Co. developed a photopolymerization imaging system based on the polymerization of barium acrylate in aqueous solution [49,50]. Barium acrylate, like acrylic acid and its other metallic salts, is very soluble in water. Furthermore, poly(acrylic acid) and poly(sodium acrylate), which form as simple long chain molecules, are also water soluble. However, barium acrylate starts to crosslink as it polymerizes to form a dense network of interconnected polymer chains. The crosslinked chains exclude the solvent and precipitate out as colloidal particles. The particles were found to be about 0.7 microns in diameter, and therefore quite effective in scattering visible light. Images were recorded in this medium as variations in the effective optical density due to variations in the density of scattering centers; the greater the exposure, the greater the density of precipitated particles.

The insolubilization of poly(barium acrylate) is due to the fact that the monomer is a multi-functional acrylic. Since the barium ion carries a double positive charge, it is associated with two negatively charged functional acrylic groups, and thus its formula is $Ba(CH_2=COO)_2$. When this di-acrylate monomer is polymerized, one of the carbon-carbon double bonds is broken to incorporate the monomer into the chain, while the other acrylic group is left pendant (literally, hanging from the polymer chain.) The same radical initiation mechanism that catalyzes the formation of the polymer chain will also bond together the pendant acrylic groups of different polymer chains, forming a dense, interconnecting network. Kloosterboer [47] has found that the relative reactivity of the pendant groups can be much greater than the reactivity of free monomer at the beginning of a reaction, and much less at the end of polymerization, due to viscosity changes in the material. He also found that the densest crosslinking is possible with di-acrylate monomers, as opposed to tri-acrylates and tetra-acrylates.

The Hughes research into the photopolymerization of barium acrylate and related monomers led to the development of a photopolymer medium for holography [51,52]. The medium was mixed immediately before use from two solutions, since the sensitized medium had a shelf life of only a few hours. The first solution was called the photocatalyst solution; it generally contained methylene blue as a light receptor, an organic sulfinate salt as a radical source, and a nitrophenylacetic acid or one of its salts as a fixing agent. The second solution was a monomer mixture, generally containing barium acrylate, lead acrylate (another di-functional acrylic) and acrylamide. (Acrylamide is a mono-functional acrylic acid derivative, with the acidic OH group replaced by an NH_2 amide group.)

The photochemistry of free radical production in the Hughes photopolymer system involves the interaction of a phenothiazine dye, such as methylene blue, with a sulfinic compound [53]. Methylene blue exists as a positive ion in solution; its narrow absorption band peaks in the red. The structure of methylene blue is shown in Figure 2-6. When the dye ion absorbs a photon, it is excited to a singlet state, and quickly undergoes internal conversion to an excited triplet state. This can be written as

$$D^+ + h\nu \rightarrow (D^+)^1 \rightarrow (D^+)^3 \qquad (2\text{-}10)$$
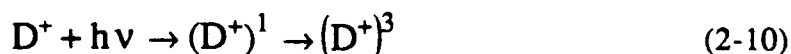
where D represents the dye. The triplet state of the dye has a higher oxidation potential than the singlet state, and can be reduced by the transfer of an electron from a sulfinate ion [54]. The sulfinate ion source could be either benzenesulfinic acid, toluenesulfinic acid, or a salt thereof. The redox reaction between the triplet dye and the ion can be written as

$$\left(D^+\right)^3 + RSO_2^- \rightarrow D\cdot + RSO_2\cdot \qquad (2\text{-}11)$$
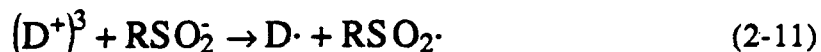
where R represents the organic benzene or toluene group. The sulfinate radical is the one that initiates polymerization; the dye radical is much less reactive.
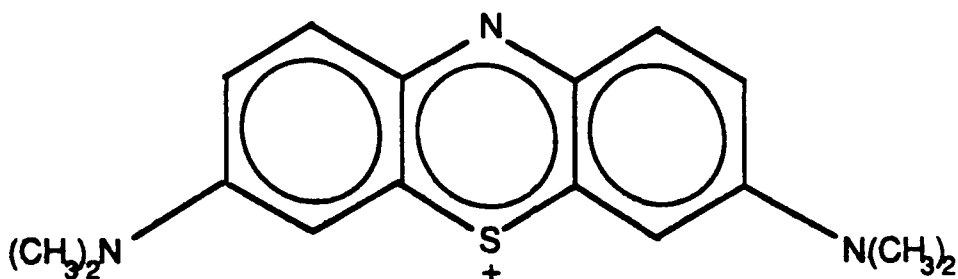
Figure 2-5: Structure of methylene blue.

The polymerization of this system exhibited an induction period, that is, with constant illumination, there was a measurable time lag between the beginning of illumination and the beginning of polymerization. This behavior is common in photopolymer materials, and reflects the scavenging of free radicals by oxygen or other inhibitors contained in the material. After sufficient radicals had been produced to neutralize the scavengers, the reaction would begin. For holographic exposure, this effect was compensated for by illuminating the plate with an overall visible light exposure on the order of 1 mj/cm^2, so that polymerization would start promptly with the exposure.

After exposure and polymerization, the remaining dye, initiator, and monomer could still react under ambient light and degrade the hologram. Two approaches were used to fix the recorded image [54,55]. First, thermal fixing of the exposed hologram in the dark desensitizes the medium by causing sulfinate ions (not radicals) to react directly with monomer molecules. The product is not photochemically active. Typically, heating at 80 degrees Centigrade for minutes or even hours was required. The second approach used a UV photochemical reaction to desensitize the medium. Nitrophenylacetic acid was added to the mixture, and after exposure the hologram was exposed to approximately 200 mj/cm^2 of UV light. The mechanism here was that the photochemical decomposition of the nitrophenylacetic acid produced aci-ions that reduced the methylene blue to its colorless (leuco) form. If the plate was not protected from atmospheric oxygen, the dye would gradually re-oxidize and the plate would regain sensitivity.

24

The ratio of the various monomers in this system was always a compromise between sensitivity and scattering noise. Pure acrylamide monomer could be made to polymerize and form a phase grating, but it required a large exposure. Pure barium acrylate was much more sensitive, but the scattering from the colloidal, polymerized particles made the reconstructed holograms very noisy. A mixture of acrylamide with barium and lead acrylates formed a noisy, scattering hologram that became transparent and formed a phase hologram after a few hours under ambient light [52]. No explanation for this transformation is known. The substitution of potassium acrylate for lead acrylate was also found to reduce scattering, as well as extending the shelf life of the material.

As a holographic material, the Hughes formulation was found to be capable of yielding 45% diffraction efficiency transmission gratings in 25 μm layers. Most of the diffraction was due to the formation of a surface relief grating, but since the maximum diffraction efficiency of a thin phase transmission grating is only 34%, the presence of a weak volume phase grating was deduced. The phase modulation was linear with exposure up to exposures of several mj/cm^2 [56]. Later work yielded a composition that required 0.5 to 1.0 mj/cm^2 for exposure, a resolution of 2500 cycles/mm, and a diffraction efficiency of up to 80% in a thick grating [57].

2. The DuPont Holographic Photopolymer

In the early 1970's, researchers from DuPont revealed the properties of a dry photopolymer medium suitable for holography [24]. No specifics of the composition were given, other than the fact that the material consisted of a photopolymerizable monomer, an initiator system, and a polymeric binder to hold the liquid monomer on the substrate.The initiator was most sensitive in the UV at 360 nm, but could be made sensitive in the blue and the green. In the UV, a pre-exposure of about 1 mj/cm^2 was required prior to the holographic exposure, which required anywhere from 1 to 50 mj/cm^2. The spatial frequency response of the material, defined as the diffraction efficiency vs. the spatial period of the holographic grating, was insignificant below 100 line pairs per millimeter (lp/mm), rose to a peak at 1100 lp/mm, and declined again to half its peak value at about 1900 lp/mm. The scattering noise due to granularity in the photopolymer medium was measured to be an order of magnitude lower than the scattering from comparable holograms recorded on Kodak 649F plates.

For a clue as to the actual composition of the original DuPont photopolymer, it is necessary to consult the relevant patent literature, with the understanding that the photopolymer composition was a closely held proprietary formula, and that patents are written as broadly as possible to cover all possible variations of the basic invention. The holographic photopolymer composition is revealed in one patent [58], and the function of the various components is described in a prior invention [59]. The basic system consists of an unsaturated monomer capable of free-radical initiated polymerization, a free-radical producing electron donor agent (i.e. initiatior), a binder, and a lophine dimer capable of cleaving under the influence of light. (Lophine is the name of a class of compounds in which three phenyl rings are attached to a central carbon-nitrogen ring, as in Figure 2-6.) In addition, the system may contain an energy transfer dye for sensitization in the visible, and an oxygen scavenger to increase the overall sensitivity (since oxygen tends to poison the free radicals and slow the polymerization reaction.)
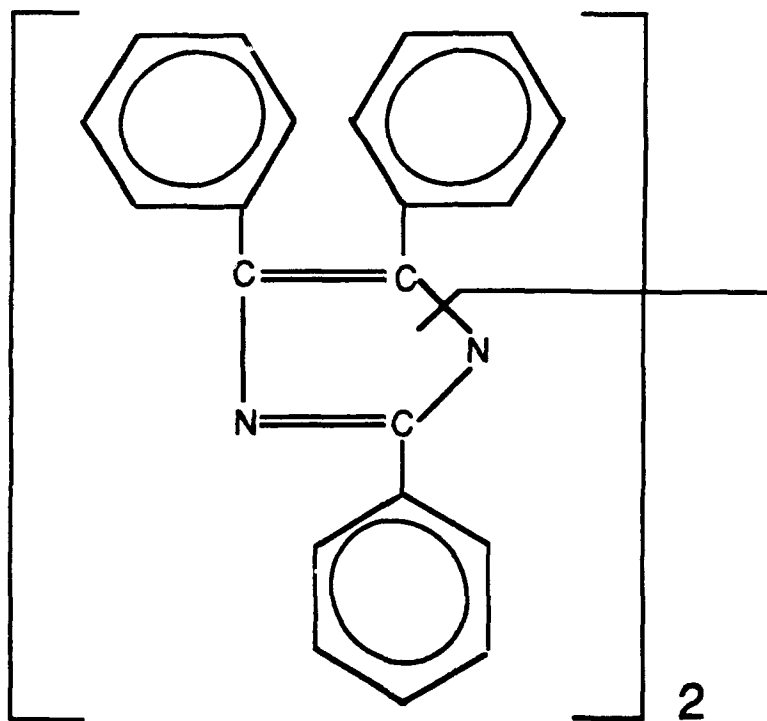
Triphenylimadazoyl Initiator
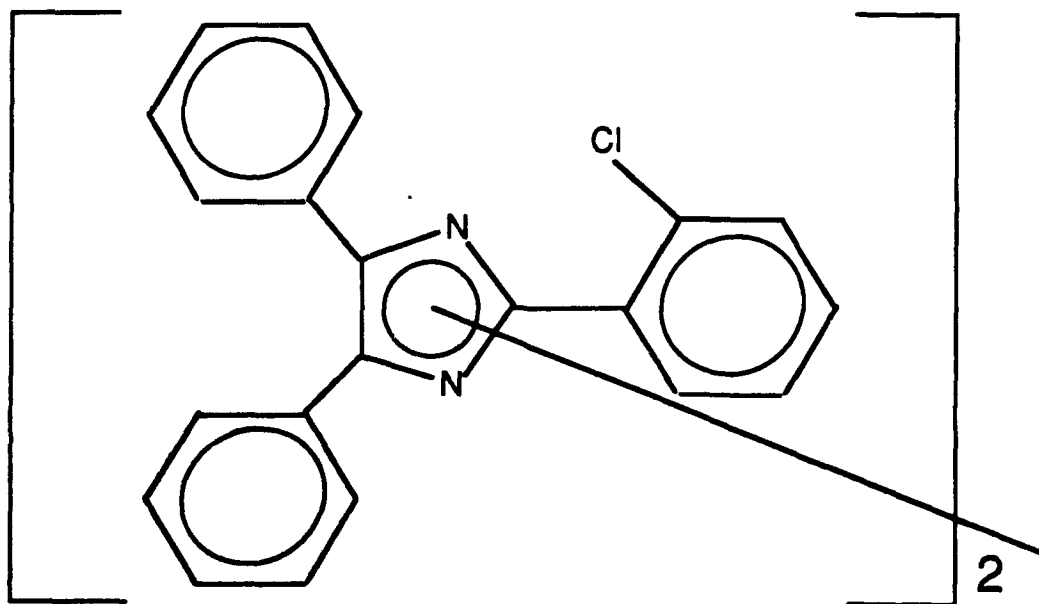
HABI initiator

Figure 2-6: <u>Lophine dimer initiators used in DuPont holographic photopolymers.</u>

The sequence of reactions for photopolymerization in this system was similar to Oster's dye-sensitized photopolymerization, discussed earlier. A lophine dimer would fission into two equal parts, either directly by the absorption of a UV photon, or indirectly by energy that was first absorbed by a sensitizing dye. (Lophine is better known as a chemically luminescent compound.) The dimer fragment was then reduced by accepting an electron from the initiator. The preferred initiators were of a class known as the amine substituted leuco dyes. The ability of these dyes to produce free radicals depended upon the number and the structure of the organic amine groups. Leuco (a Greek root word for "pale") indicates that the color-bearing group of the dye can undergo a reversible reduction to a colorless state, as in many other organic dyes. After oxidizing the dimer fragment, the reduced leuco dye served as the free radical to initiate polymerization.

A number of multi-functional acrylate monomers were deemed to be suitable for the holographic photopolymer, including pentaerythritol triacrylate, polyethyleneglycol diacrylate, and triethyleneglycol diacrylate. The binder was usually a cellulose derivative, such as cellulose acetate butyrate. The free-radical producing agent, or initiator, was usually an amine substituted leuco dye, such as Crystal Violet or Methyl Violet. The preferred dimer was 2,4,5-triphenylimidazoyl. N-phenylgycine or stannous chloride were both suitable oxygen scavengers. The energy transfer dyes, used to sensitize the system to the visible, were chosen from the xanthene dyes such as Rose Bengal or Eosin. Note that the initiator was also a dye, but the initiator dye was exploited for its radical producing properties, not for its ability to absorb photons.

To produce a holographic emulsion, the components of the photopolymer system were dissolved in an organic solvent, such as dichloroethane or dichloromethane, and spread out to dry on a plastic substrate, such as polyethylene terephthalate (Mylar). Once dried, the emulsion was still soft and tacky, so it would be covered with another layer of plastic for protection. Later, the protective coating could be stripped off and the emulsion laminated directly onto a glass plate or other substrate. A holographic grating was formed immediately upon exposure, with no further processing or fixing. Further exposure to ambient light might degrade but would not destroy the recorded hologram. The sensitizing dye remained in the emulsion, and could be bleached to colorless state by a long exposure to fluorescent light.

Twenty years after the development of the original DuPont holographic photopolymer, DuPont researchers again started to publish papers on the subject [60,61]. They had developed a family of holographic recording materials optimized for different end uses, but all derived from the original compositions. For a sensitizing dye, they used a compound identified as DEAW, with a range of 400 to 560 nm, with peak response at 480 nm. (See Figure 2-7 for DEAW structure.) The initiator was identified as hexaarylbiimadazole (HABI), but it is obvious from its structure that it is nearly identical to the triphenylimadazoyl dimer used in the old composition. (See Figure 2-6). In addition to the initiator, a chain transfer agent was added that aids the formation of free radicals. The new compositions use a wide variety of mono and multi-functional acrylates. Cellulose derivatives are again used as binders, as well as other common polymers, such as poly(methyl methacrylate). The major innovation in the new composition is the addition of a plasticizer, a compound which prevents the hardening of the emulsion when it polymerizes. The DuPont researchers believe that diffusion plays a vital role in hologram formation, and that the

27

plasticizer enhances index of refraction modulation by allowing diffusion to continue even when the polymerization is substantially complete.
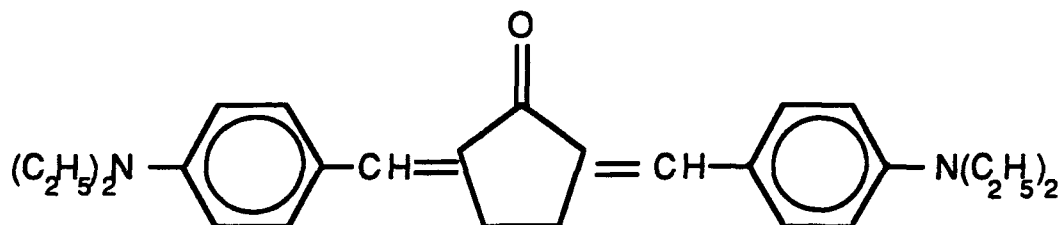
Figure 2-7: Structure of DEAW sensitizing dye.

The new DuPont photopolymers record volume phase holograms. Transmission gratings have been shown to have an index of refraction modulation, Δn, that is usually less than 0.01. For reflection holograms, Δn is sometimes as much as 0.04. The exposures that were used generally ranged from 20 mj/cm^2 up to 400 mj/cm^2. After exposure, the latent hologram is weak. A UV or visible light flood is used to polymerize all remaining monomer. Oven heating for up to 2 hours at 100° C increases the index modulation by a factor of three or four. Once again, diffusion is thought to play a role, due to the increased mobility of (unspecified) material at elevated temperatures. High diffraction efficiency is claimed, but it is unclear whether or not these efficiencies are corrected for the absorption of the sensitizing dye, which remains in the emulsion. Optional wet processing techniques have been developed that cause changes in the grating properties by means of swelling or chemical reaction with the emulsion.

3. The Polaroid (DMP-128) Holographic Photopolymer

In 1985 researchers from Polaroid disclosed the existence of a new photopolymer system for holography [17]. The new photopolymer system, named DMP-128, could be sensitized for exposure in the visible, and requires an exposure on the order of 1 to 5 mj/cm^2 for transmission gratings, and about 30 mj/cm^2 for reflection holograms. The material is coated on a glass or plastic substrate, and stored in dry air over a dessicant. The plate is made sensitive to light by placing it in moist air (approximately 50% humidity) for several minutes. After holographic exposure, the plate is washed in an alcohol bath to bring out the latent image, and then dried, resulting in a high efficiency phase grating.

The composition of DMP-128 is revealed in two patents [62,63]. It consists of a light absorbing dye, a sensitizer, an acrylate monomer, and an inert binder. Methylene blue is used as the dye for sensitivity in the red, especially at the Helium-Neon 6.'³ nm line. The sensitizer, or free radical source, is a complex polymer called branched polyethylenimine. The preferred monomer is lithium acrylate, although other acrylic acid monovalent salts may be used, such as sodium acrylate. The inert binder is N-vinyl pyrollidone. Since the film is sensitive only when moist, this solid binder is necessary simply to prevent the film from flowing off the plate during the coating process and during exposure. Lithium acrylate is very soluble in water, and the branched polyethylenimine is hygroscopic (absorbs water from the

28

air).

As with other photopolymerization systems, initiation begins with the excitation of the dye molecule to its triplet state, and then the transfer of energy to the sensitizer. The branched polyethylenimine structure is based on a saturated carbon chain with occasional nitrogens substituted for carbons, as shown below.

$$H_2N-(-CH_2-CH_2-N-)_x-H$$
$$|$$
$$R$$

where R is

$$-(-CH_2-CH_2-N-)_y-H$$
$$|$$
$$R'$$
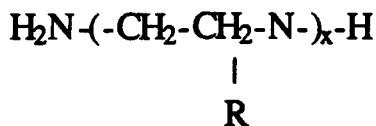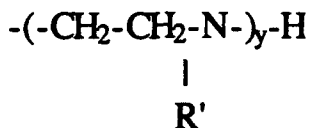
and R' is some other pendant organic group. The branched structure can be quite irregular, depending on the placement of the tertiary (triply connected) nitrogens, and the molecules can have a wide spectrum of molecular weights. DMP-128 uses the form of the initiator with a molecular weight of about 60,000. It is believed that the excited sensitizer dye abstracts a hydrogen from a carbon atom adjacent to a tertiary nitrogen, forming a free radical at that site. Unlike the common dimer initiators, the free radical does not break off and wander about on its own, but rather remains attached to the branched polyethylenimine molecule. Numerous free radicals can co-exist simultaneously on one molecule. The free radicals initiate polymerization of the lithium acrylate. The patent also suggests that after polymerization, the polyethylenimine can bond ionically to multiple acrylic chains, thus crosslinking them together.

Several wet processing steps are recommended to secure an efficient and durable hologram from the DMP-128 plate. After exposure, the plate is agitated in a methanol solution of acetic acid and zirconium acetate and then dried in air or over the boiling vapors of isopropanol to bring out the maximum refractive index modulation. (Prior to wet processing, the recorded hologram is very weak.) Treatment with a zirconium acetate solution stabilizes the finished hologram against the damaging effects of high humidity, which can swell the film and destroy the hologram. The zirconium acetate probably inhibits the absorption of moisture by crosslinking the acrylic polymer. A previous Polaroid patent demonstrated the utility of zirconium acetate in crosslinking dichromated gelatin [64].

A second wet processing step in a mixture of zirconium acetate and a fatty acid (such as stearic acid) further protects the hologram against moisture and humidity. In this step, the zirconium ion forms a soap with the stearic acid, just as common household soap is the sodium salt of stearic acid. Like any soap molecule, it has a hydrophilic end (the zirconium carboxylic group) and a hydrophobic end (the hydrocarbon chain). Bonding of the hydrophilic end to the DMP-128 polymer puts the hydrophobic end facing "outward," so it can resist the inflow of moisture.

29

The moisture sensitivity of DMP-128 before, during, and after exposure demands careful control of ambient relative humidity at 50% ± 5%. Too much moisture results in a hazy hologram. If the material is dry, the film may crack and split; if the material is too dry, no hologram will be recorded at all. Balanced against this need for stringent processing is the advantage of the very high index of refraction modulation that can be obtained, with Δn measured to be as high as 0.2. [65] This enables high efficiency gratings to be recorded in films that are only a few microns thick. Through electron microscopy and examining the effect that index matching fluids have on DMP-128 gratings, Polaroid researchers have concluded the grating is recorded as alternating solid and porous planes in the material [66]. Index matching fluids with low viscosity and low surface tension will fill the voids in the porous regions, and can be used to modify the properties of the developed hologram. In contrast, the DuPont researchers have found no detectable voids, cracks, or micro-pores in their holographic gratings.

4.   Miscellaneous Holographic Photopolymers

Many holographic photopolymer systems have been developed that have never been commercialized for holography. A good deal of work has been published on the recording of holograms in poly(methyl methacrylate) (PMMA), one of the most common and well-characterized industrial polymers [67,68,69]. PMMA is better known by its trade names of Lucite and Plexiglass. PMMA prepared by a typical batch polymerization process contains about 10% unpolymerized methyl methacrylate (MMA). If the light sensitive compound titanocenechloride is added before the batch polymerization, the remaining monomer can undergo photopolymerization within the PMMA matrix. Holograms can be recorded at 514 nm, but high intensity exposure (250 mw/cm^2) may be needed for fifteen to thirty minutes, followed by a slow polymerization reaction within the matrix, assisted by curing in an oven. The index modulation Δn is on the order of 10^{-4} to 10^{-3}. With a modulation this low, the volume hologram must be millimeters thick to have reasonable diffraction efficiency. This property can be used to advantage; a thick, low modulation volume phase hologram is precisely the type necessary to record multiple exposure holograms. The angular sensitivity of the grating is inversely proportional to thickness, so multiple holograms can be recorded and read by angular deviation of the reference/readout beam.

Some interesting variations on the basic holographic photopolymer scheme have been developed by researchers working at Bell Laboratories. In one system, two monomers were chosen such that one underwent polymerization slowly, while the other one had a rapid reaction rate. They were mixed in one film, on the theory that diffusion would cause the two species to be partitioned unequally in the dark fringes and bright fringes of the holographic interference pattern [70]. There was evidence for this mechanism, but the total index modulation was only 10% of the expected value. In another innovative system, a polymerization initiator alone was added to a porous glass matrix [71]. A holographic exposure at 364 nm selectively destroyed the initiator in the bright fringes, leaving a latent image in initiator concentration. Monomer was then introduced into the porous glass, which then formed a phase grating as it polymerized according to the amount of initiator present. The totally latent image formed during exposure was intended to avoid the undesirable interaction that sometimes occurs between an incident beam and the grating that forms during exposure.

A number of groups have also pursued the development of photopolymer systems based on the polymerization of acrylamide, along the lines of the early Hughes compositions [72,73]. One interesting development in acrylamide polymerization is a biphotonic process that enables hologram recording in the near IR. UV radiation is used to make a sensitizer molecule react with atmospheric oxygen; thus prepared, the sensitizer produces a free radical when it absorbs a second photon in the near IR, at 715 nm [74].

III. IMAGE FORMATION IN PHOTOPOLYMER PHASE HOLOGRAMS

This chapter addresses the issue of how phase holograms are formed in a photopolymer medium. First, it will be shown that the index of refraction in organic dielectrics is determined largely by two inherent properties of a material; namely, the mass density and the molecular polarizability. This will be followed by a review of the properties of phase gratings or phase holograms that are recorded by means of an index modulation. Photopolymerization will be shown to produce effects in the medium that lead to a modulation of the index of refraction, including photochemically induced changes in the molecular polarizability, and changes in the mass density brought about by internal mass transport (diffusion) or external mass transport (selective loss of material to solvents, etc.) In subsequent chapters, a model will be presented to account for the temporal evolution of the diffraction efficiency in a photopolymer medium during and after the exposure, and this model will be compared to observations made in previous research efforts.

A. The Index of Refraction and the Dispersion Relation

The response of matter to light is due largely to the electronic polarization that is induced in an atom or molecule by the electric field of the light. The rapidly oscillating optical field induces a charge separation in a molecule because the electrons respond to the local field more readily than the massive nuclei. There are also polar materials such as water whose molecules have a net dipole moment even in the absence of a field. The bulk polarization of a polar material is caused mostly by the alignment of the polar molecules with the applied field, from DC up to microwave frequencies. However, at optical frequencies, the rotational inertia of even a small polar molecule is large enough so that the molecule cannot keep up with the oscillating electric field [75].

A simplified but useful model of induced polarization assumes that the (classical) electrons are bound to their molecules by a harmonic oscillator potential. The motion of the heavy atomic nuclei is assumed to be negligible. The problem is then that of a damped, driven harmonic oscillator [76]. The damping is provided by intermolecular reactions and the radiation from the moving charges, while the driving force is the effective optical field seen by the molecule, $\mathbf{E}'$. (Henceforth bold-face type will be used to represent vector quantities.) The equation of motion for the electron is

$$m\ddot{\mathbf{r}} + \gamma\dot{\mathbf{r}} + k\mathbf{r} = e\ \mathbf{E}' \qquad (3\text{-}1)$$

where m and e are the electron mass and charge, γ is the damping factor, and k is the "spring constant" of the harmonic oscillator. The response of the oscillator is given by

$$\mathbf{r} = \frac{e\mathbf{E}'}{m(\omega_0^2 - \omega^2) - i\omega\gamma} \qquad (3\text{-}2)$$

where ω_0 is the resonant frequency

$$\omega_0 = \sqrt{\frac{k}{m}} \qquad (3\text{-}3)$$

32

The separation of positive and negative charges induced by the optical field induces a molecular dipole moment p, expressed as

$$p = e\ r \qquad (3\text{-}4)$$

or in terms of the molecular polarizability, α

$$p = \alpha\ E' \qquad (3\text{-}5)$$

Since **p** has units of length times charge [el], and E' has units of [el^{-2}], the polarizability has units of [l^3] or volume. Henceforth it will be assumed that the material is isotropic insofar as α does not depend on the direction of the applied field. Although this is not a good assumption for a small single molecule, where electrons are constrained within directional bonds, it is a good approximation for the mean polarizability per molecule, averaged over a bulk, amorphous material, such as a polymer.

The macroscopic constitutive relations, or material equations often used with Maxwell's equations can be used to tie together the macroscopic bulk polarization with the molecular picture. For the electric field, the material equation relates the electric field **E** to to the electric field displacement **D**

$$D = \varepsilon\ E \qquad (3\text{-}6)$$

via the dielectric constant, ε, also known as the permittivity . This multiplicative relation is supplemented by an equivalent additive relationship

$$D = E + 4\pi\ P \qquad (3\text{-}7)$$

Here, **P** is the bulk polarization. In terms of the microscopic view, **P** is the dipole moment per unit volume. If the material response to electric field is linear, as is usually the case,

$$P = \chi\ E \qquad (3\text{-}8)$$

and

$$\varepsilon = 1 + 4\ \pi\ \chi \qquad (3\text{-}9)$$

where χ is called the dielectric susceptibility. The macroscopic polarization **P** is simply related to the molecular polarization **p** by the number of molecules per unit volume, N:

$$P = N\ p \qquad (3\text{-}10)$$

The index of refraction of a bulk material is dependent on the polarization response of the material to the optical field, since, at optical frequencies

33

$$\varepsilon = n^2 \qquad \text{(3-11)}$$

The material equations are written in terms of **E**, **D**, and **P**, which are macroscopic quantities, averaged over a large number of molecules. However, polarization occurs on the molecular level, and the relevant field strength is **E'**, the field strength actually felt by the individual molecule, as in Equation 3-5. Unless the material medium is a gas so rarefied that intermolecular interactions are insignificant, **E'** will be due in part to the polarization of the surrounding medium, as well as the applied field **E**.

To derive the effective field **E'**, take a single molecule in a dielectric material where there is a uniform applied field **E**. Consider an imaginary sphere centered at the molecule; the sphere is macroscopically small, but much larger than the molecular dimensions. On the outside of the sphere, one may treat the surrounding dielectric medium as continuous. On the inside of the sphere, it can be shown [27] that various distributions of molecular dipoles (cubic lattice, random distribution, etc.) yield no net field at an internal observation point. Therefore, the problem reduces to the electrostatic boundary value problem of a single molecule in the center of a spherical vacuum, surrounded by a continuous polarized medium subjected to an applied field **E**.

Let ϕ indicate the desired potential, which is the potential due to the continuous polarized medium and the bound charges at the boundary between the vacuum and the medium. Consider the complementary potential Φ, which is due to the complementary configuration; namely, a sphere filled with a continuous polarized medium subject to the applied field **E**, surrounded by vacuum. One can define the zero of potential such that

$$\phi + \Phi = 0 \qquad \text{(3-12)}$$

Therefore, if the two complementary configurations were physically combined to yield one continuous polarized media without a boundary, the combined potential at the center of the sphere would be zero.

The potential ϕ can now be found in terms of Φ and the known relationship for the potential due to a volume distribution of polarization is

$$\phi = -\Phi = -\int d^3x' \; \mathbf{P(x')} \cdot \nabla'\left(\frac{1}{|\mathbf{x-x'}|}\right) \qquad \text{(3-13)}$$

Since the polarization **P** is constant and ∇' is equal to $-\nabla$, ϕ can be written as

$$\phi = -\Phi = -\mathbf{P} \cdot \nabla\phi_0 \qquad \text{(3-14)}$$

where the quantity ϕ_0 is defined as

34

$$\phi_0 \equiv -\int d^3x' \left(\frac{1}{|x - x'|} \right) \tag{3-15}$$

The auxiliary quantity ϕ_0 has the form of a potential function, but it is not a true potential. Specifically, it is similar to the integration of potential over a spherical volume with a uniform charge density of $\rho_0 = -1$. This is only an analogy, since ρ_0 is a dimensionless quantity. The quantity $(-\nabla\phi_0)$ can be obtained by means of Gauss' law to give

$$-\nabla\phi_0 = \frac{4\pi}{3} r \tag{3-16}$$

The actual field being derived here is the contribution the polarized medium makes to the effective electric field. By combining Equations 3-14 and 3-16, this can be written as

$$-\nabla\phi = -\nabla\left(-P \cdot \frac{4\pi}{3} r \right) = \frac{4\pi}{3} P \tag{3-17}$$

Therefore, the total effective electric field seen by a molecule in the dielectric medium is

$$E' = E + \frac{4\pi}{3} P \tag{3-18}$$

The dielectric constant can now be related to the number density of molecules and the molecular polarizability. Equations 3-5, 3-10, and 3-18 may be combined to give

$$P = N\alpha E + N\alpha\frac{4\pi}{3} P \tag{3-19}$$

Equation 3-8 may be used to eliminate P and E from the expression, leading to

$$\chi = \frac{N\alpha}{\left(1 - \frac{4\pi}{3} N\alpha \right)} \tag{3-20}$$

A new expression for the dielectric constant ε can be written by combining Equations 3-9 and 3-20; after a little re-arranging, one arrives at

$$\alpha = \frac{3}{4\pi N} \frac{\varepsilon - 1}{\varepsilon + 2} = \frac{3}{4\pi N} \frac{n^2 - 1}{n^2 + 2} \tag{3-21}$$

Equation 3-21 is known as the Lorentz-Lorenz formula, or sometimes as the Clausius-Mossotti equation, named after its various discoverers. Equation 3-21 is still expressed partially in terms of microscopic quantities, the molecular polarizability α and the number density of molecules N. Usually a macroscopic quantity R, known as the molar refraction or molar refractivity is defined as

$$R = \frac{4\pi \, N_A \, \alpha}{3} \qquad\qquad (3\text{-}22)$$

where N_A is Avogadro's number, the number of molecules in one mole, approximately 6.023×10^{23}. The molar refraction R is then the total polarizability of one mole of a material. Like the molecular polarizability α, the molar refraction has the units of $[l^3]$, and is conventionally expressed in units of cm^3. The expression may be further simplified by introducing the molecular weight M, and the mass density of the material ρ to yield a totally macroscopic relationship between the molar refraction and the index of refraction,

$$R = \frac{n^2 - 1}{n^2 + 2} \frac{M}{\rho} \qquad\qquad (3\text{-}23)$$

The form of the Lorentz-Lorenz relationship shown above has general applicability to understanding the refractive indices of liquid and solid materials and is not limited, as some would suggest, only to the case of rarefied gases. The molar refractivity of air varies by only 3% as the pressure is increased from 1 atmosphere to 176 atmospheres. The molar refractivity of common inorganic substances such as carbon dioxide and water changes by less than 1% in the phase change from vapor to liquid. Furthermore, the concept is also valid for mixtures. If two compounds of refractivities R_1 and R_2 form a mixture of N_1 and N_2 molecules, a good expression for the resulting refraction [77] is

$$R = \frac{N_1 R_1 + N_2 R_2}{N_1 + N_2} \qquad\qquad (3\text{-}24)$$

In particular, the Lorentz-Lorenz relationship and the assumptions that underlie it have been shown to be useful in the study of various polymers [78,79]. The Lorentz-Lorenz relationship is not perfectly accurate for polymeric materials, and several empirical relationships work just as well. However, none of the empirical relationships work any better, and they lack physical significance.

The most exacting test of the Lorentz-Lorenz formula in polymers has come from an optical technique used to determine the glass transition temperature T_g of a polymer. (Below T_g a polymer is hard and glassy; above T_g it is soft and rubbery.) The thermal expansion of a polymer tends to decrease the density and thus decrease the index of refraction with increasing temperature. When the index of refraction is measured accurately over a wide range of temperatures around T_g one generally observes a linear change of index with temperature. The slope of the n vs. T plot changes abruptly at the glass transition, as shown in Figure 3-1. [80,81] Other research [82] has shown that for two of the most commonly used optical polymers (poly(methyl methacrylate) and polycarbonate), the change of index with temperature is due almost totally to the variation of mass density, in agreement with the Lorentz-Lorenz relationship. However, the agreement with experimental data is improved if R is allowed to vary slightly as density changes, by means of an empirical correction factor.
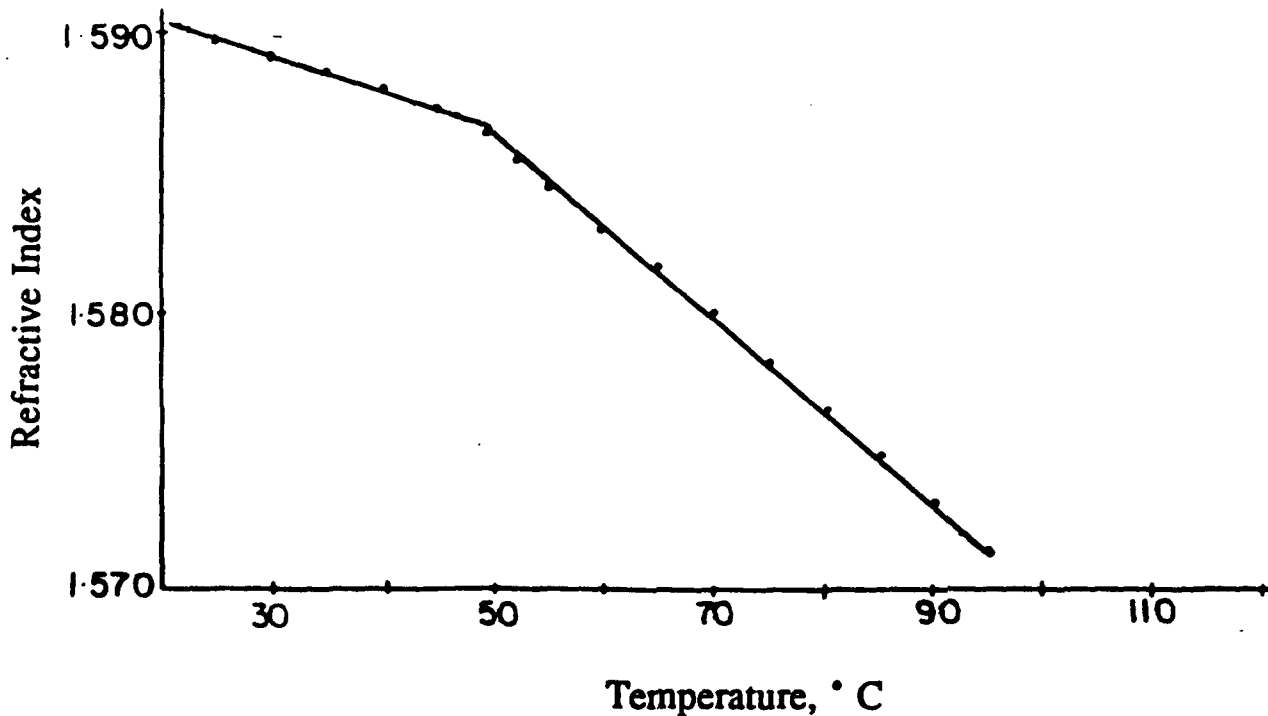
Figure 3-1: Refractive index of polystyrene vs. temperature near the glass transition temperature. (Adapted from Reference 81)

The molar refractivity of a substance varies substantially with the wavelength of light, just as the index of refraction does. This dispersion relationship can be described as the ensemble response of all the harmonically oscillating molecules in the substance, in response to the incident light, as given in Equation 3-2. Summing over all the modes of the molecular structure, and assuming an oscillator strength f_k, which is proportional to the intensity of the kth mode, one can write [83]

$$R = \frac{4\pi N_A}{3} \frac{e^2}{m} \sum_k \frac{f_k}{\omega_0^2 - \omega^2}$$

(3-25)

It is appropriate in this dispersion relation to neglect the effect of the molecular damping factor γ. The reason is that only polymers that are transparent to the illuminating radiation are of interest as holographic media. The effect of the damping factor in Equation 3-

37

2 is only significant when ω is near $ω_0$, that is to say, when near a resonant absorption line. This is the case of anomalous dispersion, which will not be considered here. At frequencies well below the major optical resonances of a substance, one has the case of normal dispersion, where the index of refraction generally increases with frequency. The normal dispersion of substances transparent in visible light is generally dominated by the effect of their resonant absorptions in the ultraviolet [23].

As a practical matter, the refractivity of a compound is usually estimated by means of an empirical relationship that is consistent with the oscillator model of molecular polarizability. It is assumed that each chemical bond in a molecule has a bond refractivity associated with it. The molar refractivity is simply calculated by summing the refractivities for all the bonds in the molecule. The justification for this procedure is that each chemical bond in a molecule represents electrons that are shared and localized between two atoms. The strength and nature of the bonds determine the response and polarizability of the molecule as a whole.

Denbigh [84] deduced several bond refractivities that are useful in estimating the index of organic compounds. The values, valid for n_D (the index of refraction at the sodium D line) are listed in table 3-1. In an analysis of one hundred and thirty organic compounds, Denbigh concludes that the "average error" between the measured and the additive molar refraction is about 0.7%. In a more recent compilation of bond refractivities, Goedhart [79] performed a regression analysis of one thousand organic compounds containing between them 43 different types of functional organic groups. The mean standard deviation of error in predicting the index of refraction was 0.4%.

B.   Modulation of the Refractive Index

The Lorentz-Lorenz relationship, Equation 3-23, relates the index of refraction n to the molar refractivity R, the mass density ρ, and the molecular weight M. However, when polymers are considered, one does not have three distinct degrees of freedom for changing the index of the material, as inspection of the equation might suggest. This can be illustrated by considering two polymer molecules built up from the same monomeric material, but each containing a different number of monomeric sub-units. Let the first molecule be composed of A monomeric units, and the second contain another number, B and also, re-write Equation 3-23 as

$$\rho = \frac{n^2 - 1}{n^2 + 2} \frac{M}{R} \qquad (3\text{-}26)$$

It is obvious that the molecular weight of a long-chain polymer is proportional to the number of identical monomer molecules that went into it. Now consider that the molar refractivity is, to a good approximation, equal to the sum of all the refractivities of its constituent bonds. Therefore, each monomer molecule incorporated into a chain contributes the same amount of molar refractivity, since each has the same molecular bonds in the same configuration. The conclusion is that the ratio M/R is constant regardless of the molecular weight of the polymeric material. Therefore, after polymerization is complete, substantial modulation of index for a single compound can only be achieved by changing the mass density. This conclusion has been experimentally verified [82].

TABLE 3-1: Bond Refractivities for Organic Compounds

(From Reference 83)

Bond	Bond Refraction cm^3
C-H	1.69
N-H	1.81
O-H	1.73
C-C	1.25
C-N	1.54
C-O	1.51
C-F	1.72
C-Cl	6.53
C-Br	9.37
C-I	14.55
C=C	4.16
C=O	3.38
C≡C	6.40
[1]C_{ar}-C_{ar}	2.73
[2]C_{na}-C_{na}	2.78

[1]Carbon-carbon bond in aromatic benzene ring structure.
[2]Carbon-carbon bond in naphthalene and derivatives.

However, due to molecular changes that occur in polymerization, the ratio M/R is not the same for both monomer and polymer. This can be illustrated by referring back to the example of acrylic acid polymerization presented in Chapter II. The acrylic acid monomer is unsaturated, that is, it contains a carbon-carbon double bond. A free radical can catalyze the transformation of the double bond into two single carbon-carbon bonds that link the acrylic monomer unit to its neighboring monomer units. (See Figures 2-2 and 2-3.) According to Table 3-1, the C=C bond with an R of 4.16 cm^3 is replaced by two C-C bonds with an R of 1.25 cm^3 each. Therefore, one would expect the molar refractivity to decrease by 1.66 cm^3 per molecular weight of acrylic acid converted.

Since the molecular weight M of a polymeric material is not a significant factor in the index of refraction, photopolymerization systems change their index of refraction in two ways when exposed to light: first, by changes in molar refractivity due to the conversion of monomer to polymer, and secondly by mass transport that changes the local mass density in the material [23]. The mechanism of molar refractivity change has already been discussed. The modulation of mass density can occur either through internal or external mass transport. Internal mass transport means that material migrates from place to place within the photopolymer, with no net gain or loss of material. Diffusion is an example of internal mass transport. A process of external mass transport involves an exchange of material between

39

the photopolymer and an external medium, such as the atmosphere or a solvent. Photoresist materials which wash away selectively in a solvent provide an example of an external mass transport that is controlled by a prior optical exposure.

To a first order approximation, the index of refraction varies linearly with both the molar refractivity and the mass density. The Lorentz-Lorenz relationship (Equation 3-23) can be implicitly differentiated to yield

$$\left(\frac{\partial n}{\partial R}\right)_\rho = \frac{(n^2 + 2)(n^2 - 1)}{6n\,R} \tag{3-27}$$

and

$$\left(\frac{\partial n}{\partial \rho}\right)_R = \frac{(n^2 + 2)(n^2 - 1)}{6n\,\rho} \tag{3-28}$$

where the subscript on the left-hand side indicates that the subscripted quantity is held constant. For small changes in index Equations 3-27 and 3-28 are usually written in terms of finite changes in index (Δn), refractivity (ΔR), and mass density ($\Delta \rho$):

$$\Delta n = \frac{(n^2 + 2)(n^2 - 1)}{6n} \frac{\Delta R}{R} \tag{3-29}$$

and

$$\Delta n = \frac{(n^2 + 2)(n^2 - 1)}{6n} \frac{\Delta \rho}{\rho} \tag{3-30}$$

In their review article on refractive index modulation in organic materials [23], Tomlinson and Chandross estimate the maximum refractive index modulation that can be achieved with photopolymers and similar photochemical systems. For a common organic solid with an index of 1.5, Equation 3-30 gives $\Delta n = 0.59(\Delta \rho / \rho)$. Density changes ($\Delta \rho / \rho$) that occur in polymerization and other photochemical reactions are rarely, if ever more than 0.3, so $\Delta n \approx 0.2$ is the most that can be expected from density changes. The index of a material can also be modulated by varying its composition. Typical organic solids range from $n \approx 1.4$ to $n \approx 1.7$, so a Δn of 0.3 is the maximum index modulation that could be achieved by varying the composition of the solid. In the limit where organic material is removed and totally replaced by air, Δn could be as large as 0.6 or 0.7. In practice, such large index modulations are never seen, because of the need for a supporting binder or matrix, and because of difficulties (such as the slow pace of diffusion over macroscopic length scales) in transporting different molecular species.

The practical problems associated with reaching these theoretical limits on index modulation can be illustrated by examining the properties of the current DuPont photopolymer compositions. Designed for use in holographic recording [60,61] and optical waveguide fabrication [85], the compositions are designed to take advantage of the inherent index

contrast between aromatic compounds, which contain benzene-type carbon ring structures, and aliphatic compounds which do not. Aromatic compounds generally have a higher index of refraction due to the high polarizability of the aromatic carbon bonds. (See Table 3-1.) A typical photopolymer of this type contains an aliphatic binder polymer, and some mixture of aliphatic and aromatic monomers. The index modulation for a given exposure decreases linearly as the fraction of aliphatic monomer in the mixture increases; the index modulation virtually vanishes when the monomer is all aliphatic, as shown in Figure 3-2.

Fraction of Aliphatic Monomer
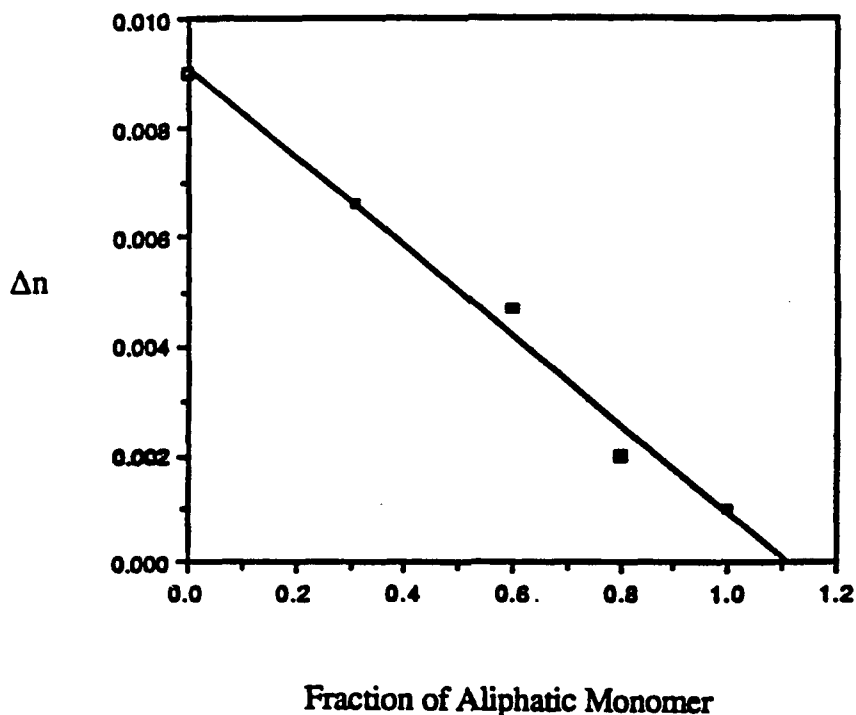
Figure 3-2: Index modulation vs. aliphatic monomer content with aliphatic binder.
(Adapted from Reference 85)

Although the mechanism of image formation is not well established, consider a simple composition containing only an aromatic monomer and an aliphatic binder. It seems likely that as aromatic monomer is consumed by polymerization in illuminated regions, the aromatic monomer flows into the depleted region by a diffusion process. Although the aromatic and aliphatic materials are initially well-mixed, the net result is a pattern of areas where the aromatic material concentration is either enhanced or depleted, with a corresponding increase or decrease of the index. The index modulation is limited first by the choice of workable acrylic binders and monomers; the difference in index between the aromatic and aliphatic acrylates is only of the order of 0.1 or less. Furthermore, the (hypothetical) diffusive mass transport cannot perfectly segregate the aromatic and aliphatic species, so for practical exposures Δn is usually around 0.01, and sometimes as high as 0.04.

C.   Properties of Phase Gratings

The index of refraction modulation that can be induced in photopolymers by an optical exposure makes them useful as media for recording phase holograms. A hologram is a

record, in a material medium, of an interference pattern. If a silver halide film is exposed to the interference pattern of two coherent wavefronts and developed normally, the interference is recorded on the film as a pattern of varying absorption. If, on the other hand, the film is bleached, then the emulsion does not vary appreciably in its absorption. However, the index of refraction varies in a way that maps the intensity undulations of the original interference pattern into undulations of the film's refractive index; this is called a phase hologram, since the index change modulates the phase of incident light, rather than its amplitude. Holographic photopolymer systems generally form phase holograms, not absorption holograms.

The most important property of a hologram is its ability to reconstruct one of the two interfering wavefronts used to record the hologram, when illuminated by the other (or conjugate) recording wavefront. It is not immediately obvious that the record of an interference pattern mapped into absorption or index of refraction should have this property. It is the intent of the current research to determine the mechanism of hologram formation in photopolymers, and wavefront reconstruction is the basis for sensitive experimental techniques for probing the evolution of a holographic grating. (These techniques will be detailed in Chapter V.) It is appropriate at this point to review the fundamental diffraction properties of holographic phase gratings, emphasizing useful results rather than rigorous derivation.

The most important property of a hologram is its ability to reconstruct one of the two interfering wavefronts used to record the hologram, when illuminated by the other (or conjugate) recording wavefront. It is not immediately obvious that the record of an interference pattern mapped into absorption or index of refraction should have this property. It is the intent of the current research to determine the mechanism of hologram formation in photopolymers, and wavefront reconstruction is the basis for sensitive experimental techniques for probing the evolution of a holographic grating. (These techniques will be detailed in Chapter V.) It is appropriate at this point to review the fundamental diffraction properties of holographic phase gratings, emphasizing useful results rather than rigorous derivation.

1.   Thin Phase Gratings

One useful approximation is that of the thin phase grating. The working definition of a thin phase grating is a planar grating, formed by a sinusoidal modulation of the permittivity ε, that exhibits diffraction in the Raman-Nath regime [86]. Raman-Nath diffraction is the diffraction of a single plane wave into a multiplicity of diffraction orders, with the electric field amplitude of the nth order proportional to an nth order Bessel function whose argument is the amplitude of the permittivity modulation. This result by Raman and Nath was the solution of the wave equation in a permittivity grating [87], and it served to explain the experimental results that Debye and Sears had obtained for the diffraction of light from acousto-optic gratings [88]. In this context, "thin" is often taken to mean that the grating thickness is less than or equal to a wavelength of light, although gratings that are many wavelengths thick can also diffract in the Raman-Nath regime.

The Raman-Nath diffraction of a thin grating can be derived simply as the Fraunhofer diffraction pattern of a sinusoidal index of refraction grating [89]. Consider a

42

square, non-absorbing aperture in the plane (x_1, y_1). Let the spatial variation of index across the aperture be given by

$$n = n_0 + n_1 \sin(2\pi f_0 x_1) \qquad (3\text{-}31)$$

where $n_1 < n_0$, and f_0 is the spatial frequency of the grating. Except for a constant phase shift across the aperture due to the mean index n_0 and the grating thickness d, the phase of a normally incident plane wave is spatially modulated according to the expression

$$\psi = \frac{dn_1}{\lambda} \sin(2\pi f_0 x_1) \qquad (3\text{-}32)$$

where λ is the vacuum wavelength of the light. The transmission function of the aperture can be written in terms of the aperture shape and phase modulation as

$$t(x_1, y_1) = \exp\left[j \frac{dn_1}{\lambda} \sin(2\pi f_0 x_1)\right] \text{rect}\left(\frac{x_1}{a}\right) \text{rect}\left(\frac{y_1}{a}\right) \qquad (3\text{-}33)$$

where a is the width of the square aperture. The Fraunhofer diffraction integral to propagate the scalar electric field amplitude U from the (x_1, y_1) plane a distance z to the (x_0, y_0) plane is

$$U(x_0, y_0) = \frac{\Phi}{j\lambda z} \int\limits_{-\infty}^{\infty}\!\!\int U(x_1, y_1) \exp\left[-j \frac{2\pi}{\lambda z}(x_0 x_1 + y_0 y_1)\right] dx_1\, dy_1 \qquad (3\text{-}34)$$

where Φ is multiplicative phase factor. Assuming a unit amplitude plane wave incident on the phase grating at normal incidence, the Fraunhofer integral reduces to a Fourier transform of the phase pattern in the grating. The integral may be simplified in terms of the following Fourier expansion of the Bessel function:

$$\exp\left[j \frac{dn_1}{\lambda} \sin(2\pi f_0 x_1)\right] = \sum_{q=-\infty}^{\infty} J_q\left(\frac{dn_1}{\lambda}\right) \exp[j2\pi q f_0 x_1] \qquad (3\text{-}35)$$

Given the reasonable assumption that the grating is large enough to contain many grating periods ($f_0 >> 2/a$), the various diffraction orders will be well-separated in the observation plane (x_0, y_0). This condition assures that there is negligible interference between the orders in the far field. Therefore, the intensity, which is the square of a sum (Equation 3-35 above) may be approximated as the sum of the squares of each term. The final result for the diffracted intensity in the (x_0, y_0) plane is

$$I(x_0, y_0) = \left(\frac{a^2}{\lambda z}\right)^2 \sum_{q=-\infty}^{\infty} J_q^2\left(\frac{dn_1}{\lambda}\right) \text{sinc}^2\left[\frac{a(x_0 - q f_0 \lambda z)}{\lambda z}\right] \text{sinc}^2\left(\frac{a y_0}{\lambda z}\right) \qquad (3\text{-}36)$$

43

where the sinc functions give the form and size of the diffraction limited spot, due to the finite size of the diffracting aperture.

The diffraction efficiency of each order is defined as the total power in that order divided by the total power incident on the grating. The diffraction efficiency in the qth order η_q can be easily derived from Equation 3-36 with the aid of the following identity [90]

$$1 = \left[J_0(x)\right]^2 + 2\sum_{q=1}^{\infty} \left[J_q(x)\right]^2 \qquad (3-37)$$

Because of the symmetry of the integral order Bessel functions, equal energy is diffracted into the +q and -q orders, and the diffraction efficiency η_q is

$$\eta_q = \left[J_q\!\left(\frac{n_1 d}{\lambda}\right)\right]^2 \qquad (3-38)$$

A plot of thin phase grating diffraction efficiency versus the modulation parameter ($n_1 d/\lambda$) is shown in Figure 3-3 for the zeroth and the ± (1,2) orders. The zeroth diffraction order is the incident beam, so at zero modulation of the phase grating it has 100% of the energy. The efficiency of the first diffracted order peaks at 33.9%, and the higher orders peak at lower values. Qualitatively, one can see that the diffraction pattern of a sinusoidal phase grating is characterized by a large number of diffraction orders, any of which can vanish when the modulation parameter is a root of the corresponding Bessel function.

A plot of a typical thin grating diffraction pattern is shown in Figure 3-4. The plot corresponds to the Fraunhofer diffraction of 500 nm light from a 5 mm square aperture containing a 0.4 mm period sinusoidal phase grating. The phase grating has an amplitude of 4 radians, and the diffraction is viewed at z = 100 m. For purposes of illustration, the assumption ($f_0 \gg 2/a$) is violated here. Because the orders are not widely spaced, the interaction of adjacent orders and their sidelobes result in an asymmetry; the peak intensity of the +n order is not, in general, equal to the peak intensity of the -n order, because the phase of the diffracted wave depends upon whether the order is positive or negative.

A special limiting case of Equation 3-38 is the diffraction from a very weak grating; i.e., ($n_1 d/\lambda$) << 1. This will be of particular interest when discussing the real-time measurement of weak phase gratings in Chapter 4. The function $J_q(x)$ can be expanded as [91]

$$J_q(x) = \frac{x^q}{2^q q!}\left[1 - \frac{x^2}{2^2 \cdot 1!(q+1)} + \frac{x^4}{2^4 2!(q+1)(q+2)} - \cdots\right] \qquad (3-39)$$

For sufficiently small x the first term alone gives a good approximation, and the diffraction efficiency of a weak thin phase grating can be written as

44
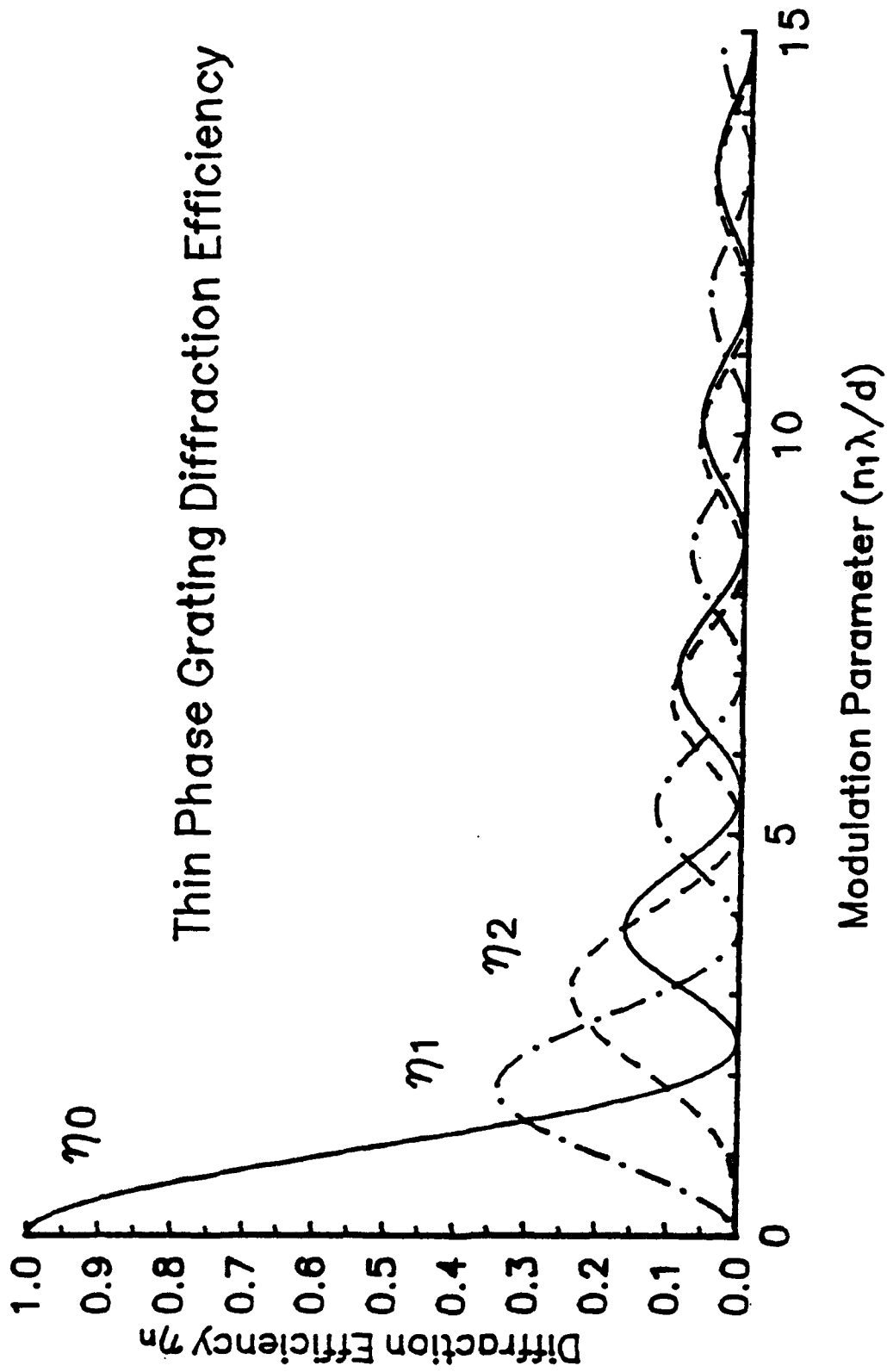
Figure 3-3: Thin sinusoidal phase grating efficiency vs. modulation for orders 0, ±1, ±2.

45
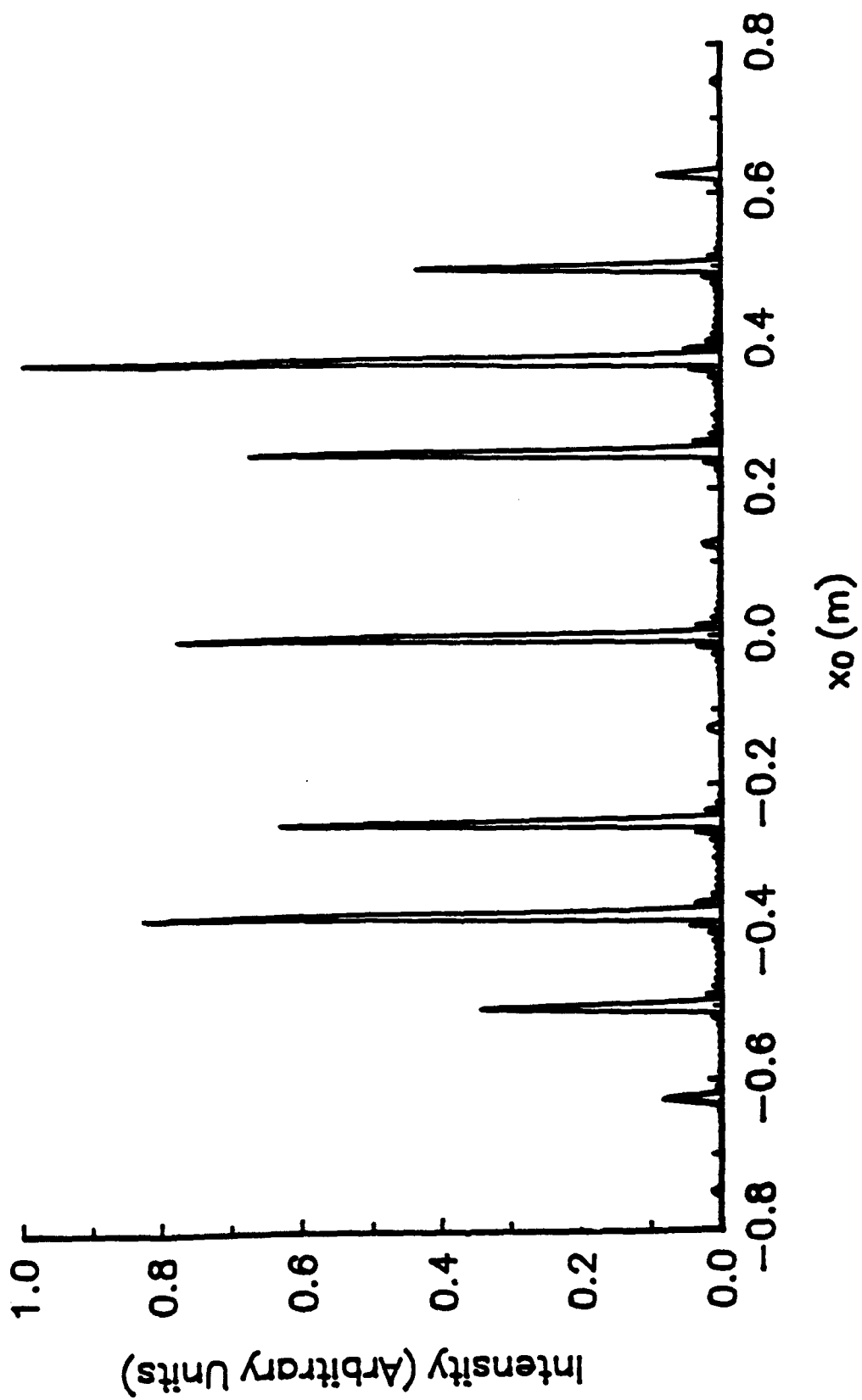
Figure 3-4: Thin sinusoidal phase grating diffraction pattern.

46

$$\eta_q = \frac{x^{2q}}{2^{2q}(q!)^2} \qquad (3\text{-}40)$$

where x is the modulation parameter $(n_1 d/\lambda)$. As with the strong thin grating, there are a multiplicity of orders, but the diffraction efficiency drops sharply with increasing q.

2. Volume Phase Gratings

Phase gratings that are much thicker than the wavelength of the incident light, especially those that are much thicker than the spatial period of the grating, are known as volume phase gratings. The volume gratings can exhibit Bragg regime diffraction. Unlike the Raman-Nath regime, Bragg diffraction is characterized by the diffraction of a plane wave into a single order. Volume phase gratings are normally recorded holographically, and the incident and diffracted orders correspond to the reference and object beams of the holographic recording. Bragg diffraction generally occurs only over a narrow range of incident angles and wavelengths.

Since a thick volume grating produces at most one diffracted order, the theoretical analysis of such a grating can be simplified by assuming that only two plane waves propagate in the grating, and that energy is transferred from one wave to the other during propagation. These two waves also correspond to the object and reference waves used to record the grating in the first place. In a classic, often cited paper, Kogelnik [92] develops this coupled wave theory to predict the properties of all types of volume gratings, amplitude gratings as well as phase gratings. The following exposition of the properties of phase gratings will closely follow Kogelnik's development for the lossless phase grating, except that first it will be useful to look at the hologram recording geometry, following the notation of Solymar and Cooke [93]. (Kogelnik simply assumes a pre-existent sinusoidal grating as his starting point.)

The holographic recording geometry for sinusoidal volume phase grating is shown in Figure 3-5. The recording medium is a uniform slab of thickness d, with the z axis normal to the surface of the medium. Two coherent plane waves are incident in the medium at angles θ_1 and θ_2 relative to the z axis. Note that these are the angles of propagation of the two plane waves in the medium, after refraction at the interface of the medium. Furthermore, the two waves are linearly polarized in the y direction, perpendicular to the plane of incidence. In the absence of attenuation, the field amplitude of the two waves may be written as

$$\mathbf{E}_1 = \mathbf{E}_{01}\, \exp(-j\mathbf{k}_1 \cdot \mathbf{x}) \quad \text{and} \quad \mathbf{E}_2 = \mathbf{E}_{02}\, \exp(-j\mathbf{k}_2 \cdot \mathbf{x}) \qquad (3\text{-}41)$$

where the x,y, and z components of the vector $\mathbf{k}_i$ may be represented as a column vector

$$k_i = \frac{2\pi n_0}{\lambda} \begin{bmatrix} \sin \theta_i \\ 0 \\ \cos \theta_i \end{bmatrix} \equiv \beta \begin{bmatrix} \sin \theta_i \\ 0 \\ \cos \theta_i \end{bmatrix} \qquad (3\text{-}42)$$

As usual, λ is the free-space wavelength of the incident light, and n_0 is the mean refractive index of the medium. Interference between the two waves will produce a total intensity of

$$E_{tot}^2 = E_{01}^2 + E_{02}^2 + 2 E_0 E_1 \cos \left[\beta (k_1 - k_2) \cdot x\right] \qquad (3\text{-}43)$$

Assume that the refractive index n and the absorption α of the recording medium are both modulated by an amount proportional to the local intensity of light,

$$n = n_0 + A E_{tot}^2 \quad \text{and} \quad \alpha = \alpha_0 + B E_{tot}^2 \qquad (3\text{-}44)$$

where A and B are proportionality constants. Then the final index and absorption patterns in the recording medium (n,α) will reflect the initial values of index and absorption (n_0,α_0) plus an overall constant shift due to the average intensity (δn,δa), and a cosinusoidal variation with an amplitude of (n_1,α_1):

and
$$n = n_0 + \delta n + n_1 \cos \left[\beta (k_1 - k_2) \cdot x\right]$$
$$\alpha = \alpha_0 + \delta \alpha + \alpha_1 \cos \left[\beta (k_1 - k_2) \cdot x\right] \qquad (3\text{-}45)$$

The resulting phase and amplitude grating forms a volume structure in the recording medium. The contours of constant grating phase are parallel, uniformly spaced planes in the medium, as shown in Figure 3-5. The geometry becomes more clear with the definition of two auxiliary angles, Ω and Ω', where

$$\Omega = \frac{(\theta_1 + \theta_2)}{2} \quad \text{and} \quad \Omega' = \frac{(\theta_1 - \theta_2)}{2} \qquad (3\text{-}46)$$

Ω is the angle that the grating planes make with the z axis; it is referred to as the slant of the grating. Ω' is the half-angle between the reference and object waves; it defines Λ, the spatial period of the grating.

$$\Lambda = \frac{\pi}{\beta |\sin \Omega'|} = \frac{\lambda}{2n_0 |\sin \Omega'|} \qquad (3\text{-}47)$$

48

The grating vector **K** is defined as the vector perpendicular to the grating planes with magnitude $2\pi/\Lambda$, or in terms of the object and reference wave-vectors as

$$\mathbf{K} = \beta(\mathbf{k}_1 - \mathbf{k}_2) \qquad (3\text{-}48)$$

When both illuminating waves come from the same side of the recording medium, as shown in Figure 3-5a the resulting hologram is a transmission grating; the grating planes tend to be nearly perpendicular to the surface of the medium. When the illuminating waves come from opposite sides of the medium, as in Figure 3-5b, the result is called a reflection grating, with grating planes more nearly parallel to the surface of the recording medium. A reflection grating with grating planes exactly parallel to the surface and a transmission grating with the planes exactly perpendicular to the surface are both called unslanted gratings, and anything else is just called a slanted grating.

The coupled wave analysis of a volume phase grating begins with a pre-existing volume grating, as shown in Figure 3-6. Since optical volume gratings are almost always formed holographically, we will use notation consistent with the hologram recording geometry just discussed. A transmission grating is illustrated, with a "reference" wave R incident in the medium at an angle θ with respect to the z axis. The grating vector **K** makes an angle ϕ with respect to the z axis; in terms of the notation used in Figure 3-5 for the holographic recording geometry,

$$\phi = \Omega + \frac{\pi}{2} \qquad (3\text{-}49)$$

A diffracted "signal" wave S is shown leaving the grating.

In the development of Kogelnik's first order coupled wave theory, it is assumed that only the two coupled waves R and S propagate in the grating, that both are polarized perpendicular to the plane of incidence, and that the waves nearly satisfy the Bragg condition in the grating. As the R wave progresses through the volume grating, it will undergo partial reflections from the grating planes. If the angle and the wavelength of the incident light is such that the partial reflections add in phase to create the S wave, the Bragg condition is said to be satisfied. In practice, the R and S waves correspond exactly to the two recording beams used to produce the hologram, unless the average index of the medium was changed in the developing process ($\delta n \neq 0$). In that case, the Bragg condition can be satisfied by radiation with a wavelength or incidence angle different from that of the recording beams. [94]

With the polarization fixed, the electric field in the medium can be expressed as a scalar

$$E = R(z)\ \exp[-j\mathbf{r}\cdot\mathbf{x}] + S(z)\ \exp[-j\mathbf{s}\cdot\mathbf{x}] \qquad (3\text{-}50)$$
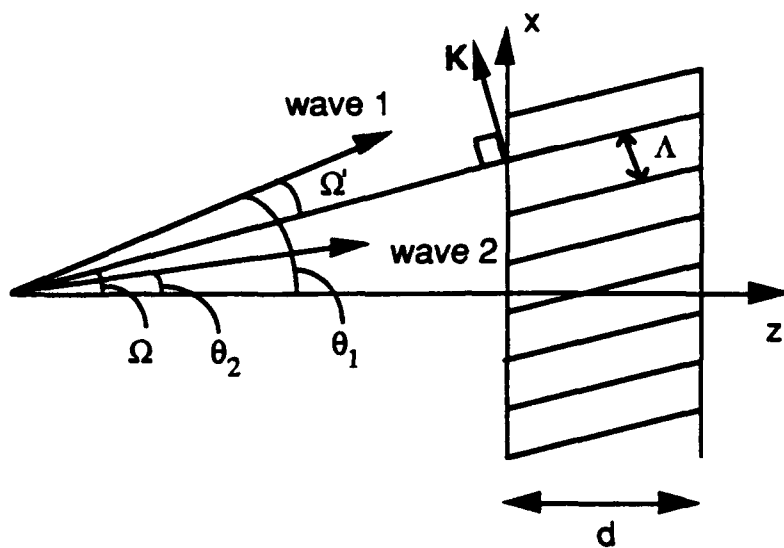
a) Transmission grating recording geometry
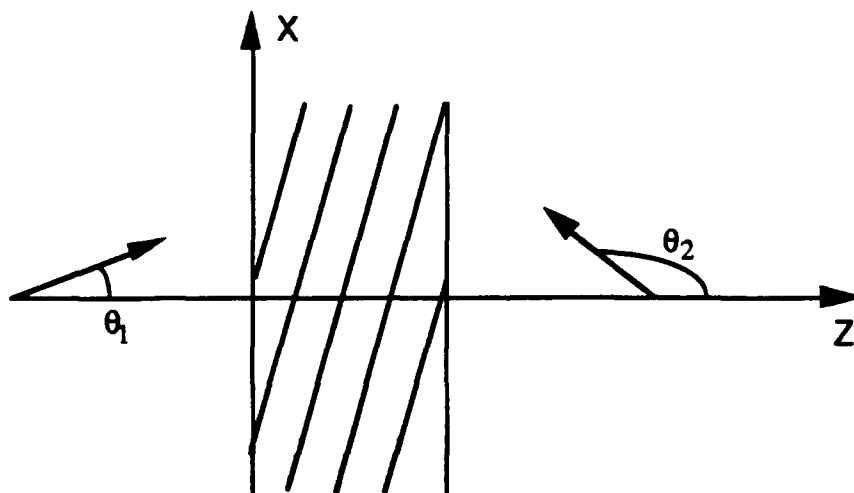
b) Reflection grating recording geometry

Figure 3-5: Transmission and reflection hologram recording geometries.
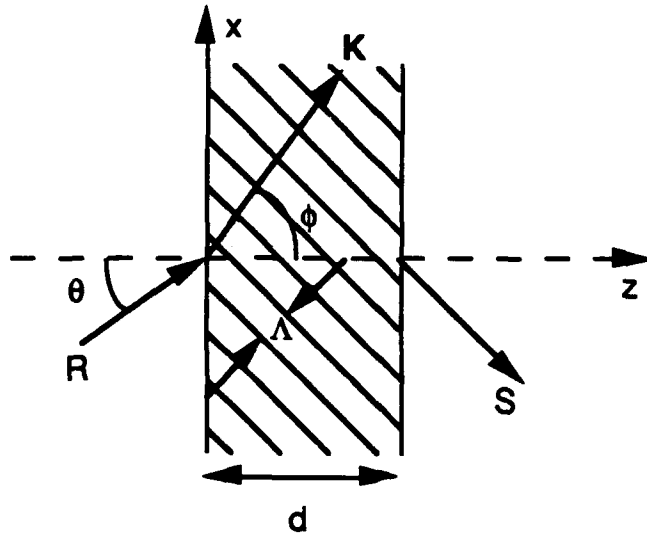
Figure 3-6: Coupled wave geometry in a thick transmission grating.

where **r** and **s** are the wavevectors of the R and S waves, respectively. Note that while the exponentials oscillate on the order of a wavelength of light, R(z) and S(z) are slowly varying envelopes that define the changing complex amplitudes of the beam, as energy is transferred from one to the other. The relationship between the wavevectors is forced by the grating

$$\mathbf{s} = \mathbf{r} - \mathbf{K} \tag{3-51}$$

with

$$\mathbf{r} = \beta \begin{pmatrix} \sin \theta \\ 0 \\ \cos \theta \end{pmatrix} \tag{3-52}$$

and

$$\mathbf{s} = \beta \begin{pmatrix} \sin \theta - \dfrac{K}{\beta} \sin \phi \\ 0 \\ \cos \theta - \dfrac{K}{\beta} \cos \phi \end{pmatrix} \tag{3-53}$$

51

The Bragg condition for a holographic grating is satisfied only by a wave with the same incidence angle and wavelength as one of the two recording beams. The Bragg condition is met exactly when the magnitudes of r and s are equal to β, as shown in Figure 3-7. In terms of the incident angle θ, the exact Bragg condition is

$$\cos(\phi - \theta) = \frac{K}{2\beta} \tag{3-54}$$

Since polarization is assumed to be fixed, wave propagation in the grating is given by the solution of the scalar wave equation

$$\nabla^2 E + k^2 E = 0 \tag{3-55}$$

where E is the total electric field as given in Equation 3-50, and k is the propagation constant of the medium. The propagation constant varies in space due to the presence of the grating. By assuming that the absorption is small and that the index modulation of the grating is much less than the mean index, one can write

$$k^2 = \beta^2 - 2j\alpha\beta + 2\kappa\beta\left(e^{jK\cdot x} + e^{-jK\cdot x}\right) \tag{3-56}$$

where κ is known as the coupling constant. It is defined as

$$\kappa = \frac{\pi n_1}{\lambda} - \frac{j\alpha_1}{2} \tag{3-57}$$

The coupling constant expresses the degree of coupling, or energy transfer between the two waves in the grating. When $\kappa = 0$, there is no diffraction. As one would expect, this only happens when the phase and absorption gratings vanish ($n_1 = \alpha_1 = 0$).

The complete second-order coupled wave equations may be written by combining Equations 3-55 and 3-56 (the wave equation and propagation constant) with Equations 3-50 and 3-51 (the form of the electric field and the wavevector relation). However, as noted before, R(z) and S(z) are slowly varying envelopes reflecting the transfer of energy between the two beams. Kogelnik assumes that the second derivatives of R and S are negligible, and writes the result as two coupled, first-order equations:

$$c_R R' + \alpha R = -j\kappa S \tag{3-58}$$

and

$$c_S S' + (\alpha + j\vartheta)S = -j\kappa R \tag{3-59}$$

52
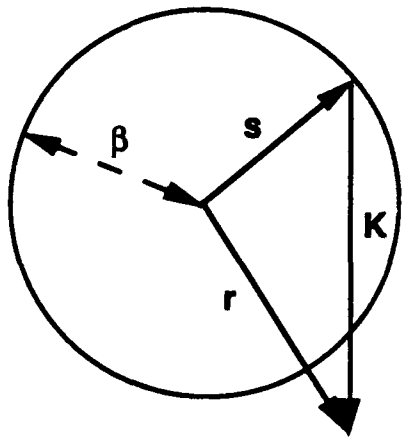
a) Near Bragg incidence
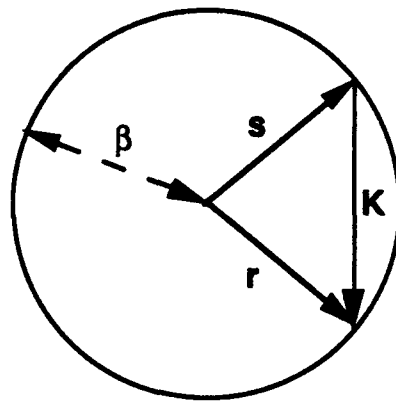
b) Bragg incidence
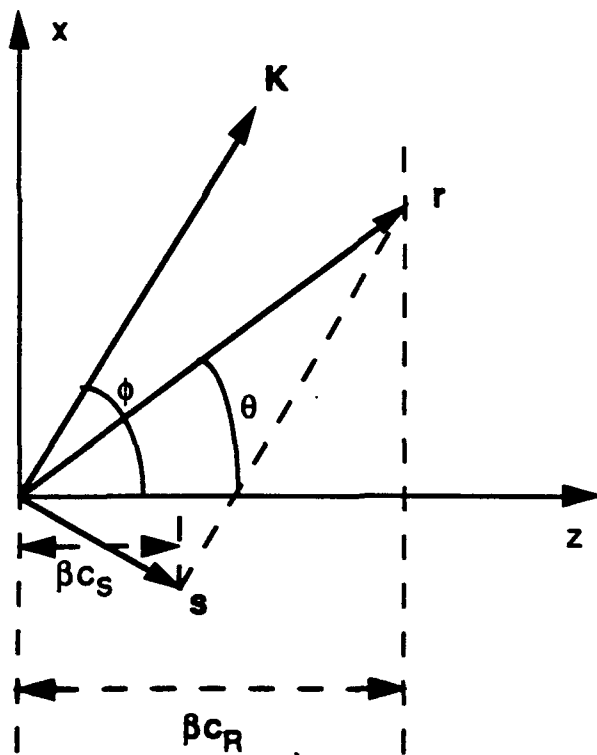
c) Definition of obliquity factors

Figure 3-7: Relationships of the grating vector and the coupled wave vectors.

where c_S and c_R are geometric factors, sometimes called the obliquity factors, illustrated in Figure 3-7.

$$c_R = \cos\theta \tag{3-60}$$

$$c_S = \cos\theta - \frac{K}{\beta}\cos\phi$$

Another important quantity introduced in Equation 3-59 is ϑ, the dephasing factor, which is a measure of how well the Bragg condition is satisfied. It is defined as

$$\vartheta \equiv \frac{\left(\beta^2 - s^2\right)}{2\beta} = K\cos(\phi - \theta) - \frac{K^2\lambda}{4\pi n} \tag{3-61}$$

By applying Equation 3-54, one can see that ϑ is zero if and only if the Bragg condition is satisfied exactly. A non-zero value of the dephasing decreases the interaction between the R and the S waves, effectively decreasing the diffraction efficiency of the grating.

Kogelnik's first-order coupled wave theory makes useful predictions about the diffraction efficiency of various types of volume holograms: reflection and transmission, slanted and unslanted, absorbing and lossless, phase and amplitude, and all the possible combinations thereof. Assuming that the incident illumination wave R is of unit amplitude, the diffraction efficiency of the grating is defined as

$$\eta = \frac{|c_S|}{c_R}SS^* \tag{3-62}$$

where S is the complex amplitude of the diffracted beam, and the obliquity factors account for the possibly different cross sectional areas of the incident and diffracted beams. Photopolymer materials tend to be phase modulating and have low absorption, so they are well characterized by the solutions for lossless phase gratings.

Consider a transmission grating ($c_S > 0$) that is lossless ($\alpha = 0$) and is a pure phase grating ($\alpha_1 = 0$). The diffracted wave appears at $z = d$, and the coupled differential equations 3-58 and 3-59 can be solved with the appropriate boundary conditions

$$R(0) = 1 \ , \ S(0) = 0 \tag{3-63}$$

The result for the general slanted grating of this type is

$$\eta = \frac{\sin^2\sqrt{v^2 + \xi^2}}{\sqrt{1 + \xi^2/v^2}} \tag{3-64}$$

54

where v is a measure of the amplitude of the phase grating, and ξ is proportional to the dephasing.

$$v = \frac{\pi n_1 d}{\lambda \sqrt{c_R c_S}}, \quad \xi = \frac{\vartheta d}{2 c_S} \tag{3-65}$$

For an unslanted phase grating at Bragg incidence, the expression for the diffraction efficiency simplifies to

$$\eta = \sin^2\left(\frac{\pi n_1 d}{\lambda \cos\vartheta}\right) \tag{3-66}$$

Likewise the case of the lossless reflection ($c_S < 0$) phase grating may be solved with the choice of suitable boundary conditions. Since the reflected wave exits the grating at $z = 0$, the boundary conditions are

$$R(0) = 1, \quad S(d) = 0 \tag{3-67}$$

The resulting diffraction efficiency is

$$\eta = \frac{1}{1 + \dfrac{1 - \xi^2/v^2}{\sinh^2(v^2 - \xi^2)}} \tag{3-68}$$

with all variables as defined before, except for v, which is

$$v = \frac{j\pi n_1 d}{\lambda \sqrt{c_R c_S}} \tag{3-69}$$

The extra factor of j is necessary because c_S is negative for a reflection grating. The diffraction efficiency of the unslanted reflection phase grating reduces to

$$\eta = \tanh^2\left(\frac{\pi n_1 d}{\lambda \cos\vartheta}\right) \tag{3-70}$$

The relative diffraction efficiencies of lossless, unslanted reflection and transmission phase gratings at Bragg incidence are shown in Figure 3-8 for various values of

55
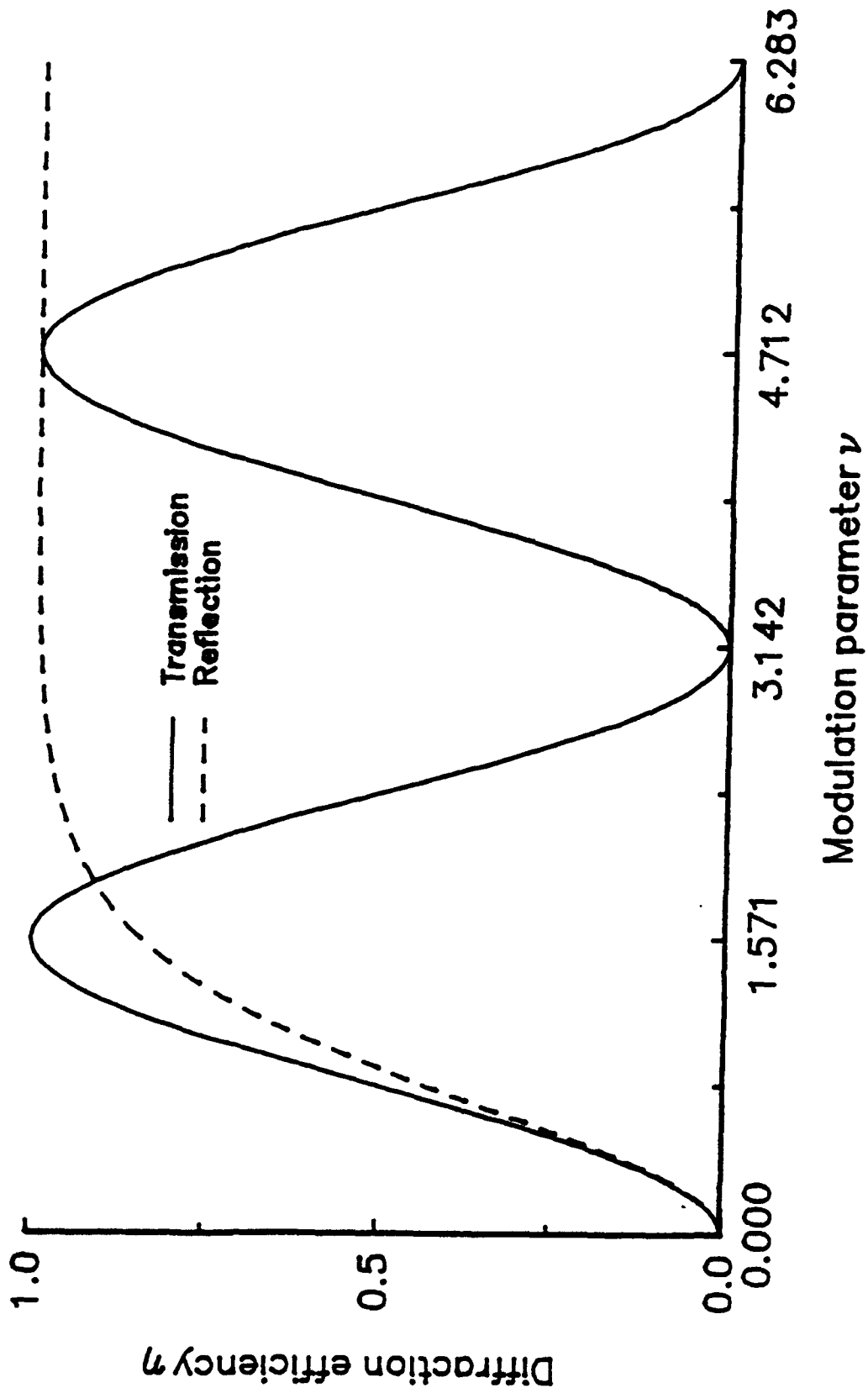
Figure 3-8: Diffraction efficiency of unslanted lossless phase gratings vs. modulation.

the modulation parameter ν. For a holographic grating, the modulation parameter depends upon the total holographic exposure, and thus Figure 3-8 can also be taken as a plot of how the efficiencies of the two types of gratings vary with increasing exposure. The unslanted reflection phase grating is essentially a stack of dielectric mirrors, so it is not surprising that reflectivity approaches 100% asymptotically as the modulation increases. The transmission grating, on the other hand, oscillates between 0% and 100% diffraction efficiency as the modulation increases. The decrease of diffraction efficiency due to over-exposure is called overmodulation. The explanation for this lies in the coupled wave equations (3-58 and 3-59). As an R wave propagates into a thick grating, it transfers energy into the S wave until all the energy is in the S wave (100% efficiency). At Bragg incidence, the coupled equations are totally symmetric, so further propagation by the S wave into the grating transfers energy back to the R wave, reducing the diffraction efficiency. Figure 3-9 shows intuitively how two volume transmission gratings of 100% efficiency combine to form a single grating of 0% efficiency. As a practical matter, overmodulation makes it difficult to record a holographic transmission grating of the highest efficiency, since any deviation from $v = \pi/2$ reduces the efficiency. On the other hand, a generous over-exposure of a reflection grating ensures nearly the highest possible efficiency.
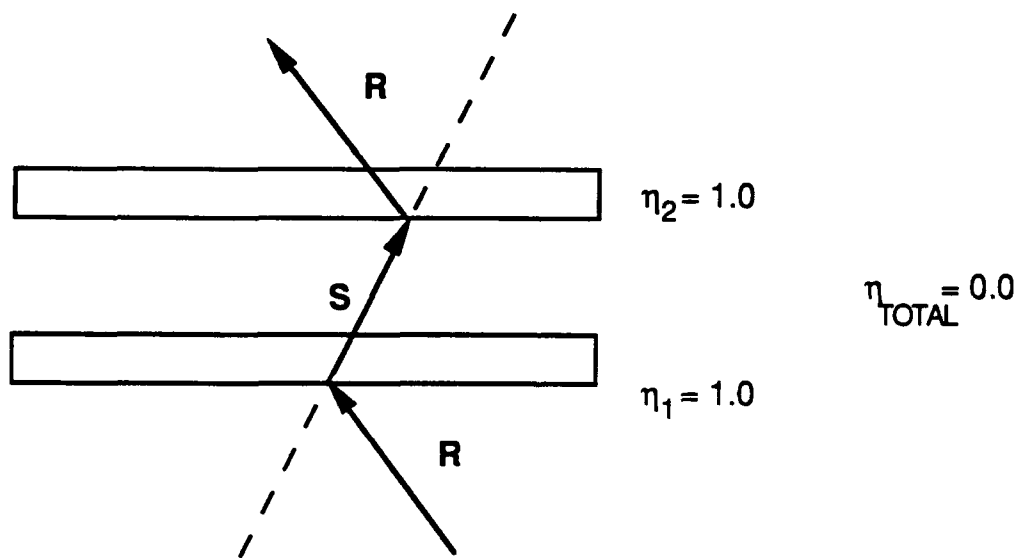
Figure 3-9: Overmodulation illustrated by two high efficiency gratings.

The expressions for the diffraction efficiency can also be viewed as functions of the dephasing to show how efficiency varies as one departs from the exact Bragg condition. Since dephasing can be brought about either by a change in the incidence angle or the wavelength of the illumination, the angular sensitivity of a grating is inseparable from its wavelength sensitivity. For thick volume gratings in general, the diffraction efficiency will be reduced by 50% when either the angular deviation from the Bragg condition $\Delta\theta$ or the

wavelength deviation $\Delta\lambda/\lambda$ are on the order of Λ/d. The dephasing behavior of a typical transmission grating is shown in Figure 3-10.

The properties of extremely weak volume phase gratings will be of interest in the experimental study of holographic image formation in photopolymers. In the limit of low modulation ($v \ll 1$) the diffraction efficiency of unslanted lossless volume gratings assumes the same form for both reflection (Eq. 3-70) and transmission (Eq. 3-66),

$$\eta = v^2 = \left(\frac{\pi n_1 d}{\lambda \cos\theta}\right)^2 \tag{3-71}$$

since for small arguments $\sin(x) \approx \tanh(x) \approx x$.

3. "Thin", "Thick", and other Gratings

This exposition of the properties of phase gratings has so far been deliberately vague on what constitutes a "thick" versus a "thin" grating, partly because one can find many conflicting criteria in the literature. Moharam and Gaylord [95] suggest that the various criteria can be reduced to two different views on what constitutes "thick" and "thin" grating behavior. The first case is that a grating is considered to be "thick" when it has a narrow angular and wavelength sensitivity, and "thin" when it exhibits diffraction for a wide range of incident angles and wavelengths. As we saw in the last section, the dephasing sensitivity of Bragg regime volume grating is of the order of Λ/d. Consistent with this, Moharam and Gaylords' suggestion for this criterion is

$$\text{Thick: } d/\Lambda > 10$$
$$\text{Thin: } d/\Lambda < 10 \tag{3-72}$$

This criterion has the advantage that it depends on the actual thickness d of the grating.

On the other hand, a "thin" grating can be defined as one that exhibits Raman-Nath diffraction with multiple orders whose intensities are given by Eq. 3-38, and a "thick" hologram is normally defined as one that shows Bragg diffraction, with only one significant diffracted order whose strength is given by Eq. 3-64. If the theoretical predictions are to be in error by no more than 1%, the criteria become

$$\text{Thick (Bragg): } \quad \frac{\lambda^2}{\pi n n_1 \Lambda^2} \geq 10$$
$$\tag{3-73}$$
$$\text{Thin (Raman–Nath): } \quad \frac{2n_1}{n}\left(\frac{\pi d}{\Lambda \cos\theta}\right)^2 \leq 1$$

Note that the condition for Bragg diffraction does not depend on the actual thickness of the grating at all.

58
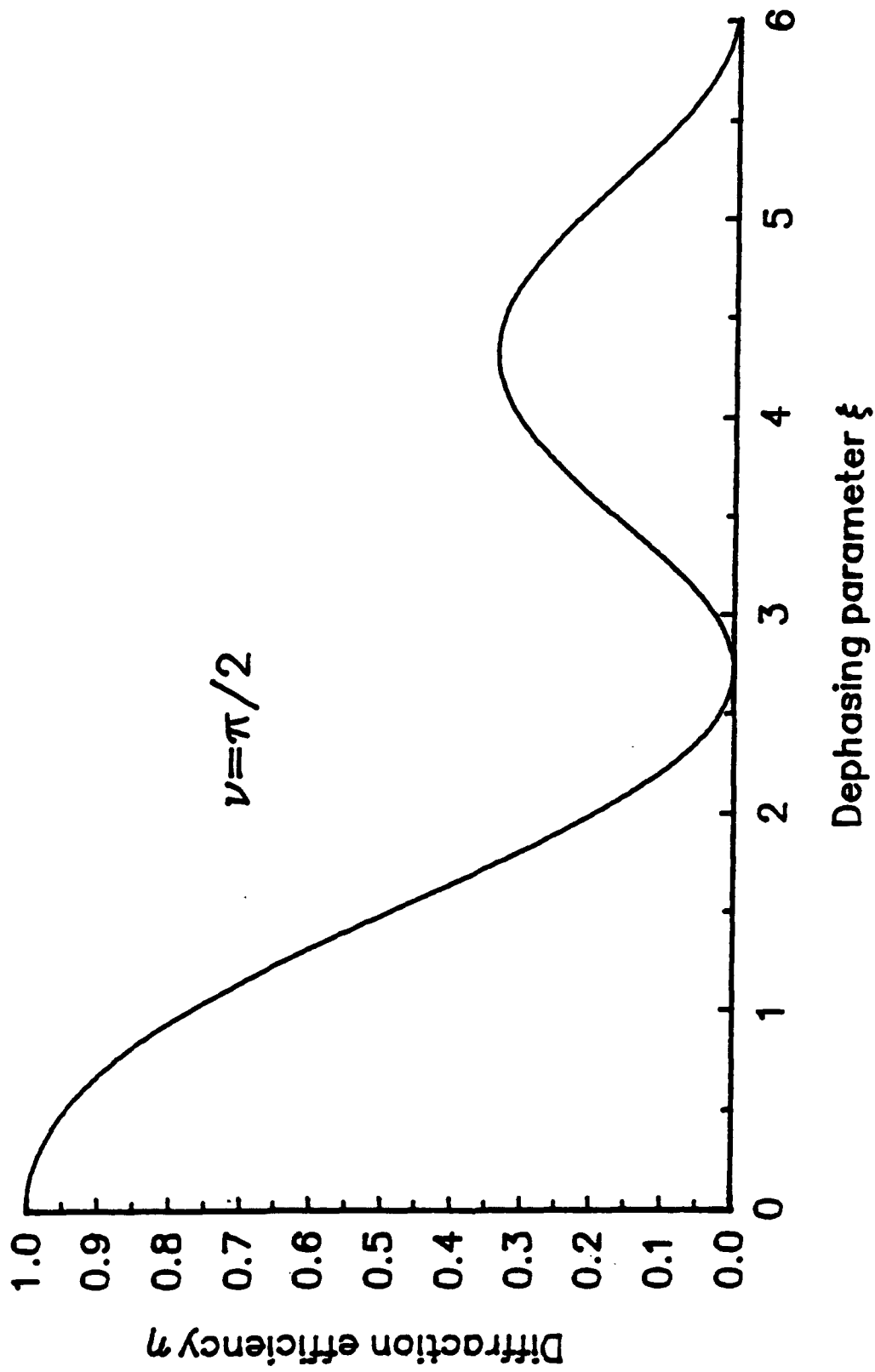
Figure 3-10: Diffraction efficiency of transmission phase grating ($\nu = \pi/2$) vs. dephasing.

The diffraction behavior of gratings that are neither thick nor thin is generally calculated by numerical methods based on rigorous wave theory. The details of these methods are outside the scope of the current research; the reader is referred to some overviews of the subject [95,96]. One approach that has proved useful in the analysis of photopolymer phase gratings has been developed by Stone [97] that is called thin grating decomposition. An arbitrary grating is decomposed into thin slices, each thin enough so that Raman-Nath diffraction is valid. The amplitudes of each diffraction order are represented by a column vector, and the transfer function of each thin grating layer is represented by a matrix, so the propagation of all the orders through the volume grating layers reduces to a matrix multiplication.

One specific result of numerical grating analysis is particularly relevant to photopolymer phase gratings; that is, the high diffraction efficiencies that can arise from a surface-relief grating [98]. Moharam and Gaylord have calculated that for sinusoidal surface relief gratings on glass (n =1.58) with $\lambda = \Lambda$ and $\theta = \pi/6$, the diffraction efficiency in transmission can exceed 99%, if the surface relief is about 2λ. This is a surprising result, since surface relief gratings are often approximated as thin gratings conforming to the Raman-Nath regime. Therefore, high diffraction efficiency alone is not proof of Bragg regime diffraction.

60

IV. DIFFUSION IN PHOTOPOLYMER HOLOGRAM FORMATION

The phenomenon of diffusion is often mentioned in the photopolymer literature as a contributing factor to the formation of photopolymer holograms. Simply put, diffusion is the motion of one material substance through another by means of the random motions of individual molecules. The macroscopic effects of diffusion can be described by differential equations similar to those for heat flow in solids [99] and a great deal of research has been done to characterize the nature of diffusion in polymers [100]. However, the prior literature in holographic photopolymers generally discusses the role of diffusion only qualitatively, without a rigorous or analytical model that might be used for prediction or control of hologram formation.

A goal of the current research is to establish a mathematical model that will show how free monomers diffuse in the volume of a photopolymer material during holographic exposure, and also show how this diffusion plays a major role in the formation of a volume phase grating. The model will be applicable to the various types of photopolymer compositions summarized in Chapter II, and the model is tested experimentally in this research against the behavior of Polaroid's DMP-128 photopolymer. The following chapters will be devoted to the techniques and results of these experiments.

In this chapter, the basics of the diffusion equation and its solution will be presented, followed by a review of the prior experimental evidence for diffusion in holographic photopolymers. The chapter will conclude with a model of holographic photopolymer diffusion based on a modification of the standard diffusion equation, and a discussion of exact and approximate solutions of the modified diffusion equation.

A. Physical Basis of Diffusion and the Diffusion Equation

Diffusion is the process by which the random motions of molecules give rise to macroscopic mass transport. Fortunately, it is possible to describe this discrete, molecular process in terms of continuous quantities such as concentrations, fluxes, and diffusion coefficients. An idealized one-dimensional diffusion process shows how random molecular jumps can be made to correspond to macroscopic quantities [101]. Consider an infinite line with evenly spaced sites where molecules may reside; each site is a distance "a" from its neighbors. Molecules may stay at a site, or jump one step to the left or right. Each site is represented by an integer "i" and N_i is the number of molecules at the ith site. Assume that each molecule can jump to an adjacent site Γ times per second. Jumps to the left and to the right are equally likely, so on average $\Gamma N_i/2$ molecules jump from site i to site i+1 per second. Likewise, the average number of molecules that jump from site i+1 to site i per second is $\Gamma N_{i+1}/2$. If one defines the net flux of particles in the positive direction from site i as J_{i+}, then

$$J_{i+} = \frac{1}{2}\Gamma(N_i - N_{i+1}) \qquad (4\text{-}1)$$

Similarly, the net flux from i-1 to i is

$$J_{i-} = \frac{1}{2}\Gamma(N_{i-1} - N_i) \qquad (4\text{-}2)$$

The time rate of change of the number of molecules at site i can be found by subtracting the number of particles leaving per second from the number of particles entering the site per second. Thus the change in molecular concentration can be expressed in terms of the fluxes

$$\frac{dN_i}{dt} = -(J_{i+} - J_{i-}) \qquad (4\text{-}3)$$

or, by using Equations 4-1 and 4-2, in terms of the distribution of molecules around site i

$$\frac{dN_i}{dt} = \frac{1}{2}\Gamma(N_{i+1} - 2N_i + N_{i-1}) \qquad (4\text{-}4)$$

Note that Equation 4-4 resembles the discrete approximation formula for the second derivative of a continuous function. Let us define a continuous, differentiable function $N(x,t)$ that is equal to N_i whenever x is the co-ordinate of the ith site:

$$N(x_i,t) = N(ai,t)) \approx N_i \qquad (4\text{-}5)$$

The difference approximation for the second derivative of $N(x,t)$ is written as

$$\left(\frac{\partial^2 N(x,t)}{\partial x^2}\right)_{x=x_i} = \frac{(N_{i+1} - 2N_i + N_{i-1})}{a^2} + O(a^2) \qquad (4\text{-}6)$$

where $O(a^2)$ indicates that the error of the discrete approximation is on the order of a^2. If a is sufficiently small, for example the few angstroms of a typical molecular jump, this error becomes insignificant in physical problems.

A continuous function for the molecular flux can also be defined by noting that Equations 4-1 and 4-2 have the form of discrete approximations to the first derivative of N. The continuous flux $J(x,t)$ can then be written as

$$J(x,t) = -\frac{1}{2}\Gamma a \frac{\partial N(x,t)}{\partial x} \qquad (4\text{-}7)$$

The negative sign indicates that material diffuses from areas of high concentration to areas of low concentration.

With two further definitions, the process of diffusion can be expressed entirely in terms of macroscopic differential equations. First define a diffusion coefficient

$$D = \frac{1}{2}\Gamma a^2 \qquad (4\text{-}8)$$

and a concentration function u(x,t) in terms of molecules per unit length

$$u(x,t) = \frac{N(x,t)}{a} \qquad (4\text{-}9)$$

With the previous definitions and development, Equation 4-3 can be transformed into the continuity equation, which is an expression of the conservation of mass.

$$\frac{\partial u(x,t)}{\partial t} = - \frac{\partial J(x,t)}{\partial x} \qquad (4\text{-}10)$$

The relationship between flux and the concentration gradient in Equation 4-7 becomes

$$J(x,t) = - D \frac{\partial u(x,t)}{\partial x} \qquad (4\text{-}11)$$

which, for historical reasons, is known as Fick's first law [101]. Finally, the diffusion equation itself may be written by combining Equations 4-4, 4-6, and 4-8, or directly from the macroscopic Equations 4-10 and 4-11.

$$\frac{\partial u(x,t)}{\partial t} - D \frac{\partial^2 u(x,t)}{\partial x^2} = 0 \qquad (4\text{-}12)$$

This form of the diffusion equation is sometimes known as Fick's second law.

The diffusion equation derived here has widespread applicability, but it is not a fundamental law of physics. The continuity equation (4-10) is fundamental in that it expresses the law of conservation of mass; the change of mass in a unit cell must be accounted for by the flow of mass across the boundaries of the cell. On the other hand, Fick's first law, (Eq. 4-11) is a constitutive relation, that depends on material properties and the exact nature of the diffusion process. Even when Equation 4-12 is only a good approximation of diffusion behavior, it is often used because it is relatively easy to solve. In fact, this form of the diffusion equation is exactly the same as the classical heat conduction equation developed by Fourier [102] in 1822. Numerous exact solutions of the diffusion/heat conduction equation are tabulated for various geometries, boundary conditions, and initial conditions [103], and specialized algorithms have been optimized for the numerical solution of this equation [104].

In general, the diffusion coefficient may be a function of space, time, and/or concentration. The continuity equation and Fick's first law keep the same form, but the diffusion equation becomes

$$\frac{\partial u(x,t)}{\partial t} - \frac{\partial}{\partial x}\left(D(x,t,u) \frac{\partial u(x,t)}{\partial x} \right) = 0 \qquad (4\text{-}13)$$

The diffusion equation can be further generalized from a one-dimensional to a three-dimensional equation [105]. The continuity equation takes the form

$$\frac{\partial u(x,t)}{\partial t} = -\nabla \cdot J(x,t) \qquad (4\text{-}14)$$

where the spatial co-ordinate x and the flux J are both vectors, and ∇ is the gradient operator. Of course, the concentration u is still a scalar quantity. Fick's first law takes the form

$$J(x,t) = -D(x,t,u) \, \nabla u(x,t) \qquad (4\text{-}15)$$

and the diffusion equation becomes

$$\frac{\partial u(x,t)}{\partial t} = -\nabla \cdot [D(x,t,u) \, \nabla u(x,t)] \qquad (4\text{-}16)$$

Fortunately, common diffusion problems such as diffusion through a thin membrane, spherically isotropic diffusion from a point source, and cylindrically symmetric diffusion from a line source can all be effectively reduced to one-dimensional problems, due to symmetry. Furthermore, the solutions of the diffusion equation for idealized point, line, and plane sources (Dirac delta functions) that have infinite density at t = 0 are Green's functions of the diffusion equation. Therefore, the solution for an arbitrary initial distribution of material can be expressed as a spatial integral of the Green's function, since the initial distribution can be expressed as a spatial integral over Dirac delta functions.

The solution for diffusion from an infinitely dense point source gives some insight into the nature of diffusion. Consider a one-dimensional case, with an initial concentration of a diffusing material embedded in a non-diffusing matrix with a constant diffusion coefficient D. The initial condition on the concentration of the diffusing material is $u(x,0) = S\delta(x)$, that is, an initially infinite concentration at x = 0, and none elsewhere. The total amount of diffusing material S is equal to the integral of the concentration profile over all space

$$S = \int_{-\infty}^{\infty} u(x,t) \, dx = \int_{-\infty}^{\infty} S \, \delta(x) \, dx \qquad (4\text{-}17)$$

With these conditions, the solution for the one-dimensional diffusion equation is [106]

$$u(x,t) = \frac{S}{2\sqrt{\pi D t}} \exp\left(\frac{-x^2}{4Dt}\right) \qquad (4\text{-}18)$$

The concentration profile of the diffusing material is a Gaussian with a time-dependent amplitude. The solution satisfies the normalization condition 4-17, which is equivalent to the conservation of mass. Since the diffusion constant D has units of (cm²/sec), the square root of Dt defines a time-dependent length scale for the diffusion process. As material diffuses outward from the origin, the width of the Gaussian profile varies as $(Dt)^{1/2}$. Of course, the Gaussian function is infinite in extent; its width can be suitably defined in terms of the width at half-maximum, or the 1/e points. Figure 4-1 illustrates this solution for various values of Dt.

The solution of spherically symmetric three dimensional diffusion from an infinite point source is similar to the one dimensional case. Only the radial co-ordinate $r^2 = (x^2 + y^2 + z^2)$ is significant. The initial condition is infinite concentration at the origin of co-ordinates, and zero elsewhere, or $u(r,0) = S\delta(r)$. The normalization is given by

$$S = \int_0^\infty u(r,t)\,4\pi r^2\,dr = \int_0^\infty S\delta(r)\,4\pi r^2\,dr \qquad (4\text{-}19)$$

and the solution is

$$u(x,t) = \frac{S}{(4\pi Dt)^{3/2}} \exp\left(\frac{-r^2}{4Dt}\right) \qquad (4\text{-}20)$$

Once again $(Dt)^{1/2}$ defines the length scale of the diffusion. After a time t, the diffusing material forms a Gaussian "fuzzball" with a characteristic radius on the order of $(Dt)^{1/2}$. The amplitude factor in front of the exponential factor varies as $(Dt)^{-3/2}$, because the material fills a volume proportional to the cube of the characteristic radius.

In general, solutions to the diffusion equation are unique. Once one has found a solution to the diffusion equation for a particular geometry, initial conditions, and boundary conditions, one can be assured that there is no other solution [107]. The equation is linear, and the solutions satisfy the superposition principle. Solutions to the diffusion equation, in the limit of large times, tend to be insensitive to the exact form of the initial distribution of material. In other words, diffusion has a smoothing property, as shown in Figure 4-2. Since the time rate of change of the concentration varies with the second spatial derivative, bumps will be flattened, hollows will be filled in, and edges will erode. Equivalently, if the initial distribution can be expressed as a Fourier series, the high frequency components decay very rapidly, until the lowest order Fourier term predominates [102].
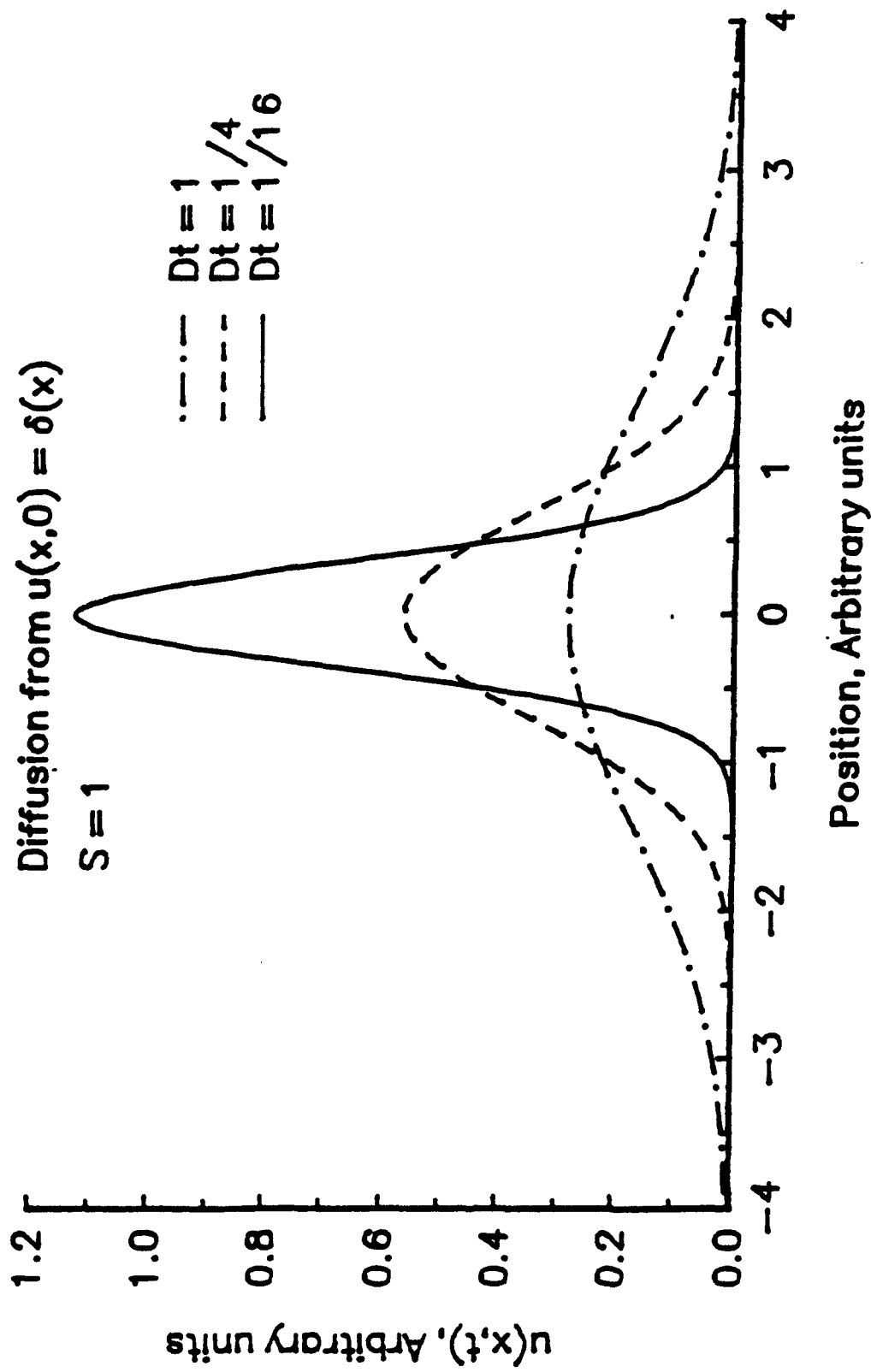
Figure 4-1: One dimensional diffusion from a delta function source, for various values of time.

66
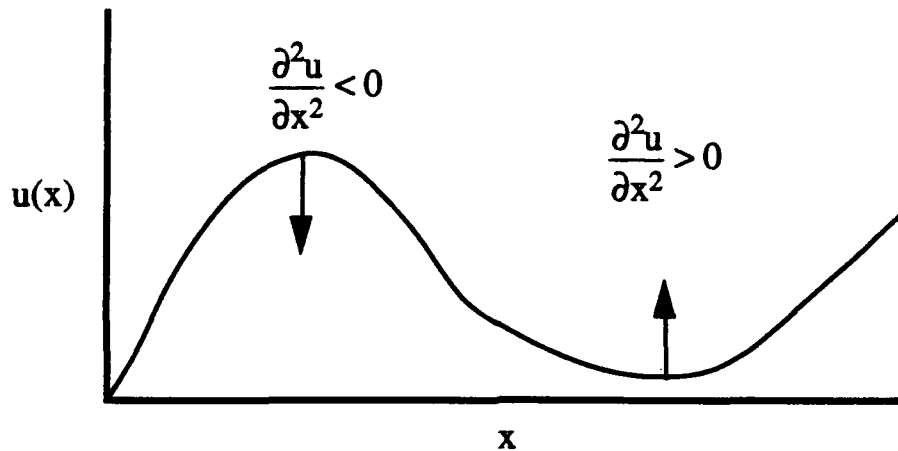
Figure 4-2: The smoothing property of the diffusion equation. $u_t = Du_{xx}$.

From the simplistic discrete model of diffusion derived earlier, one might over-estimate the magnitude of typical diffusion coefficients. Using Equation 4-8, we might estimate the particle jump distance $a=2\text{\AA}$, and use the Debye frequency from solid-state physics [108] as an estimate of the jump frequency Γ. The characteristic Debye frequency of solids is on the order of 10^{14} Hz, so the estimate for D would be on the order of 10^{-2} cm^2/sec.

However, this estimate for diffusion in solids at room temperature is too large by many orders of magnitude. Diffusion coefficients of one metal in another can be of the order 10^{-31} cm^2/sec or less. Gases in water and other organic solvents diffuse more rapidly, with D around 10^{-4} or 10^{-5} cm^2/sec, and vapors in air diffuse with D near 0.1 cm^2/sec. The simplistic estimate of diffusion coefficients is much too large because a molecule in a solid does not jump to a new location with every cycle of vibration. To make a diffusive jump, a molecule must "push" other particles aside, or surmount some type of potential barrier. Diffusion can be characterized in terms of an activation energy, and the diffusivity is related to how likely it is that a molecule will have the necessary thermal energy to surmount the activation barrier. Therefore, diffusivity can be expressed in terms of the Arrhenius relation [105]

$$D = D_0 \exp\left(-\frac{E_D}{RT}\right) \qquad (4\text{-}21)$$

where E_D is the activation energy per mole, R is the gas constant, and T is the temperature. As one would expect, diffusivity increases with temperature. The pre-exponential factor D_0 is often called the frequency factor. It is usually determined empirically, but in some theoretical models of diffusion it is approximated as $D_0 = \Gamma a^2/6$, which is derived by extending the one dimensional jump model to three dimensions.

A possible problem with the diffusion equation is that its solutions are sometimes non-physical. Consider Equations 4-18 and 4-20, which represent the diffusion of an infinite

point source at the origin from t = 0 onward. Even after an infinitesimal time, the concentration is non-zero over all space, implying that diffusing matter propagates with infinite velocity. The classical Fourier theory of heat conduction makes the same prediction for heat propagation. A recent review of theories on heat conduction [110] indicates that in order to obtain more realistic solutions, it is necessary to consider in detail the collisions between molecules that mediate the transfer of heat. Likewise, diffusive processes are controlled by the mean free path of the diffusing particles, and their characteristic time between collisions, τ. One way to incorporate this behavior into the diffusion equation is by modifying Fick's first law:

$$ \mathbf{J} + \tau \frac{\partial \mathbf{J}}{\partial t} = -D \nabla u \tag{4-22} $$

The resulting transport law is a wave equation characterized by a finite propagation speed c, which is on the order of the speed of sound in the material. It is known as Cattaneo's equation

$$ \frac{\partial^2 u}{\partial t^2} + \frac{1}{\tau} \frac{\partial u}{\partial t} = \frac{D}{\tau} \nabla^2 u \tag{4-23} $$

where $c = (D/\tau)^{1/2}$. Although the time scale τ is not well characterized, it is thought to be extremely small, perhaps on the order of the inverse of the Debye frequency, 10^{-14} sec. At ordinary time scales, Equation 4-23 reduces to the diffusion equation. Also, the speed c is of the order of the velocity of sound in the medium, which can be effectively infinite for diffusion over a short distance.

B.   Diffusion in Polymers

The literature of diffusion in polymers is primarily concerned with the diffusion of gases and vapors. This type of diffusion is of great practical interest, as in determining how long a tire will stay inflated. Also, the standard experimental technique for measuring diffusion in polymers only works with gases and vapors. In the sorption-desorption method, a thin film of polymer is suspended in a delicate analytical balance and exposed to vapors to determine the mass uptake with time, and then exposed to vapor-free gas as the weight loss of desorption is measured. If the film thickness is known, diffusion coefficients can be calculated [111].

In this research, the chief concern is with the diffusion of unreacted monomers through a photopolymer medium. However, the literature on the bulk diffusion of different polymer and monomer components is slim. This is due to experimental difficulty. In the standard technique, at least one of the components must be isotopically tagged, and traced by natural or induced radioactivity [111,112]. Nonetheless, a brief background on vapor and gas diffusion in polymers is relevant.

The diffusion of simple gases such as hydrogen and oxygen through polymers is straightforward [113]. The diffusion coefficient is usually independent of concentration and constant except for the temperature dependence predicted by the Arrhenius relationship. The activation energy of the diffusion E_d is generally between 5 and 15 kcal/mole and D_0 is generally on the order of 1 cm^2/sec.

Sometimes a small deviation from Arrhenius behavior for simple gases is observed at the glass transition temperature of the polymer, Tg. Recall from Chapter III that below the glass transition a polymer is hard and glassy. Above T_g a polymer is soft and rubbery, due to increased mobility of the polymer chain segments. At a given temperature, a glassy polymer can be made rubbery by the addition of a small amount of a plasticizer compound. Generally, the plasticizer is a liquid that is capable of dissolving the monomer of which the polymer is composed, and/or soaking into and swelling the polymer. For example, water is a plasticizer for poly(acrylic acid) and related compounds, as well as for the organic polymers that make up living organisms. The addition of a plasticizer almost always increases diffusivity of simple gases within the polymer.

The diffusion of water and organic solvents within polymers presents a more complex case, since these compounds themselves may plasticize the polymer as they diffuse through it. Above the glass transition temperature, the diffusion of solvents within the polymer is said to be Fickian. Fickian means that the diffusion coefficient, though not constant, can be characterized accurately in terms of the concentration of the diffusing material. Often, the diffusion coefficient D(u) increases exponentially with the concentration u This behavior is most marked in materials that plasticize, swell, or dissolve the polymer, and thus show a strong molecular affinity for the monomer sub-units. It is thought that, at low concentrations, most of the diffusing solvent molecules become immobilized by attaching themselves to the polymer, and do not take part in the diffusion. At high concentrations, these bonding sites are filled, and a larger fraction of the penetrant is able to diffuse through the polymer [105].

Below the glass transition temperature, the diffusion of compatible solvents in polymers is very complex and is said to be non-Fickian. The diffusion coefficient is a function of the past history of the polymer/solvent system, without any clear dependence on concentration [115]. The diffusing solvent moves through the glassy polymer with a sharply defined boundary of penetration. The swelling induced by the penetrating solvent sets up strains in the rigid, glassy material and can actually cause the polymer to fracture [116]. The cracks and voids formed by the fracturing affect the diffusivity within the polymer, as well as its other physical properties.

The literature on water diffusivity in polymers bears directly on the current research with the Polaroid DMP-128 photopolymer. DMP-128 is activated for exposure by removing it from its storage in dessicated air and allowing it to absorb moisture from air with a controlled humidity of near 50% [117]. Experience with the film indicates that it is hard and glassy when dry, and quite soft and tacky after humidification. Since lithium acrylate, the chief monomer component in the photopolymer is very soluble in water, it is not surprising that the medium is plasticized by the absorption of water.

The amount of water absorbed in DMP-128 is quite large for such thin films; the manufacturer's recommendation is that the amount of water absorbed should amount to about

7 milligrams for a 7 micron film on a 2"x2" plate. This is 40% of the weight of the dry photopolymer film. Sorption-desorption measurements performed on sodium acrylate show that it also will absorb 40% of its own dry weight from air at 50% relative humidity, with much more sorption at higher humidity levels [118,119]. Similar measurements on lithium acrylate were not available, but the sodium acrylate sorption-desorption data suggest that the diffusion of water into and out of acrylic acid and the acrylate salts is non-Fickian, with an approximate diffusion coefficient of 5×10^{-10} cm^2/sec.

C. Diffusion in photopolymers

The diffusion of monomers during and after exposure is thought to be an essential mechanism for grating formation in most holographic photopolymer systems. However, even those researchers who accept the existence of diffusion in grating formation differ on its importance, and differ even more in interpreting their experimental data in terms of the diffusion hypothesis. In reviewing the literature on this subject, one will see that even the best explanations of photopolymer hologram formation are of a qualitative nature. Some of the ambiguities in the field might be better addressed by a quantitative model that attempts to predict refractive index modulation in terms of diffusion and the kinetics of vinyl polymerization.

Most models of diffusion in photopolymers consider primarily the diffusion free monomer within a polymer matrix [23]. The diffusion of other components in the photopolymer system is not considered to be significant for several reasons. The first reason is that photopolymer compositions are designed such that the amount of monomer far exceeds the amount of any other mobile component in the mixture. As noted in Chapter II, holographic photopolymers generally consist of an immobile matrix of a binder polymer, which holds monomer, dyes, and radical-forming initiators. Dye concentrations must be kept low enough for light to penetrate the volume of the holographic material, and since a single activated initiator radical can catalyze the reaction of thousands or millions of monomer units, little is needed. The second reason is that diffusion only occurs when there are concentration gradients. In a well mixed-photopolymer system all components initially have a uniform concentration. It is mostly monomer that is consumed by the radical chain reaction, and the concentration of monomer will then exhibit gradients that cause diffusion.

It is also conceivable that the polymer formed during the light-initiated reaction could also diffuse significantly, since the periodic holographic fringe pattern will also form gradients of polymer concentration. However, the diffusivity of particles decreases as their mass and size increases. The diffusion of organic vapors in polymers confirms a trend of decreasing diffusivity with increasing molecular size [114], and the empirically observed relationship in solid state diffusion is that the coefficient of diffusion varies inversely as the square root of the mass of the diffusing particles [120]. Intuitively, one would expect that as radicalized polymer chains grow, at any instant during the reaction there would be a wide distribution of polymer molecular weights, and a correspondingly wide range of diffusion coefficients. However, this is not true of radical initiated vinyl polymerization. Even when overall reaction times are second or hours, the growth time of a single polymer chain can be extremely fast. Consequently, during a typical vinyl polymerization, one will find unreacted monomer, large terminated polymer chains, and only about 1 part in 10^8 of growing polymer chains [36]. Even for small polymer chain lengths, on the order of 10^4 monomer subunits, the newly formed polymer will be 100 times less mobile than the unreacted monomer.

The first and perhaps clearest exposition of the photopolymer diffusion hypothesis appears in the work of Colburn and Haines [24], who investigated the properties of DuPont's original holographic photopolymer, and were not DuPont employees. One of the versions they worked with lacked sensitivity in the visible, and was exposed with the 364 nm radiation of an argon-ion laser. The standard procedure was to expose the film with both object and reference beams, then let the film briefly sit in the dark, followed by a long, uniform post-exposure (using the reference beam only) in order to fix the hologram by polymerizing all residual monomer. No other processing steps were required. Simultaneously with these steps, the hologram was illuminated by the 633 nm radiation of a helium-neon laser. The holographic film was totally insensitive to the red light, but the developing phase hologram was capable of diffracting it. The strength of the first diffracted order of the red light was recorded as a measure of the diffraction efficiency. The evolution of the diffraction efficiency was surprising. During exposure, the diffraction efficiency would rise steadily from zero. After the exposure, during the dark interval, the efficiency continued to climb briefly, then fell to zero, and immediately began to rise again. During the post-exposure illumination, the diffraction efficiency rose more rapidly, and then leveled out at its final, maximum value.(See Figure 4-4.)

Colburn and Haines explained the evolution of the phase grating in terms of photochemistry, diffusion, and constrained shrinkage of the photopolymer film. In Chapter III it was explained how the breaking of carbon-carbon double bonds in vinyl polymerization resulted in a lower molar refractivity per unit mass for the polymer compared to the monomer. However, it has been pointed out that polymerization of a monomer in bulk usually results in shrinkage and a 10 to 20% increase in the mass density [23]. This mass density increase is more than enough to compensate for the decrease in molar refractivity, so the bulk index of refraction is larger after polymerization. Colburn and Haines postulated that the shrinkage of the photopolymer film in the bright fringes is constrained by the adjacent dark fringe areas, such that the whole film shrinks by a constant amount. In support of this, finished holograms were immersed in index-matching fluid with no noticeable effect on diffraction efficiency. Therefore, any surface grating was negligible compared to the volume grating recorded in the film. (Significant surface modulation was observed in some cases, but only when the period Λ of the grating exceeded 10 microns.) Had the film shrunk differentially under the influence of photopolymerization, the material exposed to the bright fringes would have shrunk more than that exposed to the minima of the fringes to form a surface relief pattern.

The Colburn-Haines mechanism for photopolymer grating formation is essentially that rapid photochemical reactions in the brightly lit fringes cause a decrease in the refractive index due to the declining molar refractivity per unit mass, but that the depletion of the monomer in the bright fringes also causes a diffusive inflow of matter from the dark to the light fringes that increases the index. The process is illustrated in Figure 4-3. During the holographic exposure, the index decreases more in the bright fringes than in the dark fringes. The depletion of monomer in the bright fringes sets up concentration gradients, and monomer diffuses from dark fringes to bright fringes. The transfer of mass increases the index in the bright fringes and decreases the index in the dark fringes. Finally, in the post-exposure step, all remaining monomer is polymerized, so the photopolymer film is uniform in composition everywhere. The remaining phase grating, if any, is due only to a modulation of the mass density caused by the diffusive mass transfer. Figure 4-4 shows one of the efficiency vs. time

71
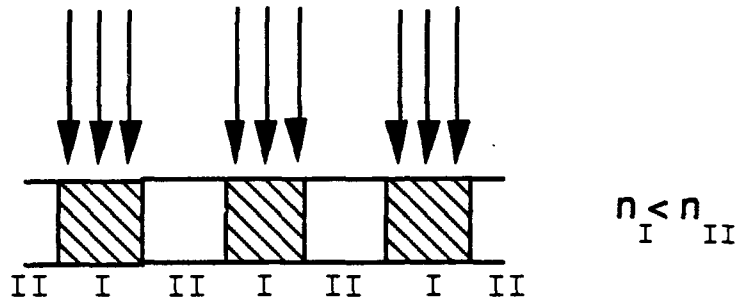
a) Photochemically induced decrease in index of the brightly lit fringes

$n_I < n_{II}$
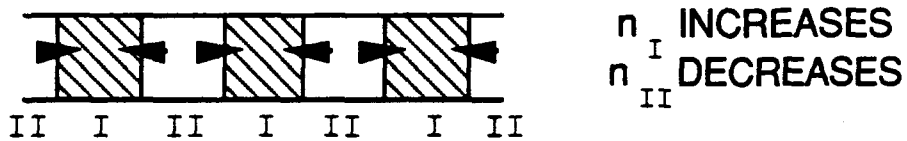
b) Diffusion transfers mass (monomer) from dark fringes to bright fringe

n_I INCREASES
n_{II} DECREASES
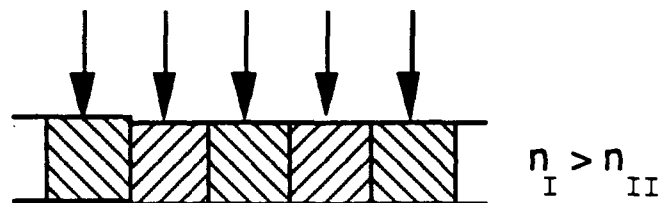
c) Flood illumination polymerizes all monomer, locking in mass-density induced index modulation.

$n_I > n_{II}$

Figure 4-3: Colburn and Haines' proposed mechanism of photopolymer grating formation.

[Adapted from Reference 24]

DIFFRACTED LIGHT
INTENSITY

EXPOSURE
INTENSITY

t=0
TIME, 5 SEC/DIV
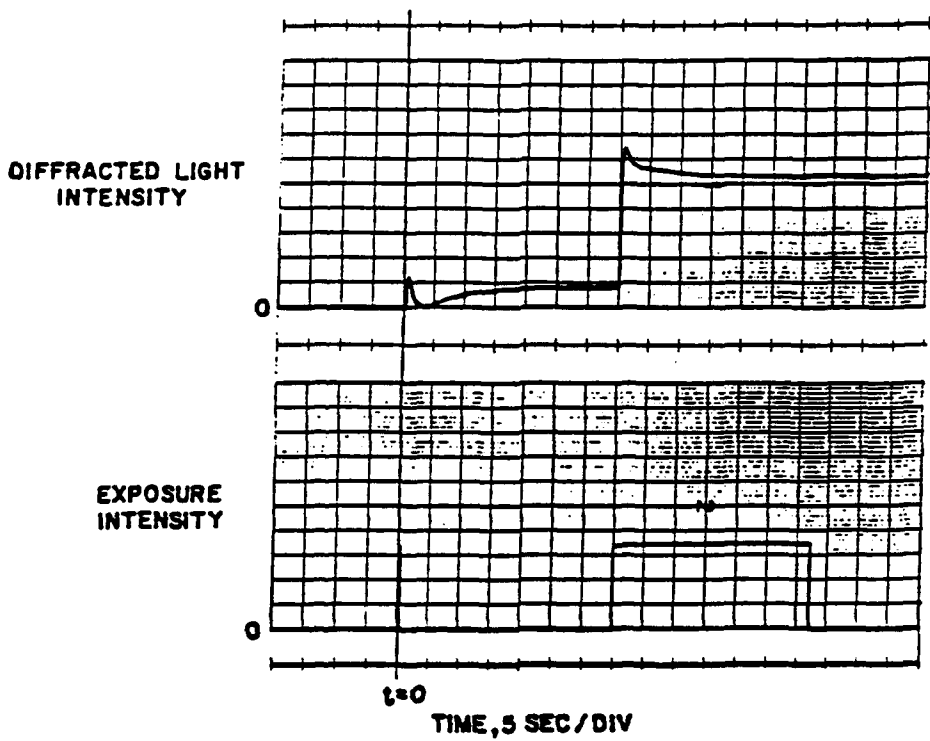
a) Evolution of a "typical" hologram

DIFFERENTIAL
INDEX δn

0

TIME

EXPOSURE
INTENSITY

0

t_1 t_2 t_3 TIME
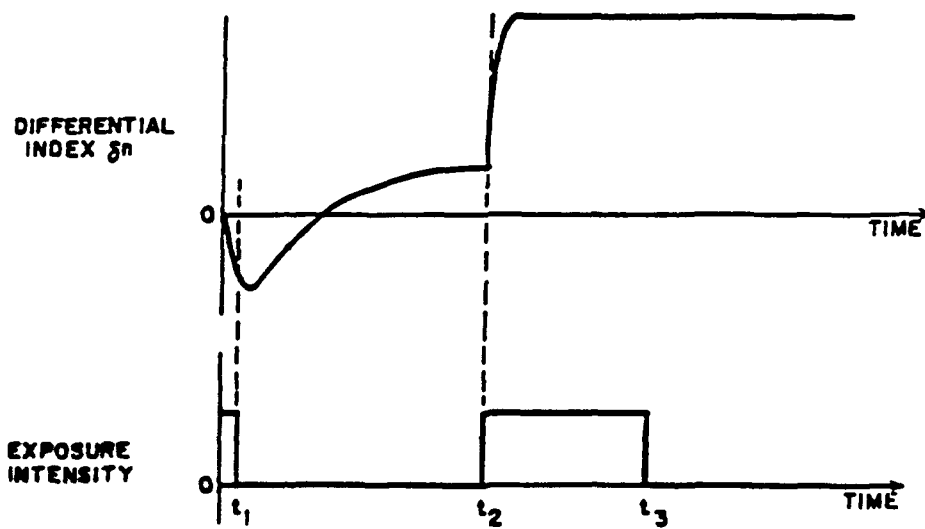
b) Postulated index changes responsible for the data seen above

Figure 4-4: Measured data and model of index change from Colburn and Haines.
[Adapted from Reference 24]

73

measurements made by Colburn and Haines, and their postulated index amplitude vs. time. For small index modulations, the diffraction efficiency in the first diffraction order is proportional to the square of the index amplitude. (See Equations 3-40 and 3-71.) Note that efficiency is always positive, but in this model the refractive index modulation can go both positive and negative.

A criticism of the Colburn and Haines theory has been that the experimentally observed dip to zero diffraction efficiency was not repeatable, and that this zero was a necessary consequence of the theory [121]. However, Colburn and Haines recognized that the dip to zero was the consequence of a special combination of grating period, photopolymer composition, and exposure intensity. Other cases were also compatible with the theory. Figure 4-5 shows the evolution of efficiency for a long, high-intensity exposure. The high-intensity illumination causes the polymerization to proceed more rapidly than the diffusion. At first there is a small peak of diffraction efficiency due to molar refractivity modulation, but as the long exposure polymerizes everything, the low level of diffusion is manifest in final diffraction efficiency of near zero. Likewise, Figure 4-6 is the evolution of a low spatial frequency grating given a short exposure, dark period, and uniform post-exposure. The diffusion time is long because of the large grating period. The molar refractivity grating plateaus soon after exposure and holds steady, but diffraction efficiency plunges to near zero once post-exposure polymerizes everything, because the mass density of the finished film is uniform. Many of these experiments were repeated and confirmed elsewhere [124].

The diffusion theory was also corroborated by MTF measurements, which consisted of measuring the diffraction efficiency of numerous holograms made with identical exposures but different values of the grating period Λ. The holograms were gated in index matching fluid to exclude the effect of surface gratings, which appeared for $\Lambda > 10$ microns. Final diffraction efficiency of the volume phase holograms fell to very low values for $\Lambda > 10$ microns, consistent with a diffusion limited process.

Researchers employed by du Pont have generally accepted the importance of diffusion in holographic photopolymers. They determined [122] that the monomer diffusion coefficient in their dry polymer film varied exponentially as a function of percent polymerization, ranging from about 10^{-7} cm^2/sec at 0% polymerization to an extrapolated value of 10^{-12} cm^2/sec at 100 percent polymerization. Continued studies of the time evolution of gratings [121,123] showed that at low exposure intensities or high spatial frequencies, diffraction efficiency during exposure rose monotonically from zero. If the exposure intensity was high or if the spatial frequency was low, the diffraction efficiency would often rise to a peak, fall, and then rise again. The interpretation of the first case is that for low intensity or high spatial frequency, the characteristic diffusion time would be much shorter than the chemical reaction time, so the density increase of the bright fringes would dominate the refractive index changes. For the other case, the diffusion time and reaction time are of the same order, so one first observes the phase grating due to the photochemical reaction, followed by a decrease in the phase grating amplitude due to diffusion. The experimentally observed decay time of the diffraction efficiency for various values of Λ was consistent with a diffusion coefficient of 2×10^{-8} cm^2/sec. The effect of the post-exposure illumination on the gratings was complicated. Sometimes efficiency would increase, decrease, or remain the same, depending on whether the exposure had been dominated by diffusion or photochemical reaction.
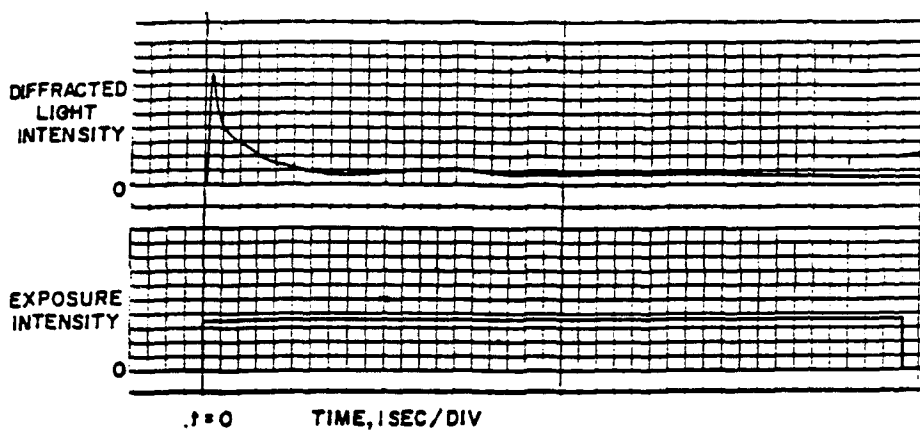
74

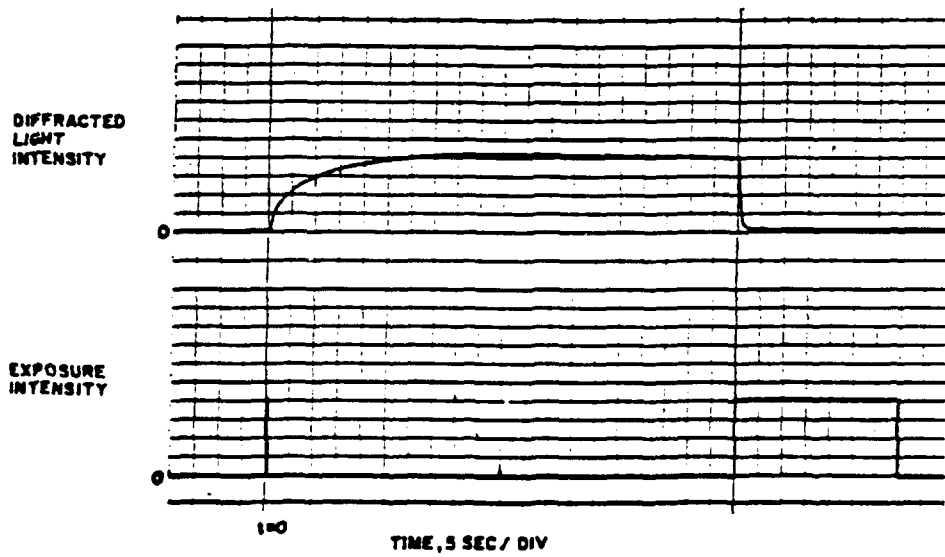Figure 4-5: Diffraction efficiency of a long, high-intensity exposure.

Figure 4-6: Effect of short exposure for a low spatial frequency grating.

Though accepting diffusion, du Pont researchers have universally agreed that the Colburn and Haines hypothesis is wrong, though they do not always agree on why it is wrong. One criticism was discussed above. More recent work, based on the new du Pont holographic photopolymers, does not find any evidence of an initial decrease in refractive index in the brightly lit fringes [60]. The new thinking is that mass density modulation, mediated by diffusion and shrinkage, is the sole contributor to the index modulation [61]. By working on this assumption, du Pont researchers have found three ways to boost the efficiency of their materials. First, they choose monomer/binder combinations with as large an index contrast as possible. Although uniformly mixed to start with, the holographic diffusion tends to segregate the binder and the polymerized monomer; final diffraction efficiency has been shown to depend upon the amount of index contrast between the two components. Secondly, the addition of a plasticizer to the photopolymer promotes diffusion and higher efficiency. Finally, a heat treatment after exposure increases the diffusivity of the photopolymer according to the Arrhenius relation (Equation 4-21), and promotes the diffusion of material that otherwise would have been immobile at room temperature.

The failure to observe a decrease in the index of the exposed film may be a consequence of the types of monomers used in the new compositions. The decrease in molar refractivity expected in the vinyl polymerization of an acrylate is the same no matter what the size or the complexity of the acrylate monomer. The breaking of a carbon-carbon double bond to form two single carbon bonds should reduce molar refractivity per monomer sub-unit by 1.66 cm^3. The base refractivity of a simple acrylate such as acrylic acid can be calculated, using the bond polarizabilities in Table 3-1, to be 15.37 cm^3, so the resulting percentage change in refractivity is about 11%. The monomers used in the new du Pont compositions have a more complex structure and a much higher initial refractivity. One of them, 2-phenoxyethylacrylate (POEA), would have an R value of 52.74 cm^3; ΔR for the polymerization reaction is still 1.66 cm^3, so the percentage reduction is only 3%. Photochemically induced changes in the molar refractivity may indeed be negligible in the new du Pont compositions.

Researchers at Bell Labs have also exploited the diffusion properties of polymers to enhance hologram formation. In a work that pre-dates and may have inspired the current du Pont compositions, Tomlinson et. al. [70] disclosed experimental photopolymers containing multiple monomers, chosen to have contrasting refractive indices and different reaction rates. Their model predicted a two way diffusion, with one component migrating from dark to bright fringes, and vice versa. Holographic gratings were recorded in these materials, and contact prints were made by illuminating the films through a wire mesh. Examination of the contact exposures with an interference microscope enabled the researchers to determine whether the index increased or decreased in the illuminated regions. In accordance with the model, the choice of monomers determined the relative index of the dark and bright fringe areas.

Diffusion has also been invoked to explain some of the aspects of hologram formation in poly(methyl methacrylate) (PMMA, known commercially as Plexiglass.) Normal polymerization of methyl methacrylate (MMA) leaves as much as 10% unreacted monomer embedded within the polymer matrix. The addition of a UV sensitive polymerization initiator yields an inexpensive holographic photopolymer, with PMMA as the binder, and MMA as the monomer [67]. The low refractive index modulation, a Δn of about 10^{-4}, means that high efficiency gratings can only be achieved with polymer films several

millimeters thick, but this thickness enhances the angular sensitivity, and allows hundreds of holograms to be stored in the same volume by angular multiplexing of the reference beam. The increase of refractive index with exposure also allowed optical wave guides to be formed in the polymer [125].

The mechanism of index modulation in PMMA was found to agree with the Colburn and Haines theory in that shrinkage was negligible and the index of illuminated regions increased due to diffusion of monomer [126]. After thick volume holograms were recorded in PMMA, one group shaved the hologram with a microtome, measuring the diffraction efficiency after each shaving was removed. The point was to determine the index modulation as a function of depth in the material. The index modulation was found to be greater in the middle of the material than it was at the faces of the material. This was attributed to the depletion of MMA, which had diffused to the outer faces and vaporized into the air before the PMMA was holographically exposed. Measurements of this evaporative loss established that the diffusion coefficient of MMA in PMMA was about 3.8×10^{-8} cm^2/sec [69]. The time evolution of PMMA volume gratings was also measured [68]. The measurements showed only a monotonic increase in diffraction efficiency with time. Once exposure began, the amplitude of the refractive index modulation grew linearly with time, and then after a point, it would increase more slowly, as the square root of time. The square root dependence occurred in the dark after exposure, but it also occurred during exposure, if the exposure was long enough. The square root dependence was interpreted as evidence of diffusion, but it is not clear what reasoning led to this conclusion.

Other photopolymer systems have also shown some evidence of diffusion-controlled grating formation. Studies done with mixtures of acrylate salts and acrylamide, similar to some of the Hughes photopolymers, have shown that diffraction efficiency is low when the characteristic diffusion time is shorter than the polymerization reaction time, which happens when the spatial frequency is too low, or the exposure is too intense [127]. Polaroid researchers are aware of the role of diffusion in the DMP-128 photopolymer, but have only mentioned it in passing [66]. MTF measurements on DMP-128 holograms by Stone indicate that they exhibit a low spatial frequency cutoff [128]. For an exposure level of 64 millijoules/cm^2, the refractive index modulation was about 0.15 for a grating of 1000 cycles per mm; the effective modulation is only .02 at 100 cycles per mm, and falls even more at lower spatial frequencies. Stone also found that the surface modulation of DMP-128 photopolymers was significant only at low spatial frequencies, suggesting that shrinkage is constrained at high spatial frequencies.

D.   A Mathematical Model of Diffusion in Holographic Photopolymers

The preceding discussion of diffusion in photopolymers indicates that there are many areas of disagreement among researchers as to what constitutes evidence for diffusion in a photopolymer system. Even when the time evolution of the hologram is recorded, the wide variety of efficiency vs. time profiles makes the interpretation of the data confusing. Furthermore, there is no general agreement as to the role of photochemically induced molar refractivity changes in the formation of photopolymer phase gratings. Part of the problem may be that the photopolymer diffusion theories advanced so far tend to be qualitative rather than quantitative. The common-sense, narrative exposition of the Colburn-Haines theory makes it appealing to some, and makes it seem like the product of an over-active imagination to

77

others. It seems that holographic photopolymer research could benefit from a more quantitative, analytical model of hologram formation, one that would attempt to predict the time evolution of the grating based upon the known laws of diffusion, photochemistry, and optics.

The system to be modeled is one in which monomer diffuses through a pre-existing polymer/binder matrix, with monomer disappearing as it polymerizes under the influence of a sinusoidal spatial pattern of light intensity. The resulting refractive index profile will depend upon the final composition and mass density of the photopolymer, in accord with the Lorentz-Lorenz relationship. The general problem of diffusion accompanied by chemical reaction has been addressed by Crank [99] for some particular cases. For an irreversible reaction such as vinyl polymerization, the diffusion equation (4-12) is modified by the addition of a loss term L that accounts for monomer lost to polymerization

$$\frac{\partial u(x,t)}{\partial t} - D\frac{\partial^2 u(x,t)}{\partial x^2} = L(x,t,u) \qquad (4\text{-}24)$$

where the loss due to the photochemical reaction could be a function of location, time, and the concentration of the reacting monomer. This form of the diffusion equation was used by Odian and Kruse [129] to predict the one-dimensional diffusion of monomer into a polymer film, under the influence of uniform gamma radiation that graft polymerized the monomer as it diffused through the film. (This was essentially a photopolymerization reaction with high energy photons.) Marotz [68], in his paper on PMMA holograms, outlined how diffusive monomer flux and photopolymerization might be combined to model index changes in a photopolymer hologram, but apparently did not pursue the model further.

The exact form of the monomer loss term must conform to the known reaction kinetics for vinyl polymerization. A useful expression for the reaction rate of photopolymerization was given in Chapter II. It expressed the time rate of change of monomer concentration (otherwise known as the propagation rate, v_p) as a function of light intensity, under the assumption that the free radical concentration remained constant during the reaction. The expression is

$$v_p \equiv -\left(\frac{d[M]}{dt}\right) = \frac{k_p}{\sqrt{k_t}}\left(f_i\,\phi_i\,I_a\right)^{1/2}[M] \qquad (2\text{-}9)$$

By collecting multiplicative constants into a loss constant k_L, and expressing monomer concentration [M] as the function u(x,t) to remain consistent with the notation for diffusion, the expression for monomer loss due to polymerization is

$$L(I,u) = -k_L i^{1/2} u \qquad (4\text{-}25)$$

In this steady state condition, the loss rate of monomer is proportional to the concentration of monomer and the square root of the light intensity. The only assumption made in deriving this condition is that the loss of radicals to termination is balanced by the photochemical creation of free radicals. After photopolymerization begins, this radical balance

78

is quickly achieved and maintained for a wide variety of reactants [130]. In particular, the reaction dependence on light intensity and concentration has been verified for the photopolymerization of simple acrylate salts. Hughes researchers verified that the polymerization rate in their composition was strictly proportional to monomer concentration [49]. Todorov et. al. [127], using photopolymers based upon the recipes published by Hughes, measured the real-time grating formation to estimate the order of the reaction with respect to incident light intensity. The order is the power to which the intensity must be raised to be proportional to the reaction rate; in Equation 4-25 the order with respect to intensity is 0.5. Todorov's estimate for the order was 0.6 ± 0.2, consistent with the theoretical value.

The prescription of the monomer loss function is complete with the specification of the holographic interference pattern. If two coherent waves of intensities I_1 and I_2 interfere the intensity pattern can be written

$$ I = I_1 + I_2 + 2 \sqrt{I_1 I_2} \cos\left(\frac{2\pi x}{\Lambda}\right) \qquad (4\text{-}26) $$

where x is defined as the co-ordinate perpendicular to the plane interference fringes, and Λ is the spatial period. If the expression for the intensity is simplified by defining the constant term $I_0 = I_1 + I_2$ and the sinusoidal amplitude $I_s = 2(I_1 I_2)^{1/2}$, and is combined with Equations 4-24 and 4-25, the monomer concentration is described by the differential equation

$$ \frac{\partial u(x,t)}{\partial t} - D\frac{\partial^2 u(x,t)}{\partial x^2} = - k_L\left[I_0 + I_s \cos\left(\frac{2\pi x}{\Lambda}\right)\right]^{1/2} u(x,t) \qquad (4\text{-}27) $$

In those cases where a concentration dependent diffusion coefficient must be considered, the monomer concentration during holographic exposure is given by the solution of

$$ \frac{\partial u(x,t)}{\partial t} - \frac{\partial}{\partial x}\left(D(u)\frac{\partial u(x,t)}{\partial x}\right) = - k_L\left[I_0 + I_s \cos\left(\frac{2\pi x}{\Lambda}\right)\right]^{1/2} u(x,t) \qquad (4\text{-}28) $$

Equations 4-27 and 4-28 will henceforth be referred to as the holographic diffusion equations.

Before these equations can be solved, initial conditions and boundary conditions must be specified. At the beginning of the holographic exposure, the monomer concentration in a well-mixed photopolymer will be some constant $[M_0]$, so the initial condition is $u(x,0) = [M_0]$. The proper boundary conditions for this problem require a look at the holographic recording geometry.

Consider an unslanted transmission grating, with the interference planes perpendicular to the two faces of the recording medium. Typically, the fringe spacing Λ might be 10 microns, so a 1 cm wide grating would be 1000 Λ wide. Suppose that the characteristic

79

diffusion time over the distance Λ is τ_D. Recalling that diffusion time increases quadratically with the length scale, the time necessary for substantial diffusion to occur across the width of the hologram would be $10^6 \tau_D$. As will be shown later, characteristic diffusion times τ_D on the order of 10 seconds have been measured in Polaroid's DMP-128 photopolymer. Diffusion across the width of such a hologram would take $10^6 \tau_D$, which is almost four months. This suggests that for experiments designed to measure the characteristic diffusion time of holographic fringe spacings, no appreciable boundary effects can be communicated to the bulk of the hologram in a reasonable time. Therefore, the hologram is effectively infinite in extent. A similar argument can be made for reflection holograms, where the fringes lie parallel to the faces of the recording medium. For reasonable reflectivity, the hologram must be many Λ thick, so diffusion through the thickness of the film is much slower than diffusion from dark fringes to adjacent bright fringes.

The effectively infinite size of the hologram with respect to diffusion, the uniform initial condition, and the periodic forcing function L are all suitable for the application of periodic or wrap-around boundary conditions. Given the same initial conditions and the same forcing function L, there is no reason to suppose that any cycle of length Λ will be different from any of the adjacent cycles. Simply put, one can assume that at all times the concentration profile $u(x,t) = u(x+\Lambda,t)$. Likewise, the fluxes, which are defined in terms of $\partial u/\partial x$, are also periodic with respect to Λ. If one has to resort to a numerical solution of Equation 4-27, it is as though one spatial cycle of the hologram were wrapped around on itself. The diffusive flux that leaves the system at $x = 0$ re-enters at $x = \Lambda$. Periodic boundary conditions of this type are commonly found in solid state physics, where the crystalline lattice imposes periodicity.

Suppose now that the holographic exposure lasts from $t = 0$ to $t = T$, where T is the length of the exposure. When the exposure ends, the polymerization ends, and the right hand side of Equation 4-27, the loss term, becomes identically zero. The holographic interference pattern has left some periodic concentration profile of monomer, expressed as $u(x,T)$. Although polymerization has ended, diffusion can still continue. The further evolution of the concentration u is governed by the free diffusion equation (4-12), with $u(x,T)$ as an initial condition. Since the initial condition is periodic, the periodic boundary conditions are still appropriate. In fact, this part of the problem, the free diffusion of an arbitrary initial profile in a periodic system, was solved long ago by Fourier [102]. The problem solved by Fourier was the conduction of heat in a ring, starting with an arbitrary temperature profile. The initial concentration or temperature profile can be expanded in a Fourier series, and the amplitude of the nth term decays exponentially in time with a decay constant of τ/n^2, where τ is the decay time of the fundamental. This is in accord with the smoothing property of diffusion; the high frequency components diminish first, leaving only the fundamental sinusoid of period Λ.

Once the monomer profile has been found, the index grating can be calculated. The index changes in the photopolymer medium can be expressed straightforwardly by using an alternate form of the Lorentz-Lorenz relationship that relates the index to a sum over all the different components of the photopolymer [23],

$$\frac{n^2 - 1}{n^2 + 2} = \sum_i \frac{\rho_i R_i}{M_i} \qquad (4\text{-}29)$$

where ρ_i, R_i, and M_i are the mass density, molar refractivity, and molecular weight of the ith component. The typical photopolymer composition has three main components

$$\frac{n^2 - 1}{n^2 + 2} = \frac{\rho_m R_m}{M_m} + \frac{\rho_p R_p}{M_p} + \frac{\rho_b R_b}{M_b} \qquad (4\text{-}30)$$

where m indicates monomer, p indicates polymer resulting from photopolymerization, and b indicates the passive binder. It is convenient to take R_p as the molar refractivity per mole of monomer subunits and M_p as the weight of one mole of monomer subunits. The ratio ρ_m/M_m is the number of moles of monomer per liter, which of course is identical to the monomer concentration function $u(x,t)$. Likewise, ρ_p/M_p is the concentration (moles/liter) of monomer sub-units in the photochemically produced polymer. The rate of monomer conversion into polymers (moles/liter-sec) is given by the right-hand side of Equation 4-27. Integration of the negative of this term with respect to time gives the polymer concentration

$$P(x,t) \equiv \frac{\rho_p}{M_p} = k_L \int_0^t \sqrt{I_0 + I_s \cos\left(\frac{2\pi x}{\Lambda}\right)} \, u(x,t') \, dt' \qquad (4\text{-}31)$$

Therefore, Equation 4-30 can be rewritten as

$$\frac{n^2 - 1}{n^2 + 2} = R_m \, u(x,t) + R_p \, P(x,t) + \frac{\rho_b R_b}{M_b} \qquad (4\text{-}32)$$

Equation 4-32 can be solved directly for n. If the change in the index is small, which is generally the case for photopolymers, a differential approximation can be made by differentiating the left hand side, and subtracting the values at $t = 0$ from the right hand side. Define $\delta n(x,t) = n(x,t) - n_0$, the difference between the final index and the initial constant index of the photopolymer at $t = 0$. Then the differential approximation is

$$\delta n(x,t) = \left(R_m u(x,t) - R_m[M_0] + R_p P(x,t)\right) \frac{(n^2 + 2)^2}{6n} \qquad (4\text{-}33)$$

where $[M_0]$ is the initial, uniform monomer concentration before exposure. As expected, the properties of the passive binder are not found explicitly in the expression for index modulation.

81

With this model of phase grating formation in a photopolymer, the solution of the holographic diffusion equation (4-27) leads to a complete description of the monomer concentration $u(x,t)$, the polymer concentration $P(x,t)$, and the index of refraction $n(x,t)$. Unfortunately, a search of the literature on mathematical physics has not uncovered an exact, analytic solution for this problem. In general, one must resort to numerical methods of solution. Diffusion equations belong to the class of parabolic partial differential equations. Standard texts describe several numerical methods suitable for parabolic equations [99,104], and the application of these methods to the holographic diffusion equation is discussed in Appendix A.

Under certain restricted conditions, the holographic diffusion equation can be made to resemble a well-characterized equation of mathematical physics, the Mathieu equation. The Mathieu equation first arose in the solution of the wave equation in elliptical cylindrical co-ordinates, as in the vibrations of an elliptical drumhead [131]. There is little agreement on the proper notation for the Mathieu equation and its solutions, but here we shall use the form given by Abramowitz and Stegun [132]. This standard form of the Mathieu equation is

$$\frac{d^2y}{dx^2} + (a - 2q \cos 2x)\, y = 0 \qquad (4\text{-}34)$$

where q arises from the physical parameters of the problem and a is an eigenvalue of the differential equation. The periodic solutions of this equation are called the Mathieu functions. There are an infinite number of Mathieu functions constituting a complete set of orthogonal basis functions over the interval 0 to 2π. An even Mathieu function is called the elliptic cosine of nth order (for $n = 0$ to infinity), $ce_n(x)$, and it is associated with the eigenvalue a_n. An odd Mathieu function is called the elliptic sine of nth order (for $n = 1$ to infinity), $se_n(x)$, and has an eigenvalue b_n. When $q \ll 1$, $se_n(x) \cong \sin(nx)$ and $ce_n(x) \cong \cos(nx)$.

The holographic diffusion equation can be cast in the form of the Mathieu equation by separation of variables after placing a condition on the photochemical loss function. Assume that the intensities of the two beams forming the hologram are very dissimilar, either $I_1 \ll I_2$ or $I_2 \ll I_1$. In either case, the amplitude of the sinusoidal component of the intensity pattern is much less than the mean value of intensity, that is, $I_s \ll I$. Since $(1+x)^{1/2} \cong 1 + x/2$ for small x, the loss function can be written as

$$L(x) = -k_L\sqrt{I_0}\left(1 + \frac{I_s}{2I_0} \cos\left(\frac{2\pi x}{\Lambda}\right)\right) u(x,t) \qquad (4\text{-}35)$$

Next it is necessary to assume that Equation 4-27 can be solved by a standard separation of variables, that is, $u(x,t) = X(x)T(t)$. Substituting Equation 4-35 in 4-27 and separating variables gives

$$\frac{1}{T}\frac{dT}{dt} = \frac{D}{X}\frac{d^2X}{dx^2} - k_L\sqrt{I_0}\left(1 + \frac{I_s}{2I_0}\cos\left(\frac{2\pi x}{\Lambda}\right)\right) = -\gamma \qquad (4\text{-}36)$$

where γ is an eigenvalue and is related to the Mathieu eigenvalues defined above. As usual, the solution for the time dependence is

$$T(t) = \exp(-\gamma t) \qquad (4\text{-}37)$$

and the ordinary differential equation for the spatial dependence becomes

$$\frac{d^2X(x)}{dx^2} + \left(\frac{\gamma - k_L\sqrt{I_0}}{D} - \frac{k_L}{D}\frac{I_s}{2\sqrt{I_0}}\cos\left(\frac{2\pi x}{\Lambda}\right)\right)X(x) = 0 \qquad (4\text{-}38)$$

The rate constant k_L multiplied by the square root of intensity gives a rate with units of inverse seconds, and the diffusion coefficient D has units of cm^2/sec. If Λ^2 could be introduced, the coefficients of the differential equation could be made dimensionless. This is accomplished by the substitution

$$\tilde{x} = \frac{\pi x}{\Lambda} \qquad (4\text{-}39)$$

which transforms Equation 4-38 into

$$\frac{d^2X(\tilde{x})}{d\tilde{x}^2} + \left(\frac{\gamma\Lambda^2 - k_L\sqrt{I_0}\Lambda^2}{D\pi^2} - \frac{k_L\Lambda^2}{D\pi^2}\frac{I_s}{2\sqrt{I_0}}\cos(2\tilde{x})\right)X(\tilde{x}) = 0 \qquad (4\text{-}40)$$

The coefficients can be expressed as dimensionless ratios of characteristic time constants with suitable definitions,

$$\tau_D = \frac{\Lambda^2}{\pi^2 D}, \quad \tau_1 = \frac{1}{k_L\sqrt{I_0}}, \quad \text{and } \tau_2 = \frac{2\sqrt{I_0}}{k_L I_s}. \qquad (4\text{-}41)$$

These three time constants are, respectively, the free diffusion time, the photochemical reaction time associated with the mean value of the illumination, and the photochemical reaction time associated with the sinusoidal component of the illumination. The equation is

$$\frac{d^2X(\tilde{x})}{d\tilde{x}^2} + \left(\left(\tau_D\gamma - \frac{\tau_D}{\tau_1}\right) - \frac{\tau_D}{\tau_2}\cos(2\tilde{x})\right)X(\tilde{x}) = 0 \qquad (4\text{-}42)$$

83

Equation 4-42 is exactly the canonical form of the Mathieu equation 4-34, with the formal identification

$$\begin{matrix} a_n \\ b_n \end{matrix} = \left(\tau_D \gamma_n - \frac{\tau_D}{\tau_1} \right), \text{ and } 2q = \frac{\tau_D}{\tau_2} \qquad (4\text{-}43)$$

where a_n and b_n are the eigenvalues of the elliptic cosine and elliptic sine solutions, and γ_n is the corresponding relaxation time of the temporal part of the solution. Note that all the coefficients of the differential equation are ratios of physically significant time constants.

Equations 4-42 and 4-43 make quantitative the previous qualitative discussion of the Colburn-Haines theory, where the relative size of the diffusion time and chemical reaction time were thought to be important. The parameter q in the Mathieu equation has been shown to represent the ratio of diffusion time to photochemical reaction time. This parameter q determines the nature of the eigenfunction solutions; for small q, the solutions are very nearly sinusoidal, while for large q, each Mathieu function is non-sinusoidal, though still periodic. If q is known, the eigenvalues a_n, b_n, and γ_n can be found. The proper Mathieu functions can be found, and the original constant monomer concentration $[M_0]$ expressed as an expansion of Mathieu functions. The evolution of the monomer concentration is found by applying the proper exponential decay time of γ_n to each term of the Mathieu function expansion.

The solution of this form of the holographic diffusion equation exhibits some interesting features in the regime $q = \tau_D/(2\tau_2) \ll 1$. This condition will be satisfied for very short diffusion times, or equivalently, very low-intensity exposures. For small q, $a_0 \cong -q^2/2$, and for all other eigenvalues $a_n, b_n \cong n^2$. The only significant eigenfunctions (not of order q^2 or smaller) with the proper symmetry are

$$ce_0(\widetilde{x};q) \cong 1 - \frac{q}{2} \cos(2\widetilde{x}) \text{ and } ce_2(\widetilde{x};q) \cong \cos(2\widetilde{x}) \qquad (4\text{-}44)$$

The constants γ_n can be determined from Equation 4-43. Ignoring the very small quantities in q^2 the approximate solution is

$$u = [M_0] \left(\left(1 - \frac{q}{2} \cos\left(\frac{2\pi x}{\Lambda}\right) \right) \exp\left(\frac{-t}{\tau_1}\right) + \frac{q}{2} \cos\left(\frac{2\pi x}{\Lambda}\right) \exp\left(\frac{4 + \tau_D/\tau_1}{\tau_D} t\right) \right) \qquad (4\text{-}45)$$

The first periodic term decays relatively slowly, while the second periodic term decays on less than the order of the diffusive time constant. For times significantly longer than the diffusive time constant, only the first term remains. Intuitively, it shows a periodic monomer concentration. However, the final solution sought here is the index grating, not the monomer concentration. Applying Equation 4-31 to calculate the total polymerization P(x,t), and using the square root expansion of Equation 4-35 yields

$$P(x,t) = [M_0]\left(1-\exp\left(-\frac{t}{\tau_1}\right)\right)f(x) \tag{4-46}$$

$$f(x) = \tau_1\left(\frac{1}{\tau_1} + \left(\frac{1}{\tau_2} - \frac{\tau_D}{4\tau_2}\right)\cos\left(\frac{2\pi x}{\Lambda}\right) - \frac{\tau_D\tau_1}{4\tau_2^2}\cos^2\left(\frac{2\pi x}{\Lambda}\right)\right)$$

The coefficient of the cosine squared term in f(x) is very small and the term can be ignored under the assumptions used here. However, it shows that a purely sinusoidal intensity pattern of period Λ can form an index grating that contains higher harmonics as well as the fundamental spatial period, since $\cos^2(x) = 1 + \cos(2x)$. The sinusoidal part of the index modulation δn_s is found from the use of Equation 4-33, after considerable algebra,

$$\delta n_s \frac{6n}{(n^2+2)^2} = [M_0]R_p\cos\left(\frac{2\pi x}{\Lambda}\right)\frac{\tau_1}{\tau_2}\left[(1-e^{-t/\tau_1}) - \frac{R_m}{R_p}\frac{\tau_D}{4\tau_1}e^{-t/\tau_1}\right]$$
$$+ [M_0]R_p\cos\left(\frac{2\pi x}{\Lambda}\right)\frac{\tau_D^2}{16\tau_1\tau_2}\left[(1-e^{-4t/\tau_D}) + \frac{R_m}{R_p}\frac{4\tau_1}{\tau_D}e^{-4t/\tau_D}\right] \tag{4-47}$$

For t = 0, this solution gives $\delta n_s = 0$, which is a good start. Since the diffusive time τ_D is assumed to be much smaller than all other relevant time scales in this problem, the exponentials that decay on the order of τ_D will go to zero quickly. If $\tau_1 \gg t \gg \tau_D$, then the value of the index grating goes negative, since it is proportional to $(\tau_D/4\tau_1) - (R_m/R_p)$, and under any reasonable assumptions the ratio of the molar refractivities is near unity. At later times, the index grating takes on larger, positive values proportional to τ_1/τ_2. This solution suggests that given the restrictive assumptions made here, the zero seen in the evolution of the phase grating is inevitable, and that it does not depend upon the differing molar refractivities of the monomer and the polymer. The ratio of the molar refractivities appears in the solution, but this ratio will never depart from unity by more than about 10%, according to the rough calculations in the previous section (p. 101).

This exercise has shown several things about the holographic diffusion equation. Most importantly, the essential parameters of the problem are the relative time scales of diffusion and photochemistry. The important parameters of the diffusion equation are the ratios of these time scales. Secondly, even a pure sinusoidal forcing function will generate higher harmonics in the index grating. Finally, a zero-crossing of diffraction efficiency during grating formation is predicted, though it is not exactly as described by Colburn and Haines, and their theory of photopolymer grating formation may be valid in other regimes of the parameters.

85

V. EXPERIMENTAL TECHNIQUES FOR MEASURING HOLOGRAM GROWTH

The theory of holographic diffusion presented in the last chapter makes specific predictions about the growth of a photopolymer hologram during exposure and its subsequent evolution in time. It might be possible to falsify or verify the theory by the detailed examination of completed holograms, but a more direct approach is to measure the properties of the photopolymer grating as a function of time from the beginning of the holographic exposure. There are a few basic techniques for doing this, all of which are based on the fact that the photopolymer phase grating is not latent, as in a silver halide film, but rather begins to form immediately upon exposure. After a review of the relevant techniques in the literature, detailed discussion will be given of how these techniques were applied in this research to the particular problem of measuring phase grating evolution in the Polaroid DMP-128 photopolymer.

A. Real-time Measurement of Grating Growth

There are two primary techniques for measuring the formation of a holographic grating. Both are illustrated in Figure 5-1. In the first method, a single laser is used to expose the hologram, and a chopper or shutter of some type is positioned in the path of the reference beam. Beyond the holographic medium, also in the path of the reference beam, is a photodetector. When the reference wave R is blocked by the rotation of the chopper or the actuation of the shutter, the only light falling on the photodetector will be the conjugate wave S' diffracted from the signal wave S. The intensities of the R and S waves are I_R and I_S. At other times, the full strength of the R wave will fall on the photodetector. Therefore, the detector is gated synchronously with the shutter, so as to take a measurement only when the reference wave is blocked. The intensity of the diffracted wave S'(referred to as $I_{S'}$) is measured at regular intervals, and the ratio $I_{S'}/I_S$ gives the diffraction efficiency η. The effect of the periodic interruptions upon the formation of the hologram can be minimized if the interruptions occur on a faster timescale than the diffusive or photochemical reactions within the medium. This technique has been used to determine the kinetics for the photochemical decomposition of various compounds embedded in a passive polymer matrix [32].

In the second method, the R and S waves expose the holographic medium without interruption, and a probe wave P of a different wavelength λ_p illuminates the grating in such a way as to satisfy the Bragg condition. The wavelength of the probe is chosen to be incompatible with the photochemistry of the recording medium, in order to have as little effect as possible on the process of hologram formation. A photodetector is stationed in the path of the diffracted probe wave P', and the diffraction efficiency at λ_p is given by the intensity ratio $I_{P'}/I_P$. This dual-wavelength method is the technique employed by Colburn and Haines and other researchers in measuring the growth of photopolymer phase gratings [24,123,124].

Both the single-wavelength and dual-wavelength methods are sufficiently sensitive to measure extremely small diffraction efficiencies, since both are effectively zero background techniques. In the absence of a grating, the only light that will reach the photodetector is that which is scattered from the optics or the holographic film. Baffling and careful positioning of the detector can reduce the scattered light. In the dual-wavelength

method, an interference filter that passes the probe wavelength can be used to block out all scattered light from the exposure wavelength.

Although real-time grating measurement is useful in characterizing holographic materials, the most sophisticated experiments and analyses of this type to date [30,31] have been developed by physical chemists to analyze a wide variety of photochemical systems, most of which are not suited to practical holography. Unlike this current research, the physical chemists have used holography as means toward the end of better understanding photochemical reactions. Any significant photochemical reaction induced by a holographic interference pattern will form an absorption or phase grating, at least temporarily. Brauchle and Burland [30] have found that the dual-beam technique allows diffraction efficiencies down to $\eta = 10^{-9}$ to be measured. With this sensitivity, they have been able to determine photochemical rate constants, distinguish one photon reactions from multi-photon reactions, measure excited state lifetimes, and determine chain lengths in polymers, as well as develop new holographic materials.

Another group led by Wang has done a great deal of work with the diffusion of photochemically active materials in a polymer matrix [133,134,135]. Camphorquinone or related compounds that undergo photochemical decomposition are doped in PMMA or some other polymer matrix and exposed to a holographic interference pattern. The evolution of the grating is measured by one of the techniques described above. The grating is initially formed by the differing molar refractivities of the reaction product in the bright fringes and the unreacted camphorquinone in the dark fringes. Generally, they have observed a decay of the holographic grating after exposure that is attributed to the diffusion, at two different rates, of the original reactant and the reaction products. The decay can be fitted to the equation

$$\eta = \left(a \exp\left(-t/\tau_a\right) + b \exp\left(-t/\tau_b\right)\right)^2 \tag{5-1}$$

where τ_a and τ_b are the characteristic diffusion times of the two species. Diffusion coefficients are then calculated from the decay times and the known grating period Λ. The diffusion coefficients thus obtained at various polymer temperatures are accurate enough to test competing theories of diffusion in polymers, and to determine the phase changes associated with the glass transition temperature T_g of the polymer.

A recent development in the use of holography as a tool in physical chemistry is a phase-sensitive method of real-time grating measurement [136] developed by Brauchle and associates. The single and dual wavelength methods already described are insensitive to the phase of the holographic grating with respect to the holographic interference pattern, because they involve the measurement of diffracted intensity only. They cannot even distinguish between phase gratings and absorption gratings. In the new technique, a single laser is used for exposure. An electro-optic modulator is placed in the reference wave, and sinusoidally modulates the phase of the reference beam with a frequency ω. A photodetector is placed in the reference beam beyond the holographic test sample. The technique is based on the observation that absorption and index are just the imaginary and real components of the complex index of refraction, so that if an absorption grating and an index grating in the same volume are spatially in phase with each other, the light diffracted from the two is out of

87
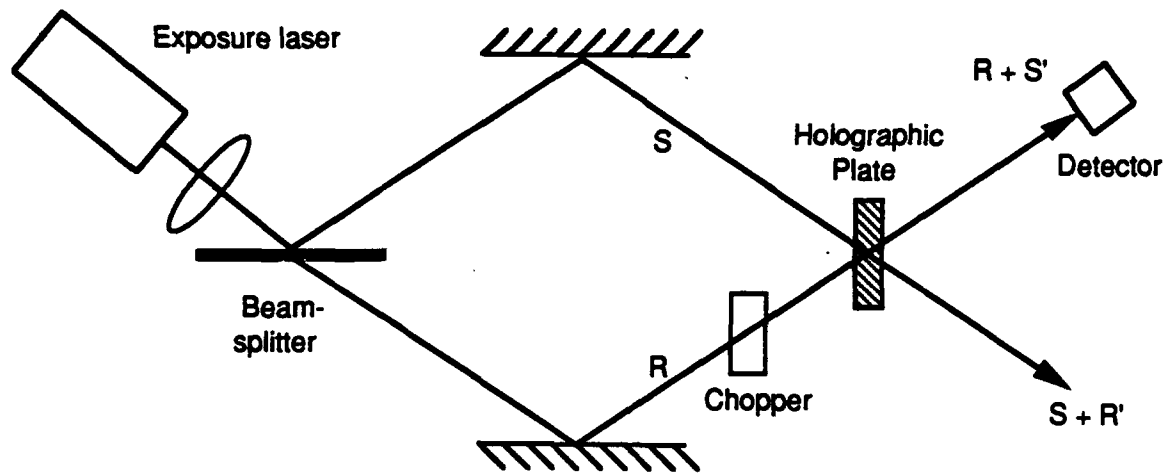
a)   Single wavelength hologram exposure and measurement
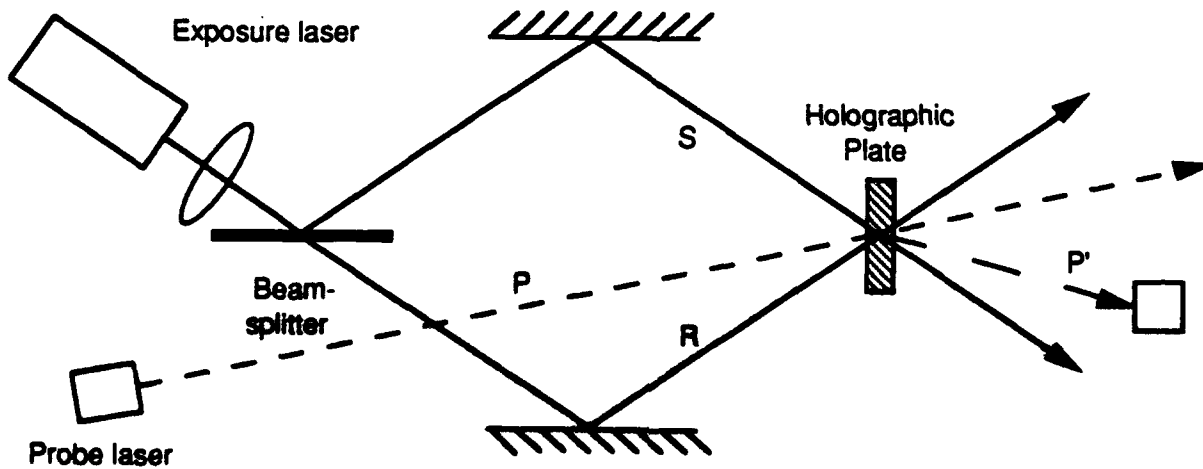
b)   Dual wavelength holographic exposure and measurement

Figure 5-1: Two techniques of real-time holographic grating measurement.

88

phase by $\pi/2$. Synchronous detection of the reference beam with a lock-in amplifier at frequencies ω and 2ω can be processed to give the amplitudes and signs of both the absorption and the phase gratings. The disadvantage of this technique is that sinusoidal modulation of the phase of the reference beam by m radians causes the interference pattern at the hologram to oscillate back and forth over a distance of $\Lambda m/\pi$, interfering somewhat with the normal grating growth process.

B. Grating Growth Measurement in Polaroid's DMP-128

The initial experiment to measure the evolution of the phase grating in DMP-128 was designed to be compatible with established techniques for the activation, exposure, and processing of DMP-128 holograms. Years of previous work with the photopolymer for the fabrication of holographic optical elements, optical interconnects, and matched filters for target recognition [18,19,20,21] has led to standard techniques, based on the processing steps recommended by the Polaroid researchers who developed the photopolymer.

Hologram recording with DMP-128 begins with the activation of the photopolymer. In this research, the photopolymer composition consisted of dry films of seven micron nominal thickness, spin-coated on 2"x2" glass plates. The dry film is smooth, glassy, and transparent, and generally is without visible defect, except for an occasional dust particle. When viewed in room light, the red-sensitive plates have a faint bluish cast, due to the methylene blue sensitizing dye. The film is stored in dry air (less than 20% relative humidity) over a dessicant, and must be activated by absorbing water from the air before it is sensitive to light.

The activation occurs in a small box held at a constant 51% relative humidity. A number of saturated salt solutions are known that equilibriate the air above them to a constant value of relative humidity [137]. At room temperature, the 51% relative humidity is maintained by a saturated solution of $Ca(NO_3)_2 \cdot 4H_2O$ in the bottom of the box. The plate is placed in a holder above the solution, and a small fan circulates the air within the activation chamber to maintain a uniform humidity. Experience has indicated that 10 minutes is a suitable activation time. If the humidity during activation is too low, the resulting holograms will be weak or non-existent; if the humidity is too high, the finished hologram emulsion will be cracked, crazed, and hazy. During subsequent exposure and processing, it is best if relative humidity in the laboratory is maintained at or near 51%, or if the plate can be sealed to prevent exchange of moisture with the air. In this research, the optical table was surrounded by a wooden framework covered with opaque plastic sheeting to form a humidor box. Relative humidity was maintained by means of humidifiers and dehumidifiers within the humidor. Humidity was one of the most important and least well-controlled variables in this work. Details on the accurate measurement of relative humidity can be found in Appendix B.

Following activation, the plate is sensitive to light, but the red-sensitive plates used in this work allowed the use of a blue-green safelight. The plate is positioned for the exposure of transmission holograms in a holder that is shown in Figure 5-2. The holder consists of a small Plexiglass stage with a glass backing mounted vertically on the rear of the stage. In previous work, the backing plate had been opaque blue glass to absorb red

89

light, thus minimizing unintentional reflection holograms. However, it became necessary to use clear glass, since the point was to measure the light diffracted from the grating during exposure. A small well at the back of the stage holds a few drops of the clear organic liquid xylene. As shown in the figure, the holographic plate is put into the well with the photopolymer film against the backing. As the plate is slowly pushed flat against the backing, a thin film of xylene is drawn up to form a continuous layer between the two. The xylene serves two purposes. First, it isolates the photopolymer film from exchanging moisture with the air, and secondly, it serves as an index matching fluid between the photopolymer and the backing, reducing reflections from the photopolymer-glass interface that might result in spurious reflection gratings being formed.
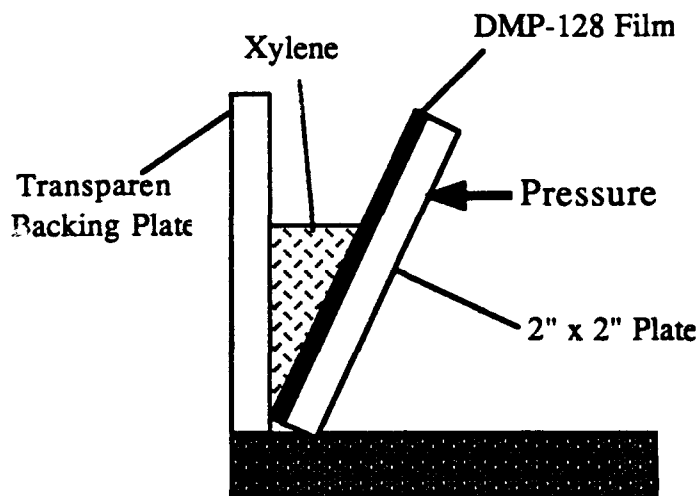
Figure 5-2: Wet mounting of DMP-128 to backing plate.

Once the plate is in place, the holographic exposure can begin. After exposure, the plate is illuminated with the light of a 75 watt incandescent bulb from a distance of one foot. This flood exposure serves to polymerize all remaining monomer in the photopolymer. At this point, the recorded grating is very weak and barely visible. The plate is removed from the backing and bathed in a developing solution consisting of methanol, isopropanol, and small amounts of water, glacial acetic acid, and zirconium acetate. The water and alcohols are solvents to extract lithium acrylate monomer and methylene blue dye from the photopolymer. The zirconium acetate promotes ionic cross-linking of the acrylate polymer [64]. The diffraction efficiency of the grating increases markedly after a few seconds in the developing bath. After a thorough rinse with distilled water, the plate is dried by suspending it in a column over the vapors of boiling isopropanol for one minute, and slowly removing it from the column back into air. At this point, the grating has become stable to normal room conditions. An optional step wil¹ increase the environmental stability of the hologram; the plate is dipped into a xylene solution of stearic acid, and then rinsed and dried as before. This optional bath forms a zirconium salt of stearic acid that resists moisture.

An experiment was devised to measure the growth of the DMP-128 grating during and after exposure while perturbing the established routine as little as possible.

Available equipment dictated the use of the single-wavelength technique shown in Figure 5-3. The laser was a Spectra-Physics 124B, with a nominal power output of 25 mW at 633 nm. The light from the laser was gated with a Uniblitz electrically actuated shutter (henceforth called the exposure shutter). After spatial filtering and collimation, the beamsplitter divides the light into object and reference waves. Polarizers were placed in the reference beam in order to equalize intensities and impose vertical polarization on both beams at the hologram recording stage, since equal intensities and polarizations maximize the fringe visibility of the holographic interference pattern. A second electrical shutter (henceforth called the reference shutter), capable of passing or blocking the reference beam was placed before the recording stage. A silicon photodetector, coupled to a Newport Research Corporation Model 880 optical power meter, was positioned in the path of the reference beam beyond the recording stage, such that it would also detect the diffracted conjugate wave when the reference was blocked. The operation of the experiment, to be described below, was controlled by a Zenith Z-100 microcomputer. The computer provided a precise digital clock, controlled the operation of the shutters, and digitized and recorded the amplified output of the photodetector.
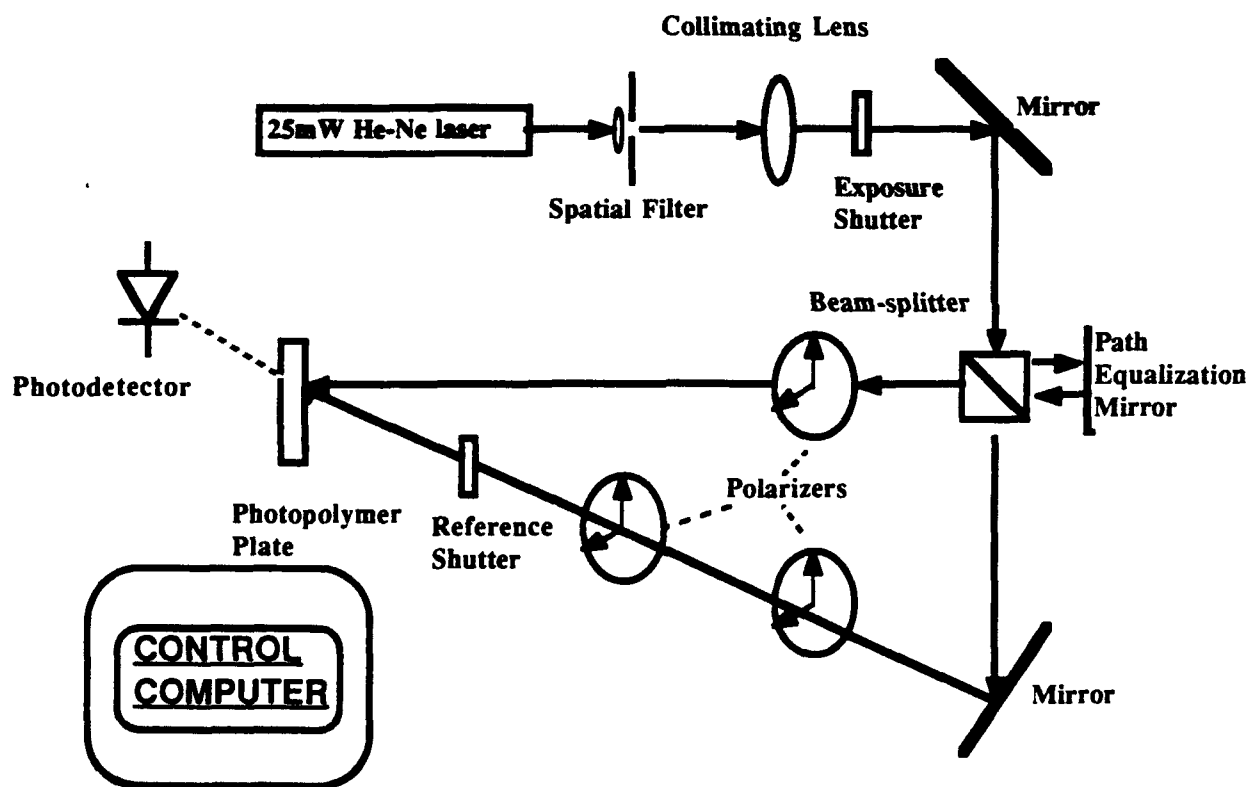
Figure 5-3: Single-wavelength set up for DMP-128 grating measurement.

The cycle of operation of the experiment closely emulated the standard operating procedure for DMP-128 hologram recording. The operation was divided into three phases [138], called exposure, cure, and flood, and is illustrated in Figure 5-4. During exposure, the exposure shutter was opened, and the reference shutter was normally open. Periodically, the reference shutter would close for a brief interval. During this interval, the

optical power diffracted from the object beam would be measured. The cure stage came next, after the end of the exposure. Recall that, in the standard procedure, a flood was supposed to immediately follow exposure. As a practical matter, the experimenter would take several seconds to set up the floodlamp, so it was thought best to simulate this interval of darkness in the experiment. One cannot keep a hologram completely in the dark and still measure the diffraction efficiency, but a workable compromise is to illuminate it with brief flashes of the object beam. This is done by keeping the reference shutter closed, and periodically opening the exposure shutter for a brief interval, while simultaneously measuring the diffracted power. Finally, in the flood phase, the reference shutter is kept closed, and the object shutter is kept open continuously to flood illuminate the grating while continuing to measure the diffracted power periodically.
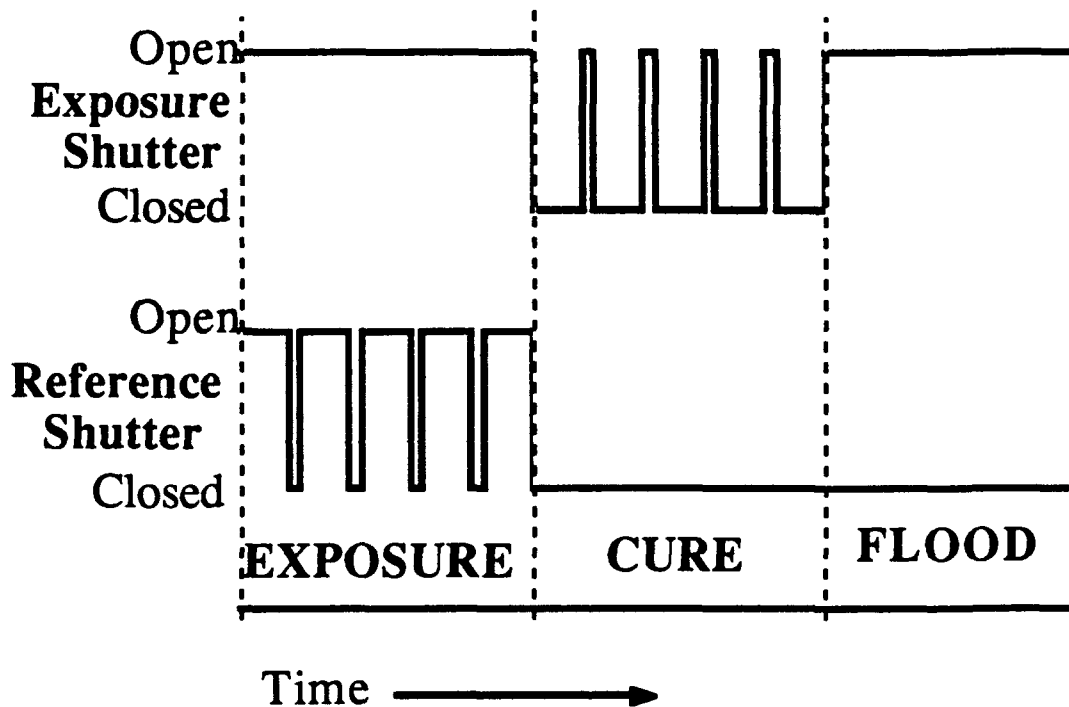
Figure 5-4: Cycle of operation for the single wavelength experiment.

In both the exposure and the cure phases it was important to keep shutter duty cycle low. During exposure, the fraction of time the reference beam is interrupted must be kept low in order to approximate a normal exposure. During cure, the larger the fraction of the time that the grating is illuminated, the less it can be said to be in darkness. It was found that the Uniblitz shutters could reliably flash off or on for intervals as short as two milliseconds. However, recall that during exposure, the photodetector was exposed to the full power of the reference beam (generally about 1 mW) and then asked to measure the power diffracted from the object beam (often much less than 1 μW). In order to have sufficient sensitivity for the measurement, the amplifier was usually set to an output gain of 1 volt (output)/1 μW (input), or sometimes 1V/10 μW. In either case, the amplifier was always saturated when the reference beam was incident on the photodetector, and required

92

several milliseconds to return to normal operation. Therefore, during exposure, the reference beam would be interrupted by the shutter for 10 msec, and the measurement would be taken near the end of the 10 msec interval. A sampling rate of one measurement every 200 msec was usually sufficient to follow the evolution of the DMP-128 grating, so the duty cycle of the interruption was only 5%. Likewise, in the cure phase, the hologram was illuminated with one, 10 msec flash every 200 msec, for an on duty cycle of 5%.

The method just outlined worked well initially. Figure 5-5 shows the first data taken with this method. It represents the evolution of four holographic gratings recorded at different locations on a single DMP-128 photopolymer plate. Object and reference beam intensities were both 1.9 mW/cm^2, and the grating period Λ was 2.50 μm. The four traces represent the growth of diffraction efficiency for four exposures that were (from bottom to top) 1,2,4, and 8 seconds in duration. The exposures were chosen to bracket the normal exposure energy for transmission holograms, 5 to 10 mJ/cm. In each case, diffraction efficiency rises linearly during exposure. Each exposure is followed by a 15 second cure, during which the efficiency declines monotonically, and a 60 second flood. The decline in efficiency usually appeared to reach an asymptote at the end of the cure, but the decline resumed when the hologram was flooded with the light of the object beam.

These initial results seemed consistent with the intuitive model of photopolymer grating formation formulated by Colburn and Haines. The decay during the cure phase looked as though it might be consistent with the exponential decline of a free diffusion process, while the further decline during flood illumination could be associated with the reduction of phase grating contrast as all remaining monomer is polymerized. The next logical step was to measure the evolution of a large number of photopolymer gratings for various values of Λ, which could be adjusted by changing the angles between the object and reference beams, and then looking for changes in the time scale of the decay. The grating period Λ was not only the most easily controlled parameter of the experiment, but also, since diffusive decay time is quadratic with respect to Λ, a reasonable choice of grating periods between 1 and 25 μm would cause the diffusive time constant, if any, to vary by a factor of 625.

However, further experience with the experiment revealed problems that called for modifications to the original experimental plan. Figure 5-6 illustrates the results of an experiment that should have been similar to the case shown in Figure 5-5. Once again, four distinct gratings were written on one DMP-128 plate. Object and reference beams were at 1.70 mW/cm^2, and the grating period was 3.39 μm. All four exposures were identical: 10 second exposure, 15 second cure, and 60 second flood. Upon inspection, it appears that the curves are similar to what might be seen if the data of Figure 5-5 were modulated by a large quasi-periodic signal. Although it might appear that some type of Fourier processing might be able to filter out the periodic corruption and restore usable data, such efforts were fruitless.

The phenomenon illustrated in Figure 5-6 occurred often and unpredictably. Various possible noise sources were tested and discounted until it was realized that the modulation could be related to the wet mounting technique used to hold the photopolymer plate. One can see from Figure 5-2 that when the photopolymer plate is pressed tightly against the backing plate, it forms a multi-layer sandwich of glass, photopolymer, xylene,
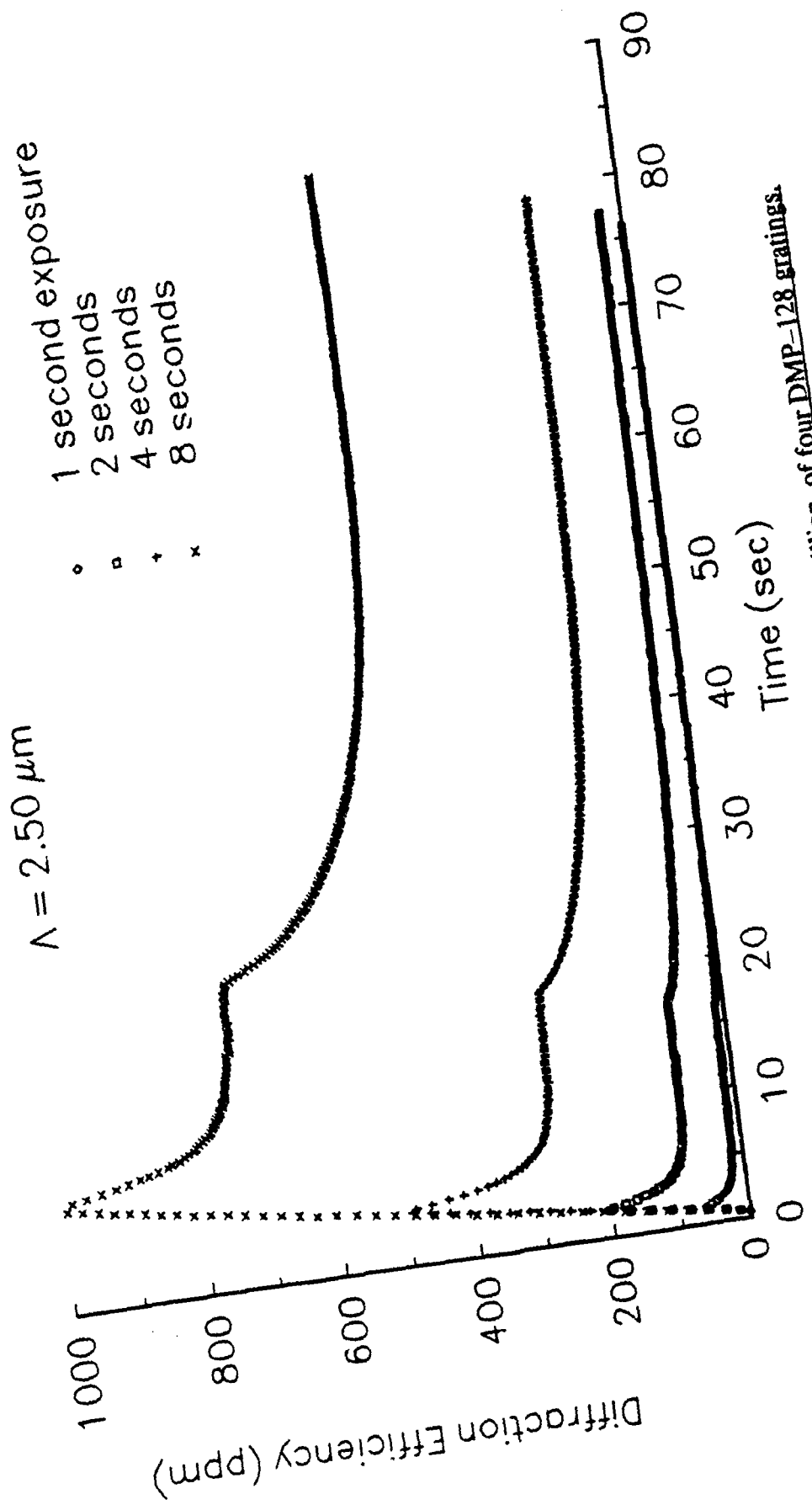
93

Figure 5-5: Evolution of diffraction efficiency, in parts per million, of four DMP-128 gratings.
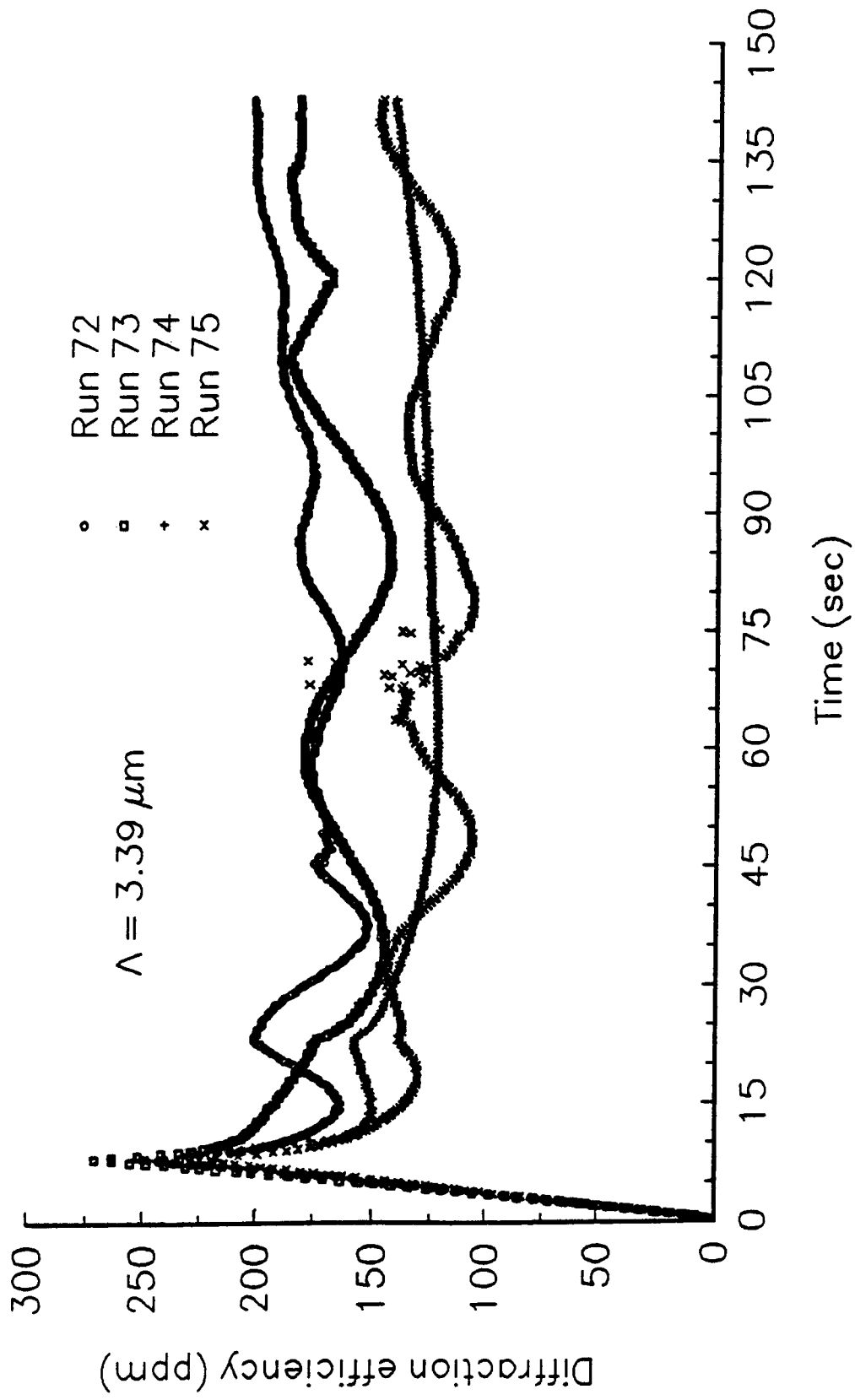
Figure 5-6: Four equal exposures on one plate, showing semi–periodic corruption.

and glass. Coherent reflections from the various interfaces will add up differently and alter the transmission if the thickness of any of the layers is changed, as in a Fabry-Perot etalon. It has been noted earlier that photopolymer films have been observed to change thickness upon exposure. Furthermore, sometimes considerable force was required to press the photopolymer plate against the backing plate, and the residual stress in the sandwich may have caused a creep or flow of the xylene layer during the experiment. Thereafter, all exposures were made with the photopolymer plate secured at its edges in a standard 2"x2" filter holder, with the photopolymer film facing away from the exposing beams. The gross periodic modulation seen in Figure 5-6 was not seen again. Unfortunately, this left the plate exposed to fluctuations in ambient humidity that occurred during an experiment. The humidity control equipment had to be shut off during holographic exposure, since it was a source of electrical noise and mechanical vibration of the optical table. The relative humidity could drift by several percent in the time that it took to expose and measure four holograms.

The single-wavelength technique for monitoring hologram growth finally had to be abandoned in this research because of a specific difficulty with some of the equipment, not a generic defect of the method. A problem was noticed that the measured diffracted light would periodically dip and then return to near its original value. The difficulty was traced to the laser. The output power of the laser was in fact dipping and then rebounding to its original level (which is something the laser did for several weeks before failing completely). To compensate for this, a second photodetector was added to the system to measure the power output of the laser, via an existing "ghost" reflection from a beamsplitter. The computer digitizer was capable of recording data sequentially from multiple channels, so the power level of the laser was recorded and used to normalize the measured diffracted power. However, normalization did not improve the signal to noise ratio of the data; on the contrary, the normalization degraded it.

The problem lay with the fact that there was a substantial time delay between each measurement of laser power and the corresponding measurement of diffracted energy. The situation is shown in Figure 5-7. The 10 msec electrical pulse that controls a single shutter actuation is shown, and the two measurement times marked. Recall that during exposure, when the reference shutter closes for 10 msec, the detector amplifier spends most of that interval coming out of saturation, and the measurement of diffracted power must take place toward the end of that interval. Therefore, the measurement of laser power on another channel must take place first, since the digitizing equipment could record different channels only sequentially, not simultaneously. There was an irreducible period of several milliseconds between the two, and the high frequency components of the noise and power fluctuations could change in that time. In other words, the noise at time t was uncorrelated with the noise at time t + 10 msec.

The obvious solution to this difficulty is to electrically filter the output of both photodetectors with an integrating, low-pass filter, with a cut-off frequency substantially below 100 Hz, since 100 Hz = (1/10 msec). However, the faithful reproduction and accurate measurement of the amplitude of a 10 msec pulse from the photodetector requires that the cutoff frequency be much higher than 100 Hz. The dilemma cannot be resolved in this case. Standard lock-in amplifier techniques are equivalent to averaging successive identical measurements to reduce noise, but the growth and decay of the grating assures that successive measurements cannot be assumed to be equal.
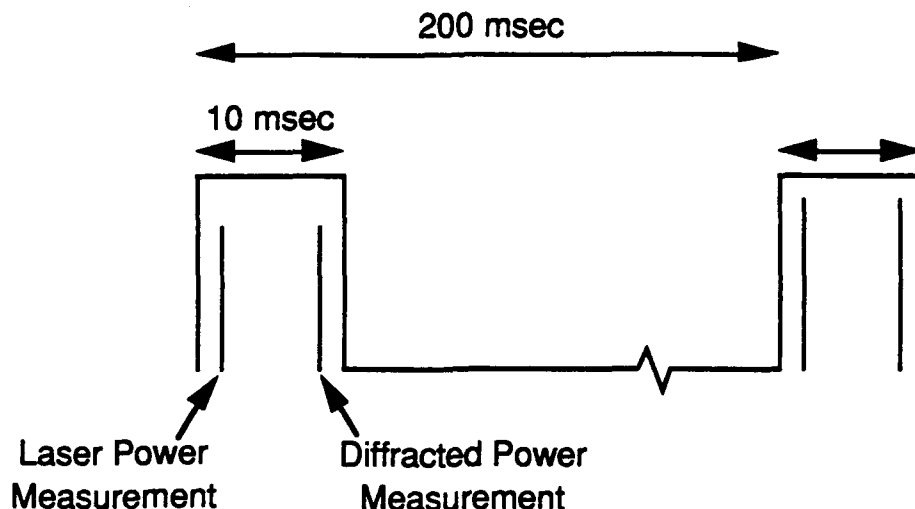
Figure 5-7: Timing of measurements relative to 10 millisecond shutter actuation.

The necessity of measuring laser power and diffracted power sequentially demanded an experiment that did not chop the signal into short, high-bandwidth pulses. The answer was to adopt the dual-wavelength technique for monitoring the grating. The probe beam stays on continuously during the experiment, and the outputs of the photodetectors that measure probe laser output power and diffracted probe power can both be filtered enough to remain correlated and allow normalization of laser power fluctuations, and still respond quickly enough to follow the dynamic behavior of the photopolymer grating.

The realization of the dual wavelength technique is shown in Figure 5-8. As before, a Spectra-Physics helium-neon laser was used to expose the red-sensitive photopolymer plates. An electrically actuated shutter in the He-Ne beam controls the exposure. The probe beam is the filtered, collimated, and attenuated output of a Spectra-Physics Model 165 argon-ion laser operated at 514 nm. The probe beam is also gated by an electrical shutter. One photodetector samples the output power of the argon-ion laser for normalization, and the signal photodetector measures the 514 nm radiation diffracted from the grating. A narrow bandpass optical interference filter in front of the signal photodetector passes the 514 nm radiation and blocks any 633 nm light that might be scattered or diffracted from the photopolymer film.

The cycle of operation of the dual-wavelength experiment is much simpler than the operation used in the single wavelength measurement. At the beginning of the exposure, the probe beam shutter opens first, to take a baseline measurement for zero diffraction efficiency. Then the exposure shutter opens to illuminate the photopolymer plate with the 633 nm holographic interference pattern. The exposure shutter closes to end the exposure. The probe beam remains on until the end of the cure phase. All the while, the digitizer is recording both the diffracted power and the argon-ion output power. The sampling rate is under computer control, but for most experiments the power was sampled five times a second. Unlike the previous experiment, there is no flood phase, since

97
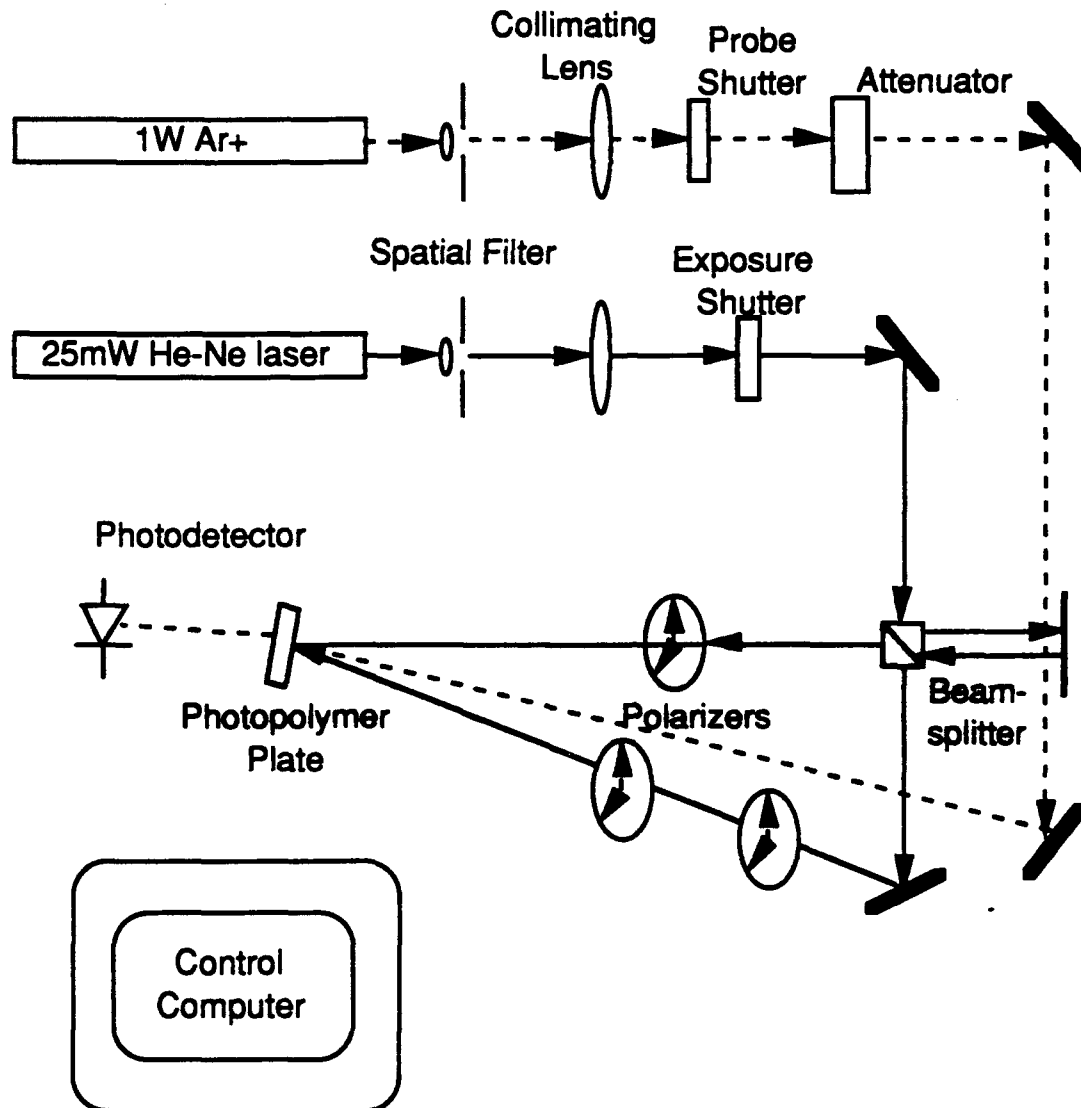
Figure 5-8: Optical layout of dual-wavelength measurement of grating formation.

continuous illumination by a weak (1 mW) 514 nm beam has no photochemical effect on the photopolymer. The only disadvantage of the dual-wavelength technique is that some care must be taken in determining the location of the first 514 nm diffracted order; in the single-wavelength method, the photodetector is just placed in the path of the reference beam.

The use of the dual-wavelength technique enabled the measurement of DMP-128 grating growth over a wide range of Λ, revealing a wide range of dynamic behavior. The grating period Λ was systematically varied from 25.4 μm down to 1.04 μm, which is almost a factor of 25 variation in grating period. Since the diffusion time τ varies quadratically with Λ,

any diffusive behavior in the grating formation should show a variation in time scale by a factor of nearly 625.

A cursory examination of the data lends credibility to the diffusion hypothesis. In Figure 5-5 one saw that the cure phase decay time at $\Lambda = 2.5$ μm was on the order of a few seconds. Figure 5-9 shows some quite different behavior which was typical of gratings recorded with a ten times greater (25.4 μm) periodicity. In this run, the intensities of the object and reference beams were both 2.7 mW/cm^2; the two traces shown represent an exposure of two seconds and an exposure of four seconds. In each case the diffraction efficiency appears to increase quadratically with time during the exposure, and then to increase more slowly after exposure. Typically the post-exposure growth would continue ever more slowly for several minutes after the exposure, though the microcomputer system could not log all of the data. The pre-development diffraction efficiency reached an amazingly high value of 2%, as opposed to more typical values of 0.1% for small values of Λ.

If it is assumed that the diffusion coefficient is the same as for the results shown in Figure 5-5, one would expect the diffusion time for a 25.4 μm grating period to be on the order of several hundreds of seconds, much longer than the actual length of the measurement shown. Therefore, the growth seen after exposure has very little to do with diffusion, and is probably due to some polymerization associated with residual free radicals in the system. In the section on data analysis, it will be shown that this slow grating growth is consistent with a first-order decay of free radical concentration.

As the grating period was decreased, there was a trend in the behavior of the hologram growth curves. At $\Lambda = 8.47$ μm, as shown in Figure 5-10, three different exposures show a slight post-exposure growth of the grating, followed by a slow relaxation on the scale of roughly 200 seconds. At $\Lambda = 6.35$ μm, the decline in diffraction efficiency immediately follows exposure, and the decline has a shorter time scale, as shown in Figure 5-11. Figure 5-12 is representative of the grating evolution at $\Lambda = 2.67$ μm, where the time scale of the post-exposure decline appears to be on the order of five to ten seconds.

A number of measurements were also made for $\Lambda = 1.04$ μm, which in some cases showed a continuation of the trend, with post-exposure declines with a time scale of only one or two seconds. In other cases, however, the growth of the grating during the exposure was anomalous. The case shown in Figure 5-13 is particularly interesting. The diffraction efficiency rose to a peak, fell to zero (to within the measurement accuracy of the equipment), and rose to nearly the same peak value before declining again, all while the holographic exposure still continued. At the end of the exposure, the diffraction efficiency relaxed upward to an asymptote. With similar exposures, other gratings showed similar oscillations of the diffraction efficiency during exposure, though none of the other gratings appeared to vanish during or after exposure.

In addition to the systematic variation of the grating period, other experiments were performed to answer specific questions that arose in the course of the research. For example, although the high diffraction efficiency of developed DMP-128 holograms proved that the volume grating dominated any surface grating effects, it was desired to know how
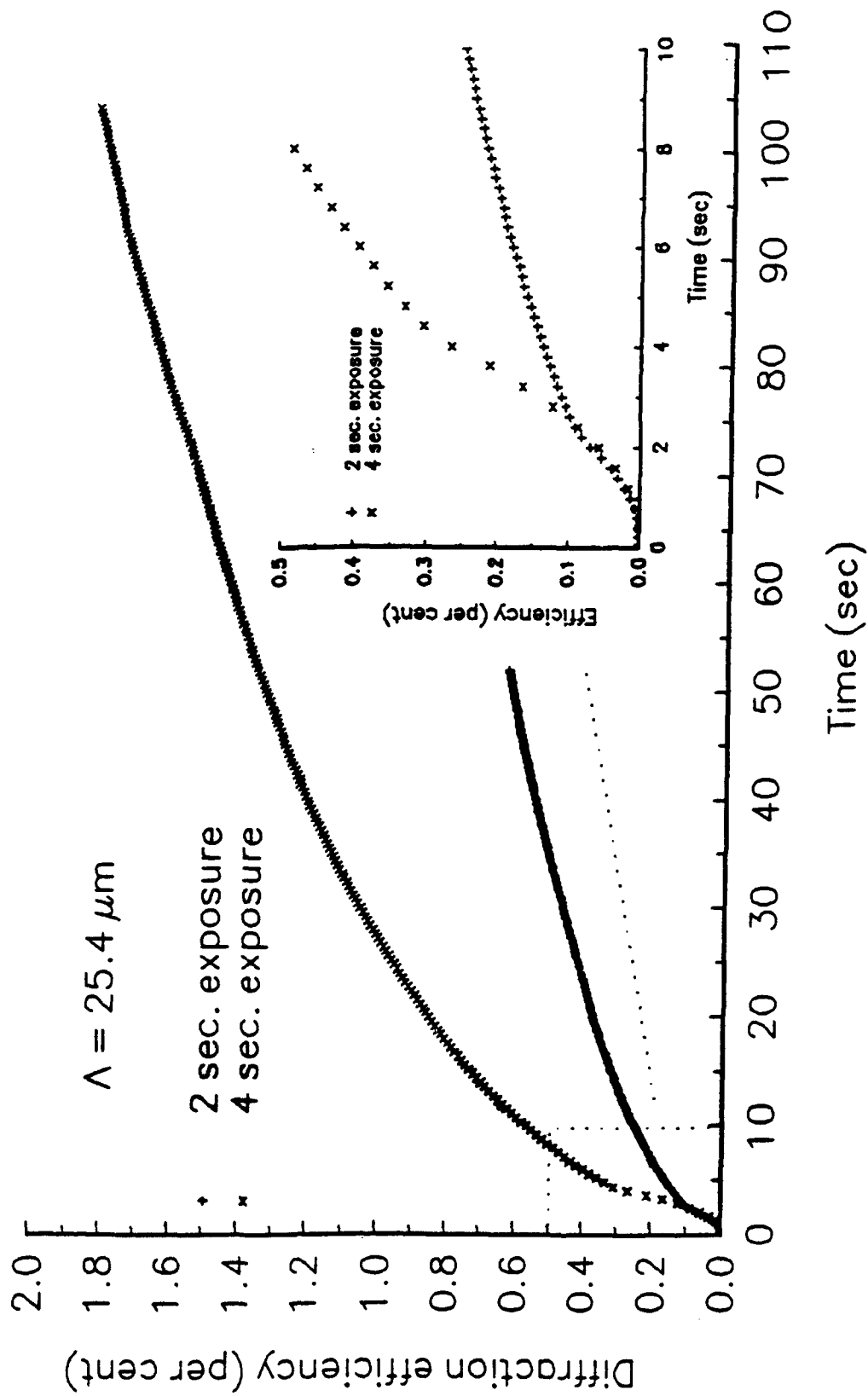
Figure 5-9: **Grating formation in 25.4 μm gratings, with exposure behavior detailed in inset.**
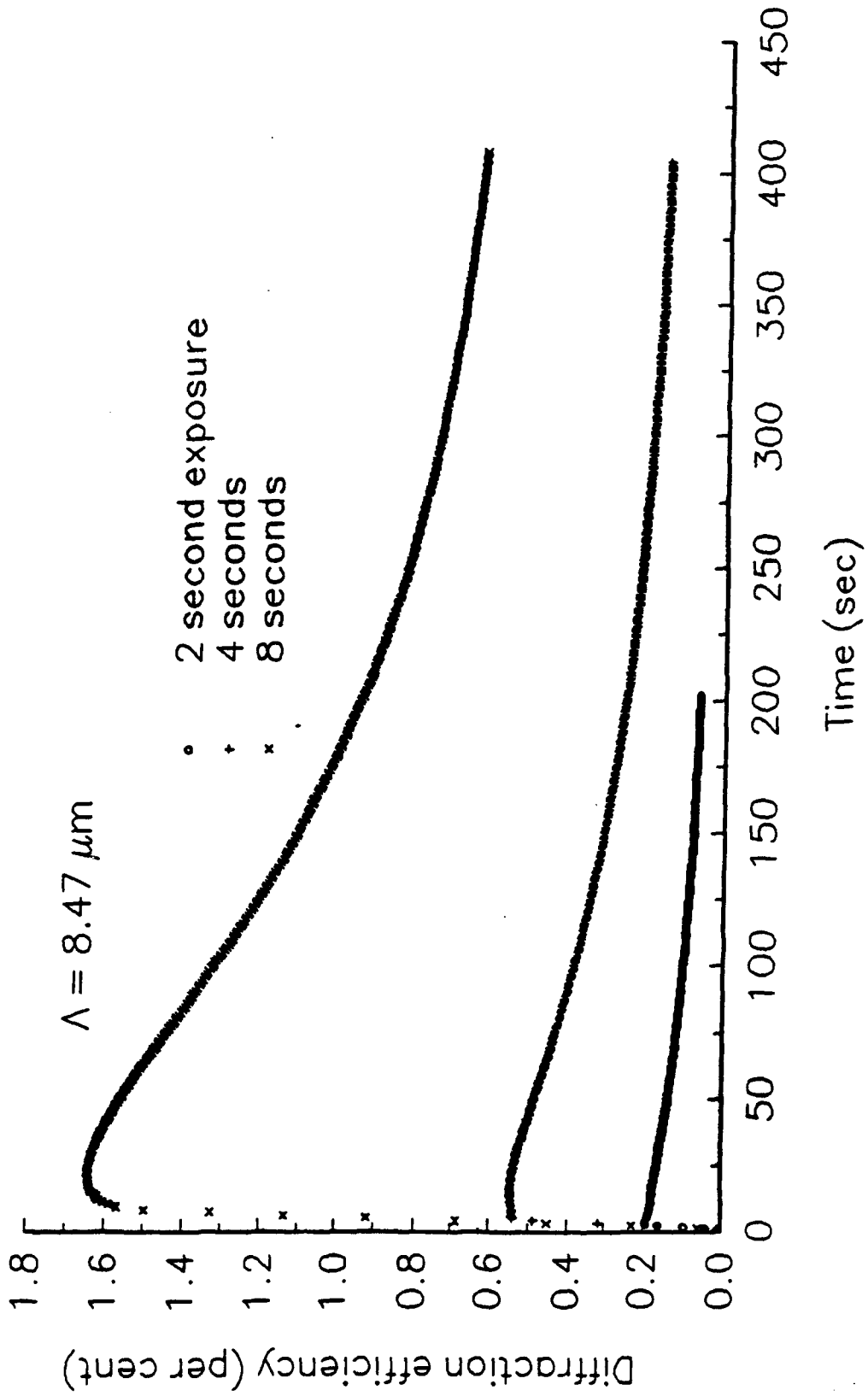
Figure 5-10: In 8.47 μm grating, efficiency increased slightly after exposure, then declined.
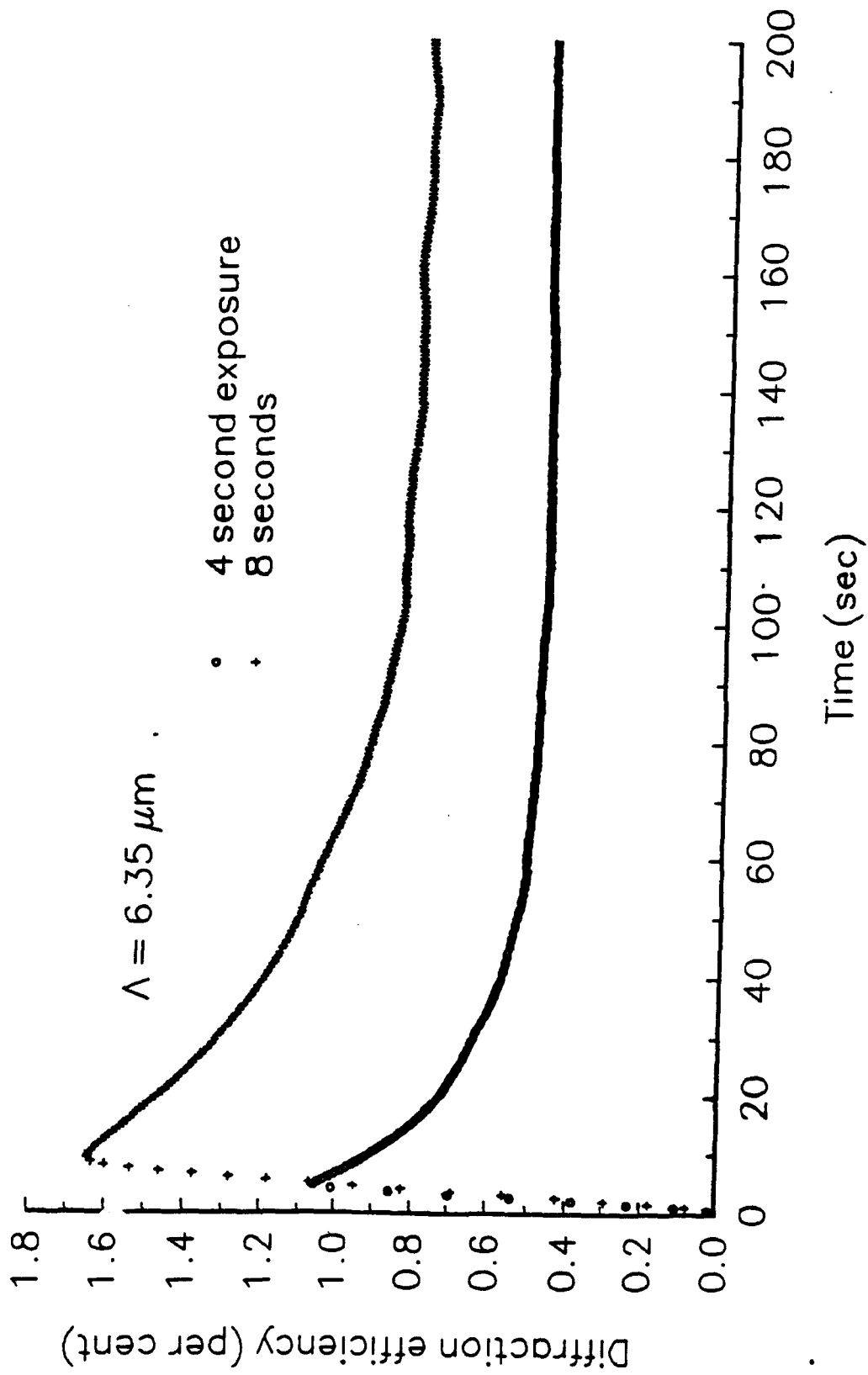
Figure 5-11: Post-exposure decline in efficiency was immediate for 6.35 μm grating.
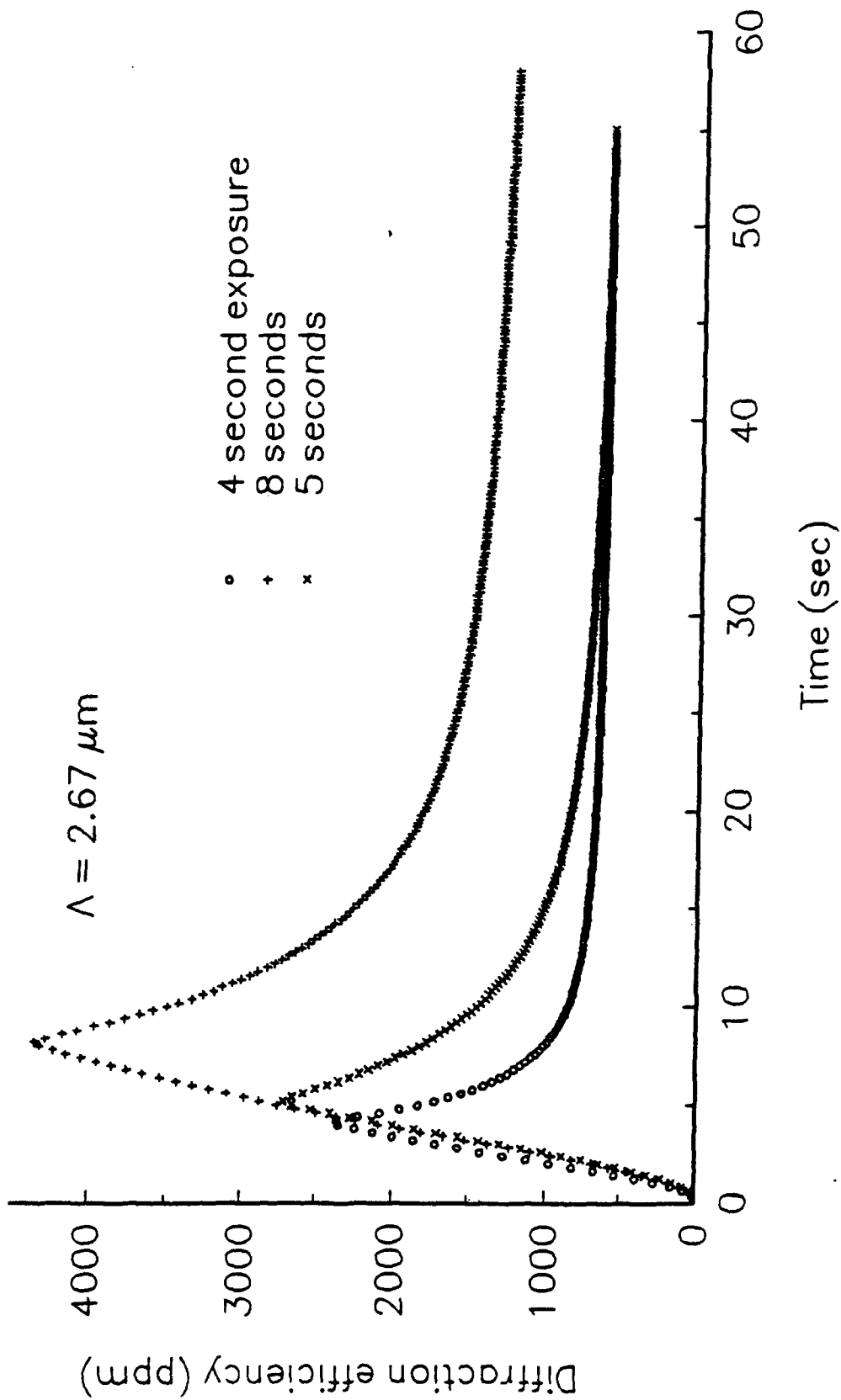
Figure 5-12: Characteristic decay time was on the order of seconds for 2.67 μm grating.
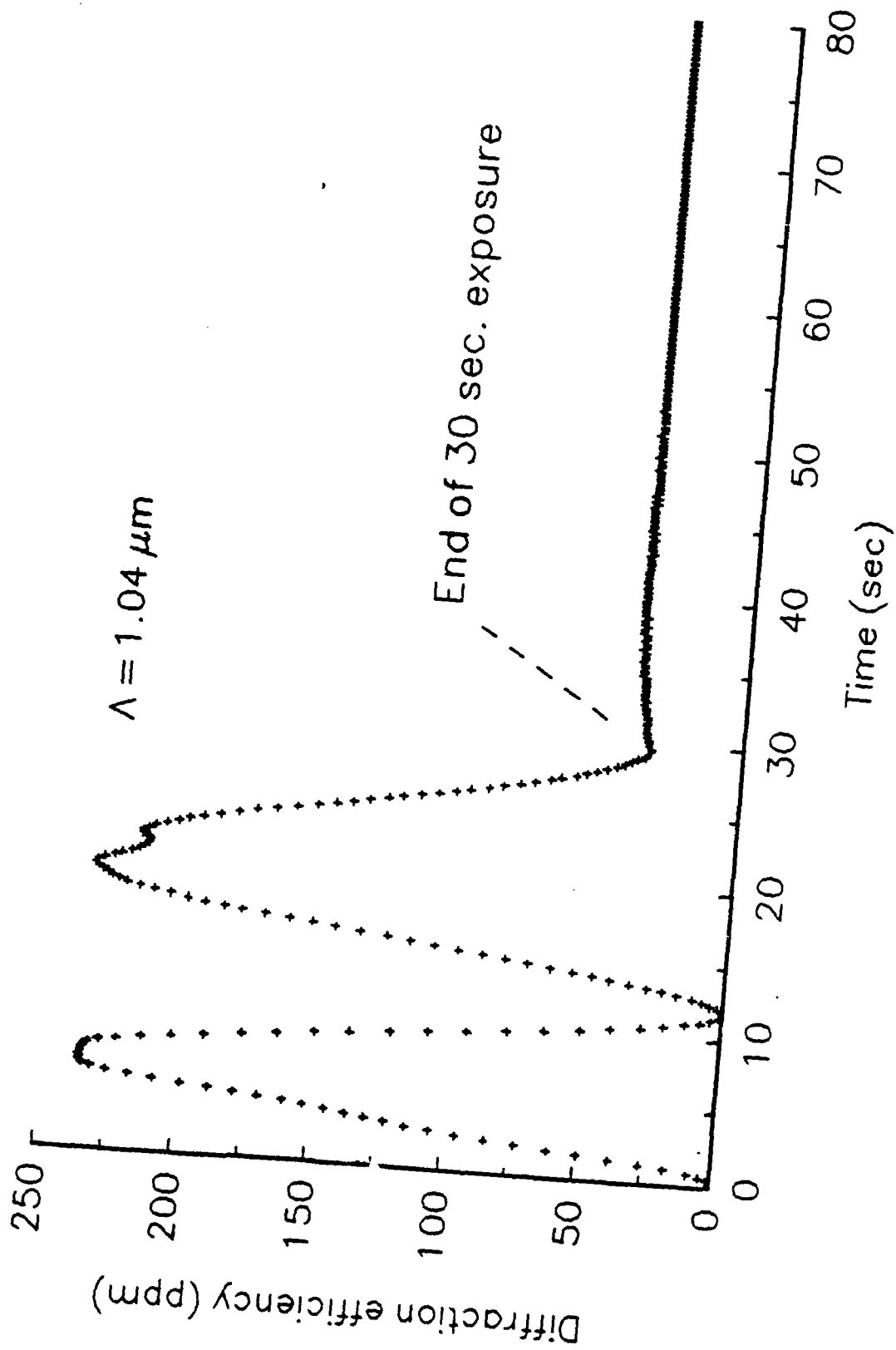
Figure 5-13: <u>A zero of efficiency and other anomalous behavior seen in 1.04 μm grating.</u>

much surface relief modulation there actually was. Dr. Jean Bennett, then at the UAH Center for Applied Optics, provided assistance in making profilometer measurements of the surface relief. Typical results are shown in Figure 5-14. The surface relief was roughly sinusoidal with the known period of the holographic grating, and usually had an amplitude of about 200 Å, or 0.02 μm. This corresponds to a shrinkage of the 7 μm emulsion by about 0.3%. The phase modulation of this surface relief grating, $\Delta nd/\lambda$, is on the order of 0.016. Using Equation 3-40 to calculate the first order Raman-Nath diffraction for small values of the phase modulation, the expected diffraction efficiency of the surface relief grating is on the order of $\eta = 6 \times 10^{-5}$.

The effect of the surface relief grating is negligible in the developed, high efficiency DMP-128 hologram, but what about during the measurement of holographic grating growth, where diffraction efficiencies were accurately measured in parts per million? To answer this question, the signal photodetector was moved to the other side of the holographic plate to measure the strength of the reflected first order. Generally, a surface relief grating will diffract light into backward as well as forward orders, while an unslanted volume phase transmission hologram of the type recorded here will only diffract energy into the forward direction [95]. Therefore, a strong reflected order would have been an indication of a significant surface relief grating during exposure. The result of this test is shown in Figure 5-15. The raw digitizer output is shown, and the discrete nature of the measurement is visible. A unit change of the digitizer output corresponds roughly to 0.6 part per million (ppm) of diffraction efficiency. The signal seems to rise slightly during the 20 second exposure, and then quickly returns to the background level. The forward diffracted signal under identical exposure conditions was greater by a factor of 200. Therefore, the formation of a surface relief grating, if any, was at most a very small perturbation to the measured diffraction in this research.

Another specific question led to an interesting experimental result regarding the continual post-exposure increase of diffraction efficiency in the 25.4 μm gratings. It was thought that an intense bright flash of light might serve to exhaust all of the photochemical reactants in the system and stabilize the diffraction efficiency. A normal 20 second exposure of a 25.4 μm grating was made, and the diffraction efficiency was monitored continuously as the hologram was exposed to several flashes from a high-intensity Nikon camera flash, held just inches from the photopolymer plate. The result is shown in Figure 5-16. There is a jump and then a decline of efficiency with each flash, superimposed on the expected envelope of slow grating growth. In retrospect, it was realized that the high radical concentrations produced by a high-intensity flash are kinetically more favorable to radical termination reactions than to increased polymerization. The repeatable response to the flash is probably due to repeated bleaching and renewal of the colored state of the methylene blue dye in the photopolymer. Bleached methylene blue slowly oxidizes in air and returns to its colored state. This was often seen during the liquid bath development of the DMP-128 holograms. Colorless dye would leach out into the developing fluid, and then the fluid would turn blue as the dye oxidized.

.
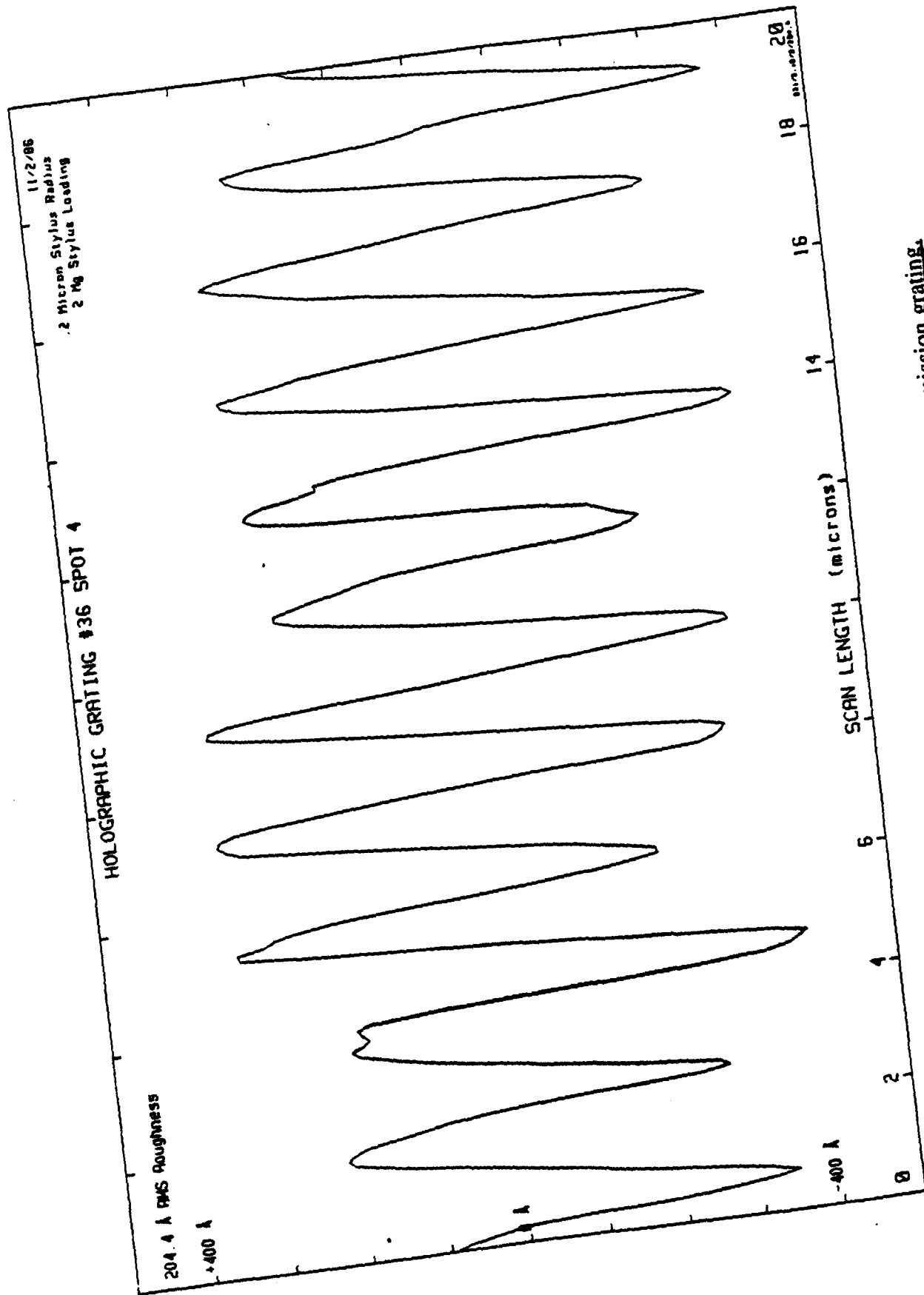
Figure 5-14: Surface profile of a typical DMP-128 transmission grating.

$\Lambda = 3.46 \ \mu m$
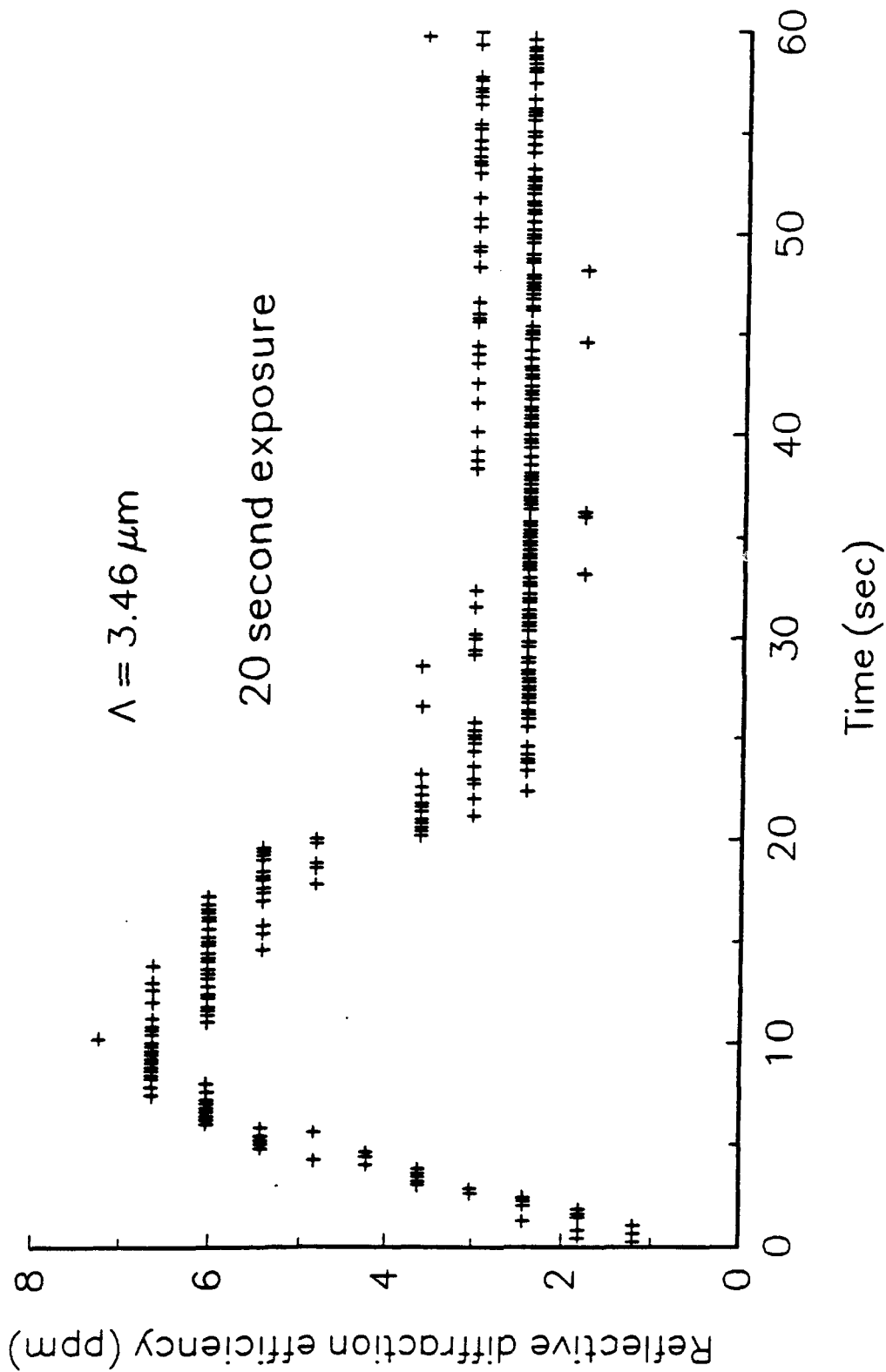
20 second exposure

Figure 5-15: First reflected order from DMP-128 grating indicated negligible surface relief effects.
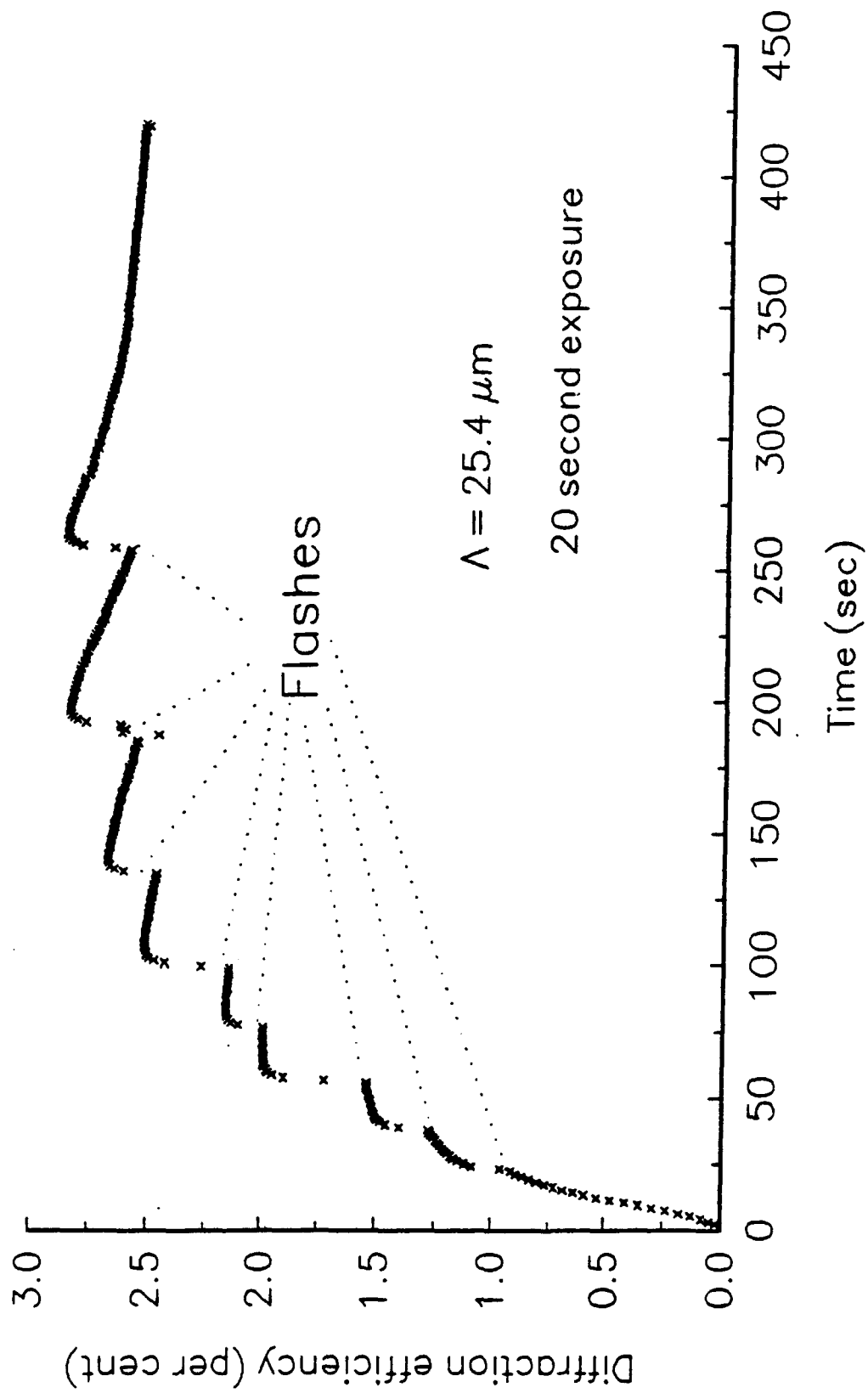
Figure 5-16: Effect of repeated post-exposure white light flashes on grating growth.

C. Data Analysis

A reading was taken from the signal detector at the beginning of each measurement of grating growth, in order to serve as a baseline value that was subtracted from all subsequent readings to zero out the effect of probe light scattered by the optics and the measurement bias of the detector. Also before each measurement, the strength of the probe beam and the fraction of the probe (argon-ion) laser power incident on the normalization detector was determined, in order to convert the measured power at the signal detector into a diffraction efficiency, adjusted for fluctuations of the laser power. It was noted earlier that corresponding signal and normalization measurements were made a few milliseconds apart, but each signal was low-pass filtered at 15 Hz before digitization, so the two were effectively correlated, and the high-frequency noise suppressed.

The measurement of the dynamics of the underlying phase grating was the goal of this research, not just the diffraction efficiency. In varying the grating spacing Λ over a wide range, holograms were produced that ranged in behavior from those that were clearly in the Raman-Nath regime (at 25.4 μm) to those that were clearly in the Bragg regime (at 1.04 μm). However, in either regime, the functional dependence of the diffraction efficiency on the amplitude of the index grating is similar. Equation 3-40 for the diffraction efficiency of a Raman-Nath grating, when the index modulation is small, can be written as

$$\eta = \frac{1}{4}\left(\frac{n_1 d}{\lambda}\right)^2 \tag{5-2}$$

where n_1 is the amplitude of the sinusoidal index modulation, d is the thickness of the transmission grating, and λ is the wavelength of the incident light. Likewise for small modulation in the Bragg regime, the diffraction efficiency is

$$\eta = v^2 = \left(\frac{\pi n_1 d}{\lambda \cos\theta}\right)^2 \tag{3-71}$$

where θ is the Bragg angle with respect to the normal. These equations indicate that for small values of the diffraction efficiency, the square root of diffraction efficiency is proportional to the index modulation.

Both equations 5-2 and 3-71 were derived from truncating everything but the first term of a power series expansion for, respectively, the first order Bessel function and the sine function. The assumption that the square root of diffraction efficiency accurately reflects the index modulation depends upon the higher terms of the power series expansion being negligibly small. In this research, the highest pre-development diffraction efficiency was about 2%, for the 25.4 μm Raman-Nath gratings. The exact expression for efficiency in the Raman-Nath regime is

$$\eta_q = \left[J_q\left(\frac{n_1 d}{\lambda}\right)\right]^2 \tag{3-38}$$

and the power series expansion for J_1 to two terms is

$$J_1(x) = \frac{x}{2}\left(1 - \frac{x^2}{8}\right) \qquad (5\text{-}3)$$

If $\eta = 0.02$, the largest value seen in this research, the error in neglecting the second term of the expansion is only 2×10^{-4}. For smaller diffraction efficiencies, the absolute and relative errors are even less. The error analysis is very similar for the Bragg regime, so one can safely take the square root of the diffraction efficiency as a measure of the strength of the underlying phase gratings measured in this research.

The evolution of the diffraction efficiency for the large period (25.4 μm) gratings was puzzling at first because instead of the rise and decay seen in other data, the efficiency only increased with time. The analysis of this data could be simplified if, as suggested in the last section, the diffusion time-scale was much longer than the duration of the experiment, which seemed consistent with the trend of the data. In that case, the post-exposure increase of diffraction efficiency had to be due solely to a continued photochemical reaction within the photopolymer medium. Recall from Chapter Two that the rate of polymerization v_p, which is also known as the rate of propagation, depends jointly on the monomer concentration [M] and the free radical concentration [M·]

$$v_p \equiv - \left(\frac{d[M]}{dt}\right)_p = k_p [M][M\cdot] \qquad (2\text{-}4)$$

where k_p is a rate constant. Also, the time rate of change of the free radical concentration depends upon the termination reaction, in which free radicals join their unpaired electrons and neutralize each other. The termination rate is given by

$$v_t \equiv - \left(\frac{d[M\cdot]}{dt}\right)_t = k_t [M\cdot]^2 \qquad (2\text{-}7)$$

In deriving the photopolymerization reaction rate during exposure, the steady state condition was invoked, which was that the rate of termination (radical destruction) was exactly equal to the rate of initiation (radical creation). Now consider the chemical reactions taking place immediately after exposure when one can safely assume that the photochemical initiation rate is zero. In the post-exposure period, one starts with a fixed, finite amount of free radical, left over from the exposure, that destroys itself through the termination process, leading to an ever-declining rate of polymerization. However, the free radical concentration reflects the spatial periodicity of the illumination that produced it; a lot of radical in the bright fringes, little or none in the dark fringes. For ease of notation, let the

110

radical concentration [M·] be represented as r(t), a function of t. Then Equation 2-7 can be rewritten as

$$\int_{r_0}^{r} \frac{dr'}{r'^2} = -k_t \int_{t_0}^{t} dt' \qquad (5\text{-}4)$$

where r_0 and t_0 are the initial radical concentration and initial time. The expression can be integrated to yield the radical concentration as a function of time

$$r(t) = \frac{1}{k_t(t - t_0) + \dfrac{1}{r_0}} \qquad (5\text{-}5)$$

If the initial radical concentration r_0 is large, and if we set the initial time $t_0 = 0$, one can see that as time increases, the radical concentration varies as $1/t$. Equation 2-4, the rate equation for polymerization, is still valid, so the rate of polymerization will also vary as $1/t$, where the end of the holographic exposure is defined as $t = 0$. The expression derived in Chapter Four for the change in refractive index of the photopolymer, Equation 4-33, can be adapted here. The assumption of very slow diffusion implies no mobility of monomer, so the loss of monomer at any point is exactly balanced by the increase in polymer, and the change of index is

$$\delta n(x,t) = \frac{(n^2 + 2)^2}{6n}(R_p - R_m) P(x,t) \qquad (5\text{-}6)$$

where $P(x,t)$ is the concentration of polymerized monomer molecules. Therefore, as the post-exposure polymerization continues, one would expect an increase in the index modulation proportional to the time-integrated polymerization rate, and a diffraction efficiency that increases quadratically with this index modulation.

Analysis of the growth curves of 25.4 μm DMP-128 gratings supports the conclusion that the post-exposure polymerization varies as $1/t$. Figure 5-17 is based upon the four second exposure, 25.4 μm grating growth curve shown originally in Figure 5-9. Figure 5-17 is an estimate of the time rate of change of the index modulation which was calculated by the finite differences of the square root of diffraction efficiency. In other words, the plotted values are

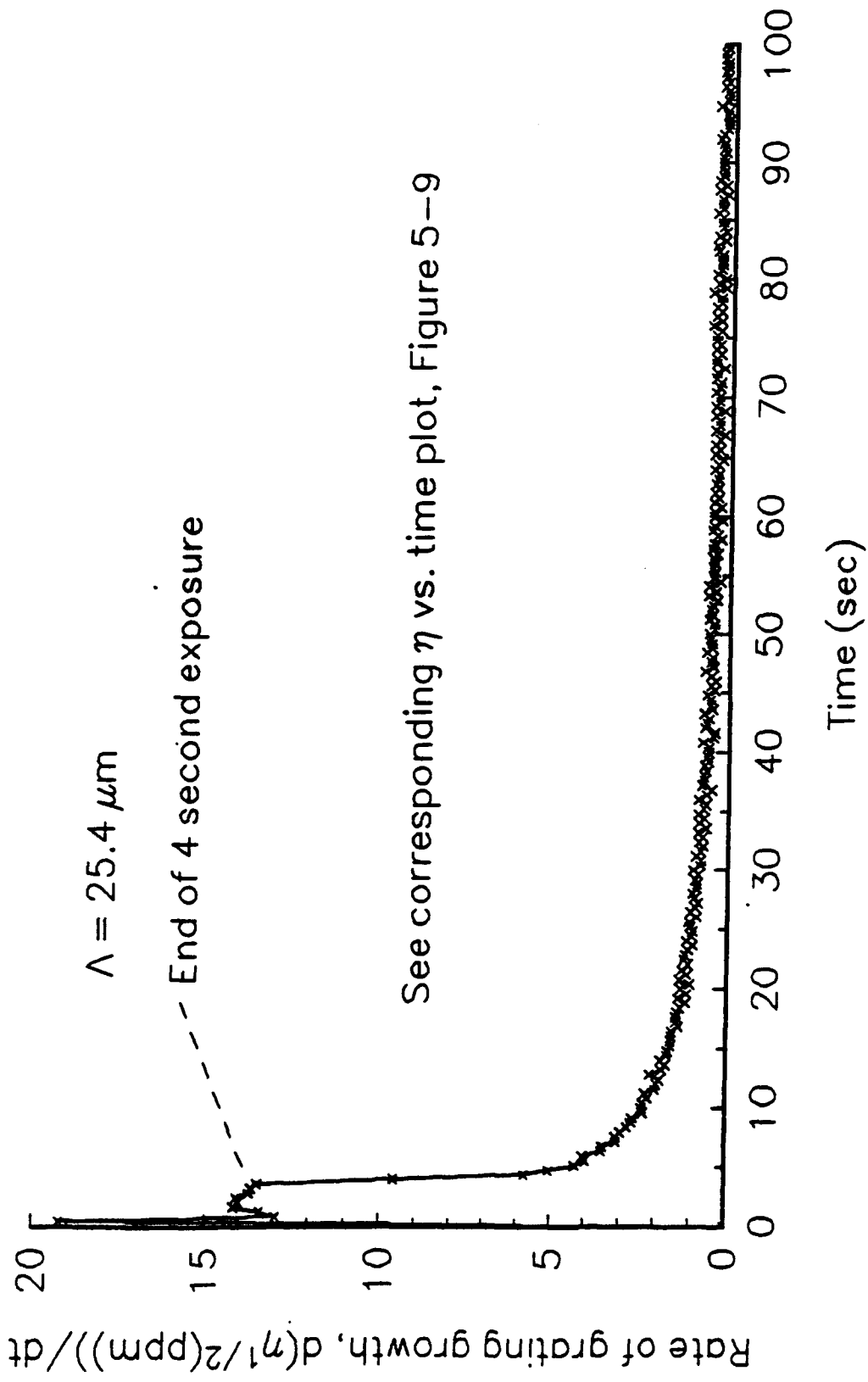$$\frac{d}{dt}\left(\frac{n_1 d}{\lambda}\right) \approx \frac{\sqrt{\eta(t + \Delta t)} - \sqrt{\eta(t)}}{\Delta t} \qquad (5\text{-}7)$$

111

Figure 5-17: <u>Finite differences estimate of grating growth rate in 25.4 μm grating</u>

where Δt is the sampling interval of the experiment, 0.4 seconds in this measurement. The numerical differentiation of measured data is usually ill-advised, since it magnifies the effect of noise and random error, but here the noise is sufficiently low to make the exercise worthwhile. The plot shows that during the holographic exposure, the growth rate of the grating is very roughly constant, in accord with the steady state photopolymerization kinetics developed in Chapter Two. The rate of growth declines rapidly immediately after exposure, but does not altogether vanish even 100 seconds after exposure. The post-exposure grating growth is presented in a slightly different form in Figure 5-18. Here, the finite difference derivative approximation has been smoothed with a polynomial spline, and plotted on log-log scales. (This derivative approximation technique is known as the Savitzky-Golay algorithm [139].) If the growth rate of the index modulation varied as $1/t$, as one would expect from Equations 2-4, 5-5, and 5-6, then the slope of this line would be exactly negative one. In this case the slope is -0.93. A similar numerical analysis was performed for the other 25.4 μm gratings. When plotted on a log-log scale, the slope of the numerical derivative of grating growth ranged from -0.74 to -1.1, confirming that the post-exposure polymerization rate varies approximately as $1/t$. Since the polymerization is irreversible, the post-exposure index modulation builds up as the time integral of the reaction rate (roughly proportional to $\log(t)$), and the square of this index modulation is seen as the ever-increasing diffraction efficiency of the grating.

The next task of data analysis was to turn to the small-period gratings and attempt to derive diffusion coefficients from the characteristic decay of the grating seen after exposure. Decay curves like those shown in Figures 5-11 or 5-12 appear as though they could plausibly be represented by a decaying exponential plus a constant, but this did not prove to be the case. Figure 5-19 is a plot of the post-exposure decay for a 2.67 μm grating; it is in fact the decay curve that follows the five-second exposure in Figure 5-12. Figure 5-19 portrays the square root of diffraction efficiency of the post-exposure decay on a logarithmic scale, after a constant representing the terminal value of the decay was subtracted out. If the decay of the index grating were well-represented by a single exponential, this data would fall along a straight line. Instead, the data follow one straight line indicating a short decay constant at first, and later follow another straight line indicating a long decay constant. This suggests that the decay of the holographic phase grating can be represented as the sum of two exponentials with different decay times, plus a constant, or

$$\sqrt{\eta} = A \exp\left(-\frac{t}{\tau_A}\right) + B \exp\left(-\frac{t}{\tau_B}\right) + C \qquad (5\text{-}8)$$

Fitting data to Equation 5-8 is very similar to the problem in radiochemistry of determining the concentrations (A,B) and lifetimes (τ_A,τ_B) of two unknown radioactive species, solely from the evolution of the total activity over time; C is always zero in this problem. A standard text on radiochemistry [140] outlines a construction much like that shown in Figure 5-19; plot the activity on a log scale, and construct lines tangent to the curve both at short and long times. The authors suggest that for actual experimental data, this procedure will not work well unless the two exponential decay times differ by more than an order of magnitude. For many practical problems in radiochemistry, there are further constraints that ease the fitting problem; for example, one radioactive species may be a known "daughter" of another "parent" radioactive species. In his book on numerical
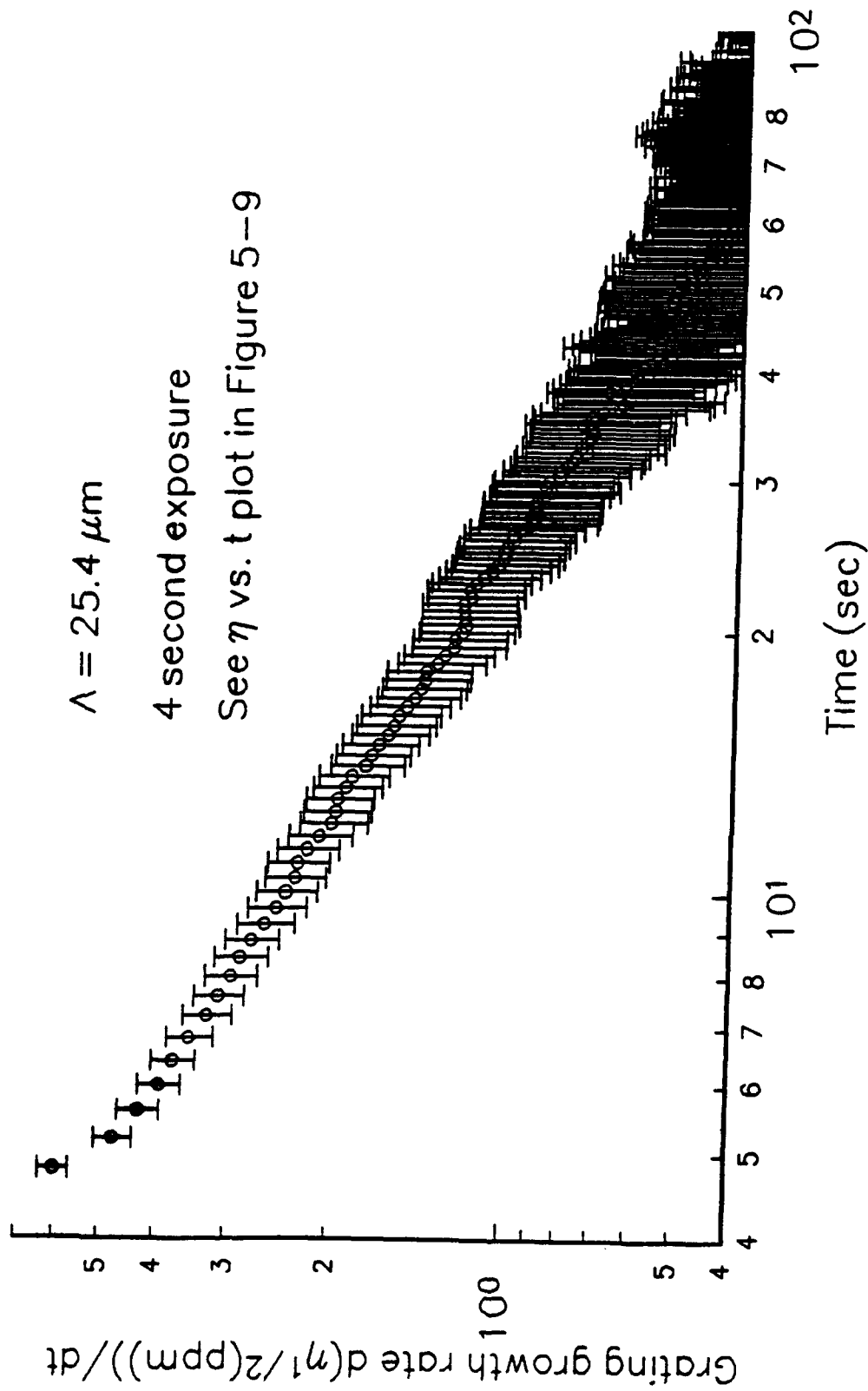
Figure 5-18: Smoothed data indicates (1/t) dependence of diffusionless grating growth.

$\Lambda = 25.4 \ \mu m$

4 second exposure

See η vs. t plot in Figure 5-9

114
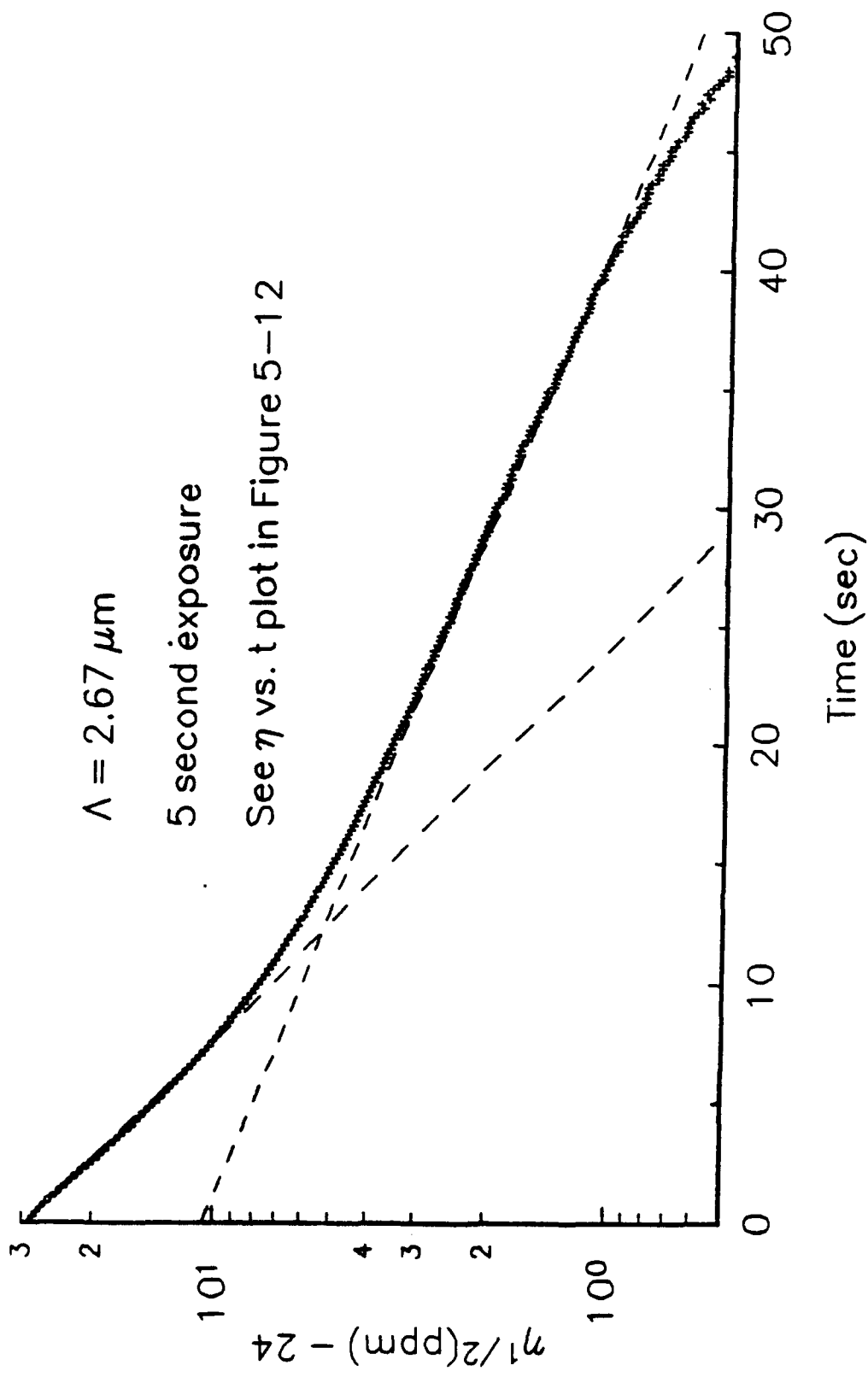
Figure 5-19: <u>Post-exposure efficiency decay seems to vary as a sum of two exponentials.</u>

The figure shows a plot with axis labels:
- x-axis: Time (sec)
- y-axis: $\eta^{1/2}(ppm) - 24$

Annotations on the plot:
- $\Lambda = 2.67 \ \mu m$
- 5 second exposure
- See η vs. t plot in Figure 5-12

analysis, Acton [141] is less sanguine about the prospects for fitting radioactive decay data as the sum of two exponentials. He states, "The answer to this problem lies in the chemical rather than the computer laboratory, and the sooner the hopeful innocent can be sent there and away from the computer room, the better off everyone will be. For it is well known that an exponential equation of this type in which all four parameters are to be fitted is *extremely* ill-conditioned. That is, there are many combinations of [the four parameters] that will fit most exact data quite well indeed (will you believe four significant figures?) and when experimental noise is thrown into the pot, the entire operation becomes hopeless."

Hopeless or not, the data still appeared to behave as a sum of two exponentials, and this functional form was consistent with a post-exposure diffusion of free components within the photopolymer. In the model developed in Chapter Four, it is assumed that exposure to the holographic interference pattern has induced a periodic, not necessarily sinusoidal, modulation of the monomer concentration u(x,t), which is taken to be the initial condition for the free diffusion taking place after exposure. The expression for the free diffusion is

$$\frac{\partial u(x,t)}{\partial t} - D\frac{\partial^2 u(x,t)}{\partial x^2} = 0 \qquad (4\text{-}12)$$

which is easily solved by separation of variables. The general solution is

$$u(x,t) = \sum_{n=0}^{\infty} h_n \cos\left(\frac{2\pi n x}{\Lambda}\right) \exp\left(-t/\tau_n\right) \qquad (5\text{-}9)$$

where

$$\tau_n = \frac{\Lambda^2}{4\pi^2 n^2 D} \qquad (5\text{-}10)$$

and the h_n are the coefficients of the cosine series representation of the initial monomer concentration.

As expected, diffusion causes the high spatial frequencies present in the monomer concentration profile to decay more quickly than the fundamental. However, Equation 5-9 is not the explanation for the multiple exponential decay constants seen in the data. In Equation 5-9, different decay times τ_n are associated with different grating periods Λ/n. In this research, only the first order diffraction of the fundamental grating period was measured. The presence of two different decay time-scales in this data suggests that two different components of the photopolymer with different diffusion coefficients were diffusing simultaneously.

Analysis of the decay data such as that shown in Figure 5-19 required an algorithm capable of fitting data to an equation that is non-linear with respect to its parameters. Equation 5-8 is linear with respect to A, B, and C, but it is non-linear with

116

respect to the time constants τ_A and τ_B. The goal of the fitting is to minimize the mean squared error between the fitting function and the measured data. The goal is the same for standard "least squares" techniques, but ordinary least squares routines are not suitable for the non-linear problem.

The fitting of the data to the model equation can be expressed as a minimization of the χ^2 ("chi-square") error [142]. Let the five parameters of the model equation 5-8 be represented by a five component vector a (i.e. $a(1) = A$, $a(2) = t_A$, etc.). The N measured data points $y_i = (\eta)^{1/2}$ are measured at equally spaced times t_i, and the standard deviation of the error at each point is σ_i. The corresponding values predicted by the model equation are $y(t_i;a)$. The chi-square error is

$$\chi^2 = \sum_{i=1}^{N} \left(\frac{y_i - y(t_i;a)}{\sigma_i} \right)^2 \qquad (5\text{-}11)$$

and the goal is to choose the parameters so as to minimize χ^2. The first critical step is to make a good estimate of the measurement errors σ_i. Early in this research, the random noise at the terminals of the computer digitizer was estimated at $\sigma = \pm 5$ millivolts, corresponding to a standard deviation of ± 4 digitizer units (5 volts = 4095 digitizer units). However, the low-pass filtering of the photodetector signals and normalization of the laser power reduced the noise substantially. Figure 5-20 shows a detail of one of the decay curves portrayed in Figure 5-9, with a best-fit straight line drawn in for reference. One can see that the measurement error is not, for the most part, due to random, Gaussian noise, but rather to the discreteness of the measurement. The digitizer has only a finite number of outputs, but the measured signal is continuous. Therefore, a simple model for the measurement error is that the error is random and uniformly distributed from -1/2 to +1/2 digitizer counts around the "true" value of the signal. A straightforward calculation of the standard deviation for this uniform distribution gives $\sigma = 0.3$ digitizer units. This is in agreement with the standard deviation of the data about the straight line fit. For each data set that was analyzed numerically, the last ten seconds of the end of the grating decay were fitted to a straight line in order to estimate the standard deviation of the error. The standard deviation varied from 0.3 digitizer units (the minimum possible) up to 1.0 digitizer units in some cases.

The first method used to fit the model Equation 5-8 is known as the Levenberg-Marquardt method [143,145]. It uses the analytic derivatives of the χ^2 function with respect to the fitting parameters to guide an iterative search for the set of parameters that will give the smallest χ^2. Unlike some other similar methods, it also gives an estimated error for each of the parameters. The problems associated with the model Equation 5-8, as predicted by Acton [141], soon became apparent. A careful graphical estimate of the initial values of the parameters was necessary in order to avoid unstable and bizarre answers. Even when results were reasonable, the errors estimated by the algorithm were not. In the units used here, all five parameters were of order 1 to 100. In a typical case, the terminal constant C was estimated to have a value of about 20 and an error of 0.1; the other four parameters
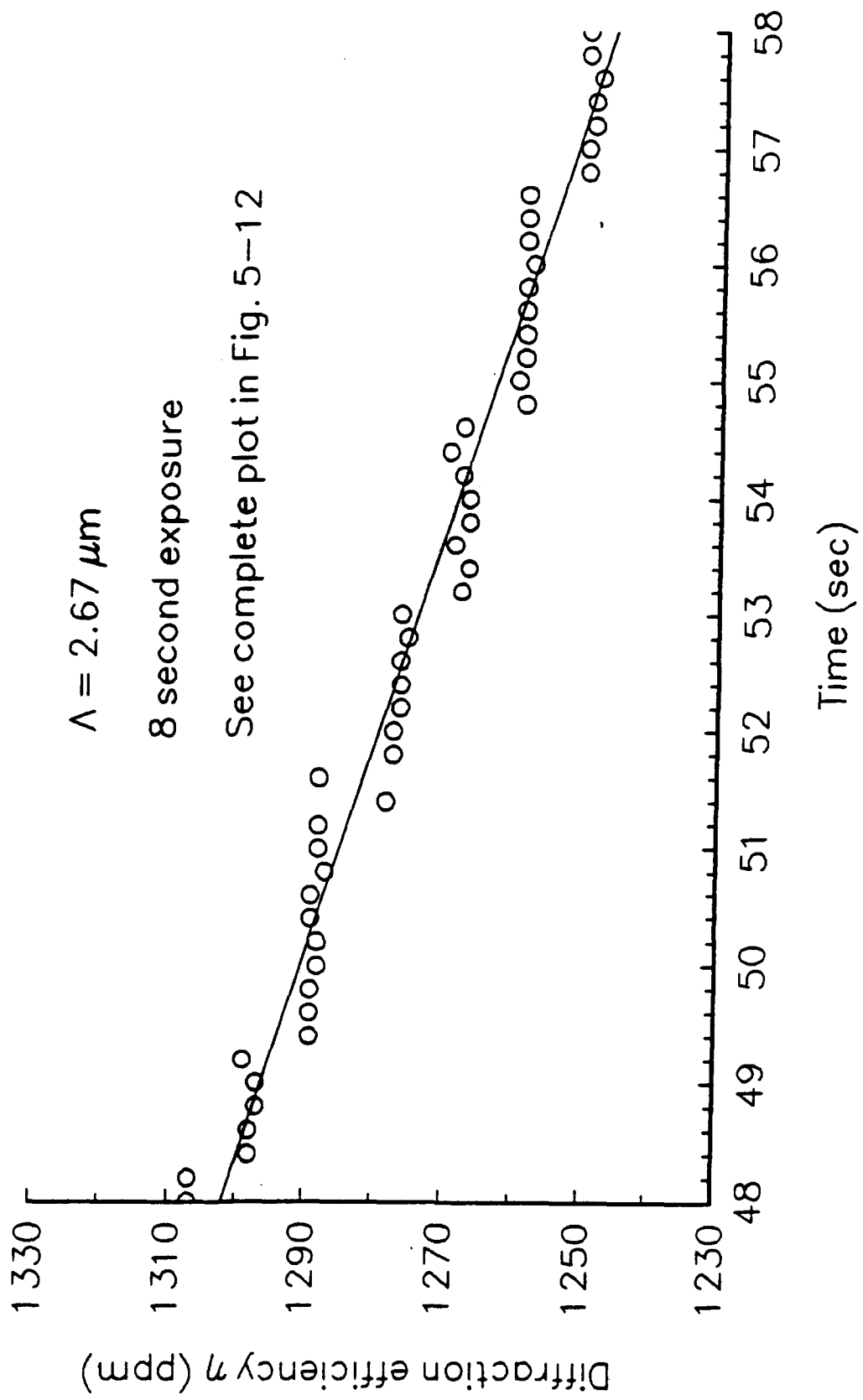
Figure 5-20: Measurement error shown to be dominated by digitizer discreteness.

118

were all of order 10, with estimated errors of 10^6. Often, the estimate of the error squared was a large negative number, which is clearly ridiculous. The use of double precision arithmetic only increased these spurious error estimates. This indicated a numerical instability. Essentially, it seems, the four exponential parameters were "competing" with each other to explain the same variations in the data.

The more stable Nelder-Mead algorithm, also called the downhill simplex method [144,146], gave more satisfactory results. The simplex method generally found lower values of χ^2 than the Levenberg-Marquardt method did with the same data. The price was an increase in computer time, and the lack of any error estimate on the parameters. Table 5-1 summarizes the results of this data fitting exercise for six holographic gratings made at two different grating periods. The table lists the grating spacing Λ, the decay times τ_A and τ_B, and the estimated diffusion coefficients D_A and D_B associated with the two decay times, as well as the ratio of the diffusion coefficients. The diffusion coefficients were estimated using Equation 5-10 with n=1, since only the first diffracted order was measured in this investigation.

TABLE 5-1: Estimated Grating Decay Parameters and Diffusion Constants

Λ (μm)	τ_A (sec)	τ_B (sec)	D_A x 10^{10} (cm^2/sec)	D_B x 10^{11} (cm^2/sec)	D_A/D_B
2.67	2.307	14.03	7.83	12.87	6.08
2.67	5.114	35.63	3.47	5.07	6.86
2.67	5.230	33.26	3.45	5.43	6.35
1.04	.701	6.77	3.91	4.05	9.66
1.04	.919	6.13	2.98	4.47	6.67
1.04	.951	8.66	2.88	3.16	9.10

From these data, one can surmise that one species in the photopolymer medium diffuses with a diffusion coefficient of approximately 3×10^{-10} cm^2/sec, while a second optically sensitive species has a diffusion coefficient of about 5×10^{-11} cm^2/sec. The ratio of the mobilities of the two species is in the range of six to nine. The only plausible candidates for the two species are lithium acrylate monomer (molecular weight 74) and methylene blue sensitizing dye (molecular weight 320). The second, smaller diffusion coefficient must be associated with the more massive methylene blue molecule.

The theoretical model of photopolymer diffusion has detailed the means of phase grating formation in the monomer, but did not take into account the role of the dye in the formation of a transient grating. It was seen earlier, however, that the bleaching of the dye when exposed to light is significant. The holographic interference pattern must form an absorption grating in the dye by differential bleaching of the dark and the bright fringes. However, methylene blue dye is soluble in water, and free to diffuse in the moist DMP-128

119

photopolymer. If the dye diffusion time is short, the diffusion will gradually eliminate the absorption grating. If the dye diffusion time is long, the absorption grating will disappear anyway as the bleached dye re-oxidizes.

A final goal of the data analysis was to tie together the observation of post-exposure polymerization seen in large period gratings, as compared to the diffusive behavior seen in short period gratings. The model for the rates was the 4 second exposure of a 25.4 μm grating, whose grating growth rate was previously discussed and illustrated in Figures 5-17 and 5-18. For a diffraction efficiency expressed in parts per million (ppm), the grating growth rate during the 4 second holographic exposure can be empirically approximated as

$$\frac{d\sqrt{\eta}}{dt} = 14 \ (ppm)^{1/2} \ sec^{1} \qquad (5\text{-}12)$$

and the continued grating growth after exposure (t > 4 seconds) can be approximated as

$$\frac{d\sqrt{\eta}}{dt} = \frac{16}{t - 2.857} \ (ppm)^{1/2} \ sec^{1} \qquad (5\text{-}13)$$

Integration of these rates leads to a fair approximation of the 25.4 μm grating growth, as shown in Figure 5-21. In this simple simulation, there was no diffusion, so the diffusion time was effectively infinite.

The addition of diffusion to the simulation reveals a problem previously overlooked. From Equation 4-33, one can write the index grating δn as

$$\delta n \ \frac{6n}{\left(n^2 + 2\right)^2} = R_m u(x,t) + R_p P(x,t) \qquad (5\text{-}14)$$

where, as before, u represents the monomer concentration and P represents the polymer concentration. In the absence of diffusion, or in an exposure that is short compared to the characteristic diffusion time, an increase in polymer concentration is exactly matched by a decrease in monomer concentration, so P = - u, and

$$\delta n \ \frac{6n}{\left(n^2 + 2\right)^2} = \left(R_p - R_m\right) P(x,t) \qquad (5\text{-}15)$$

$R_p - R_m$ is a small negative quantity, equal to approximately $0.1 * R_p$ for DMP-128. (This was calculated in Chapter Four, p.101.) However, after diffusion is complete, u(x,t) is a constant, so only the polymer concentration contributes to the final phase grating.

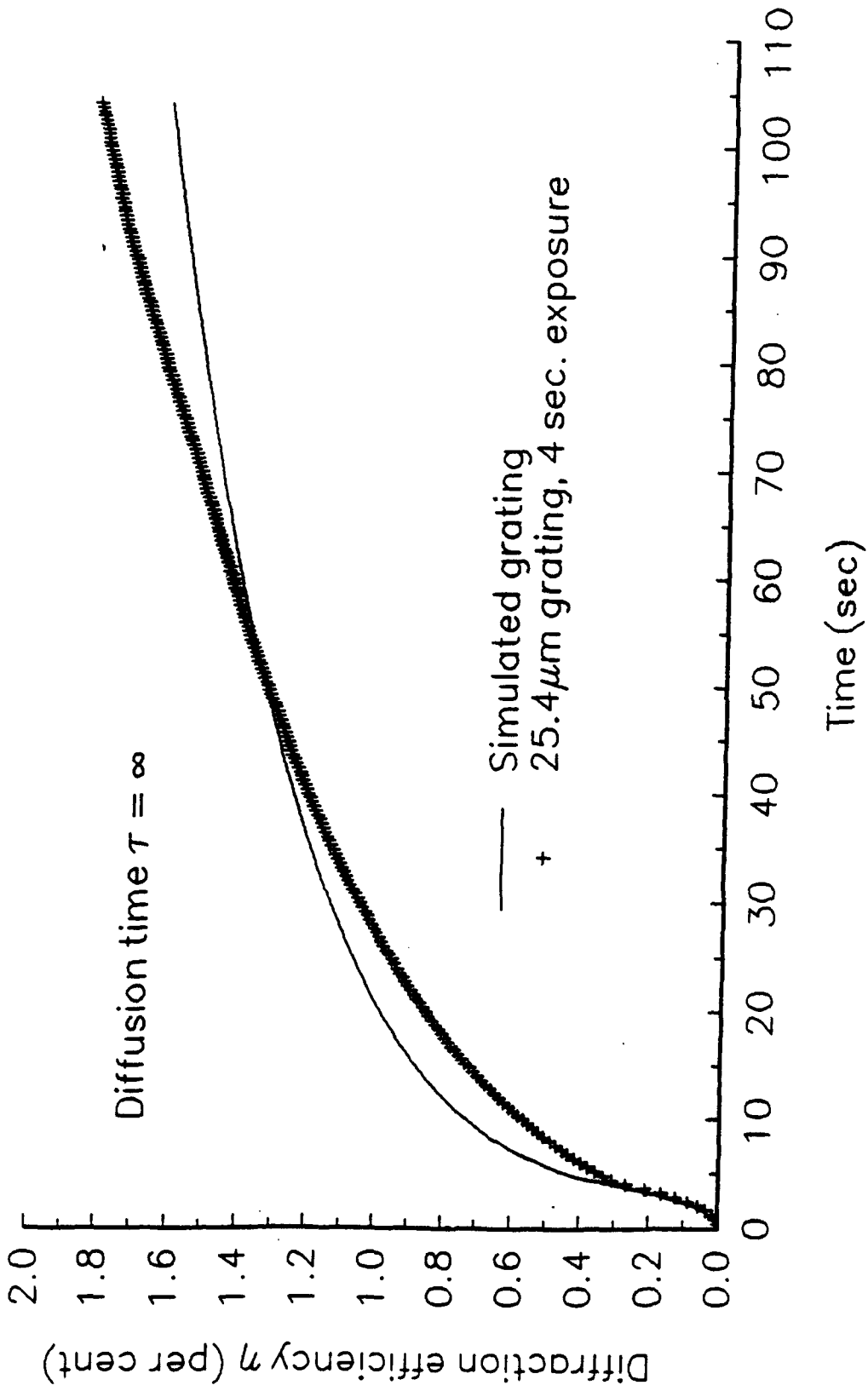$$\delta n \ \frac{6n}{\left(n^2 + 2\right)^2} = R_p P(x,t) \qquad (5\text{-}16)$$

120

Figure 5-21: Measured and simulated 25.4 μm grating growth, assuming no diffusion.

Between Equation 5-15 and 5-16, the phase grating changes sign and increases in magnitude by about a factor of ten. The diffraction efficiency would appear to rise, fall to zero, and then rise again to a much larger value. This zero of diffraction efficiency would seem to be an inevitable consequence of the photopolymer diffusion model, though it was seen only once in this investigation. Indeed, this is essentially the argument that was used against the diffusion model of Colburn and Haines.

The reconciliation of the photopolymer diffusion model with the data demands that only a fraction of the available monomer be able to diffuse freely. In many diffusive systems, only a, small fraction of the diffusing species has mobility, the rest being tied up in association with the matrix. Experimentally, this is observed as a concentration-dependent diffusion coefficient, as discussed in Chapter 4. In the case of DMP-128, much of the monomer may be immobilized by affinity for the compatible polymer, or actually "caged" by an impenetrable network of polymer, as theorized by Kloosterboer [46,47,48]. In any case, the fact that post-exposure diffusion rarely, if ever, causes the phase grating to vanish strongly implies that less than 10% of the available monomer is actually free to diffuse.

In Figure 5-22, an attempt was made to simulate the behavior of an 8.47 μm grating produced by a four second exposure. The polymerization rates implied by Equations 5-12 and 5-13 were used, along with an assumed diffusive time constant of 150 sec. Recall that Equations 5-12 and 5-13 are empirical approximations to the actual rates measured during and after a four second exposure of a 25.4 μm grating. It was further assumed that only 7.5% of the variation in monomer concentration was subject to diffusion; the rest was immobile. Aside from an overall scale factor, the form of the decay looks about right; however, the "overshoot" from the post-exposure chemical reaction is much larger in the simulation than in the actual measured data. The actual increase in diffraction efficiency after exposure was only a few percent; the simulated grating triples in diffraction efficiency after the exposure is complete. The failure of this simulation to match the measured data suggests that the rate of post-exposure polymerization is much smaller in the 8.47 μm grating than it was in the 25.4 μm grating.

It would seem that the rate of post-exposure polymerization becomes much smaller as Λ decreases. Indeed, an attempt to simulate the measured behavior of 2.67 μm gratings demanded that the post-exposure chemical reaction be zero, or very close to it. In Figure 5-23, a 3.5 second diffusive time constant, 6.5% of monomer free to diffuse, and zero post-exposure chemical activity provides a good match to the data. The best match between simulation and experiment was obtained setting the right-hand side of Equation 5-13, the post-exposure polymerization rate, to zero. The apparent lack of post-exposure polymerization in short period gratings might be explained partially by the diffusion of activated dye, which would erase the spatial periodicity of the reaction, or alternatively it might be due to the diffusion of a radical scavenger. Such scavengers are often added to acrylic acid and related compounds to inhibit spontaneous thermal polymerization at room temperature. All of the gratings recorded in this research used high visibility fringe patterns, which is to say that the light intensity of the dark fringes was near zero, so a substantial amount of radical scavenger could have survived in the dark fringes, and then diffused out to suppress any post-exposure reactions.
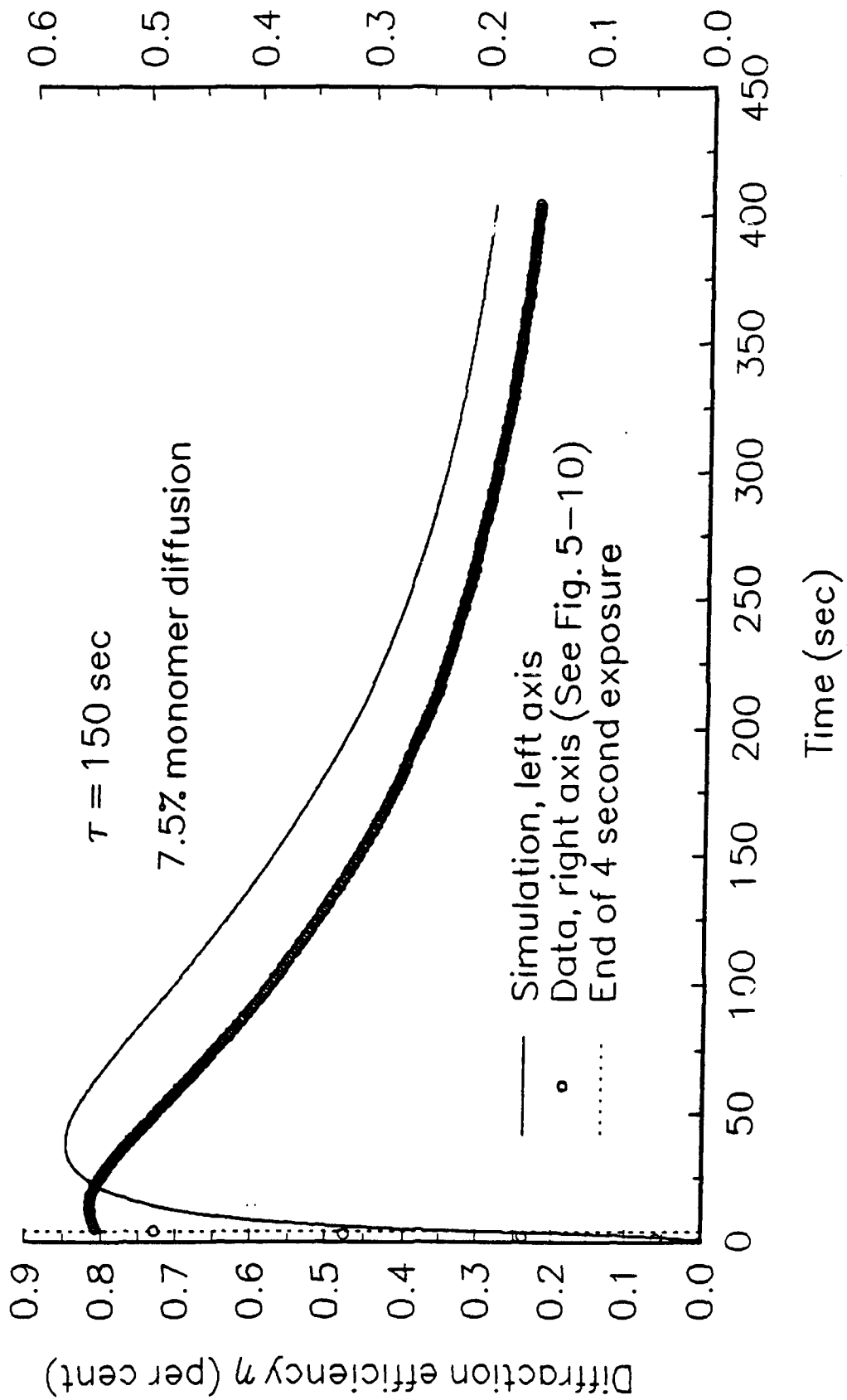
Figure 5-22: Measured and simulated 8.47 µm grating evolution.

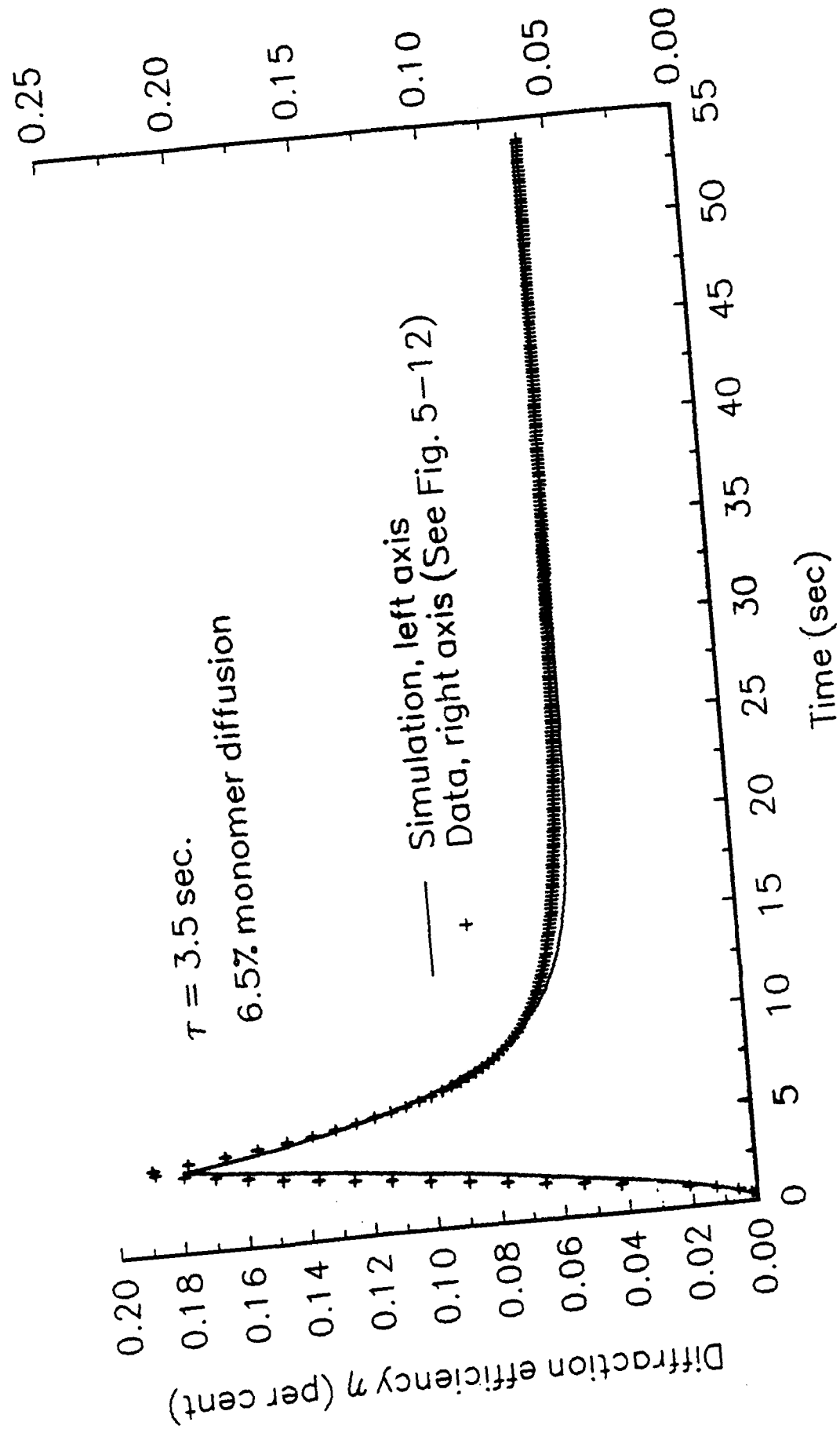**Figure 5-23:** <u>Simulation of a 2.67 μm grating suggests that polymerization ends with exposure.</u>

124

VI. CONCLUSIONS AND SUGGESTIONS FOR FUTURE INVESTIGATION

This research was inspired in part by the work of Johnson [10], who characterized the holographic reciprocity law failure in silver halide materials in terms of two relative time-scales of the system. The first time-scale was the the thermal dissociation lifetime of a developable silver pre-speck, versus the second time-scale, the mean time between photons absorbed by a silver halide grain. The relative magnitude of these two quantities determined the effectiveness of the various exposures in a sequence of multiple holographic exposures. The theoretical model was confirmed by experiment, and found practical application in the fabrication of multiple exposure holograms for the display of medical tomographic imagery.

This research effort began with the ideas, gleaned from the photopolymer literature, that diffusion might play a significant role in photopolymer hologram formation, and that it might be possible to measure the evolution of the DMP-128 grating while it was being formed. A general model of phase grating formation in photopolymer compositions was developed, consistent with the known laws of optics, photochemistry, and chemical kinetics. The model indicated that the most important processes of image formation in photopolymers depend upon photochemical reactions and the associated diffusion induced by the periodic depletion of monomer. A differential equation representing the model was formulated, and it was shown that the dynamics of the grating evolution during exposure are entirely determined by the ratios of the diffusive time-scale and two different photochemical time-scales. An analytic solution of the differential equation in terms of the orthogonal Mathieu functions was found to be valid for certain values of the parameters. The analytic solution predicts a sign change of the transient phase grating during holographic exposure, a phenomenon that has been observed before in photopolymers, but never explained before in a completely satisfactory manner.

Prior to the experimental stage of this research effort, all that was known about the latent grating in DMP-128 was that it was sometimes faintly visible to the naked eye. An experimental set-up was designed and built which allowed a microcomputer to control holographic exposure, probe beam exposure, and the digitization and recording of real-time diffraction efficiency data. Dozens of experiments were performed in which the growth and post-exposure evolution of the gratings in Polaroid's DMP-128 photopolymer were measured. Gradual refinement of the experimental technique eliminated several sources of systematic and random error that degraded the quality of the early measurements. The final and most satisfactory experimental arrangement exploited the spectral selectivity of the photopolymer by exposing it with red (633 nm) light, while simultaneously probing the grating with green (514 nm) light that had no photochemical effect on the medium.

The most important experimental observation was the qualitative and quantitative change in grating behavior as the grating period Λ was varied systematically from 25.4 μm to 1.04 μm. For large grating periods, the transient grating grew monotonically both before and after exposure. The surprising post-exposure increase of diffraction efficiency was shown to result from polymerization induced by residual free radicals, and to follow the expected kinetics for such a reaction, in the absence of any significant monomer diffusion. As the grating periods grew smaller, the post-exposure evolution of the diffraction efficiency changed into a decline rather than a growth. As the grating period became smaller, the post-exposure decline became faster. This phenomenon had been modeled as an exponential decay in the amplitude of the phase grating due to diffusion of free monomer, but the decay data were

better described as the sum of two exponentials, suggesting that two components were diffusing simultaneously in the photopolymer medium. When the grating period was reduced to about 1 micron, new behavior was observed in which the diffraction efficiency rose, and fell, and even oscillated during exposure, sometimes falling to a value indistinguishable from zero.

The double-exponential decay can be explained in terms of the simultaneous diffusion of the monomer and the sensitizing dye. Recall from Chapter Two that the DMP-128 photopolymer consists of a polymeric binder, a monomer, a polymeric initiator, and a sensitizing dye, all operating in the presence of water absorbed from the air. This composition is the one revealed in Polaroid's 1986 patent [62], and its validity for the current research has been confirmed by a Polaroid chemist [147]. Of these components, the only ones likely to contribute to a holographic grating and have diffusional mobility are the monomer and the methylene blue sensitizing dye. The mechanism of phase grating formation and decay by monomer reaction and diffusion has already been discussed at length. However, only near the end of this research was the significance of the dye behavior realized. The data in Figure 5-16 show that the photochemical reduction of the dye to a clear, colorless state, followed by its re-oxidation to the colored form can have a significant effect on the transmitted diffracted signal. A normal holographic exposure would have imposed a sinusoidal variation of bleached dye concentration in the photopolymer, forming an absorption grating, rather than a phase grating. However, both the excited and unexcited dye molecules would then have diffused, leading to an exponential decay of the absorption grating amplitude. The re-oxidation of the dye to the colored state, as seen in Figure 5-16, would take minutes rather than seconds, and would not have been significant for measurements of short grating decay times. Therefore, the most reasonable interpretation of the current research data is that holographic exposure in DMP-128 forms both a phase grating and an absorption grating simultaneously. The phase grating is due to a periodic depletion of monomer, and the absorption grating is due to a periodic bleaching of the sensitizing dye. Both gratings then decay with rates characteristic of the diffusion times of the lithium acrylate monomer and the methylene blue sensitizing dye, respectively. The methylene blue molecule, being both more massive and larger than the simple lithium acrylate molecule, diffuses more slowly in aqueous solution, and is associated with the larger of the two decay times for each data fit shown in Table 5-1.

In a more speculative vein, the dye diffusion hypothesis also suggests an explanation for the oscillatory behavior of the diffraction efficiency during the exposure of the 1 μm period gratings. Heretofore, it has been assumed that the spatial variation of the polymerization rate depends solely upon the variation of the incident light intensity. However, if a significant amount of reduced (excited) dye can diffuse from bright fringes to dark fringes during the course of an exposure, the excited dye will initiate polymerization in the dark fringes, and thus reduce the phase contrast between dark fringes and bright fringes. This would tend to decrease the diffraction efficiency even while the holographic exposure continued. Dye diffusion would thus decrease the spatial variation in the photopolymerization, and might set the lower limit on the grating period that can be recorded in the photopolymer.

Further analysis and attempts to simulate the measured data led to the realization that the data gathered in this investigation can be explained only if a small fraction of the monomer, on the order of 7%, is actually free to diffuse. In a bright fringe, the immediate photochemical effect of polymerization is a small drop in the refractive index. However, if all monomer were free to diffuse, the material that diffused in to replace the depleted monomer

would reverse the sign of the phase grating and increase its amplitude by at least a factor of ten, after briefly passing through zero. However, what is usually observed is the rapid formation of a phase grating by polymerization, followed by only a partial decline of the diffraction efficiency. This necessarily implies that only a small fraction of monomer is actually free to diffuse. The simulations also led to the conclusion that the post-exposure chemical reactions seen in large-period gratings are largely extinguished in small period gratings.

This research effort has built upon much previous work in photopolymer holography, polymer chemistry, and holographic measurement techniques, and has extended the theoretical and practical understanding of holographic photopolymers. Careful review of the literature and frequent communications with other photopolymer researchers have made clear that certain aspects of this research have been both novel and significent. The significant contributions of this research include:

1. The first and to date only measurements of the exposure and post-exposure grating evolution in Polaroid's DMP-128 photopolymer by holographically probing the latent grating.

2. The observation and modeling of post-exposure grating growth in a photopolymer due to residual free radical. The experimental results support the conclusion that the polymerization reaction is controlled by the free radical termination rate, which is quadratic in free radical concentration. However, as the grating period decreases, this post-exposure reaction rapidly becomes negligible; it may be extinguished by the diffusion of dye or some residual radical scavenger.

3. The determination of monomer and dye diffusion rates in the DMP-128 photopolymer.

4. The formulation of an analytical model of grating growth in photopolymers that can be expressed as a modified diffusion equation (Equation 4-27). It can be expressed (Equation 4-42) in such a way that the only coefficients of the differential equation are dimensionless ratios of the characteristic diffusion time and characteristic photochemical reaction times of the photopolymer system. This model equation was then solved analytically in terms of the orthogonal, periodic Mathieu functions. The solution is valid in the limit of small fringe visibility of the holographic interference pattern, and for diffusion times much smaller than the inverse of photochemical reaction rates.

5. The discovery that although diffusion plays an important role in the formation of the photopolymer grating, only a small fraction of the available monomer in the DMP-128 system is actually free to diffuse.

6. This research constitutes the first complete synthesis of a) photopolymer holographic grating measurement, b) an analytic model of grating growth and decay, and c) rigorous mathematical modeling of the experimental data in light of the analytic model. This comprehensive approach to photopolymer grating formation is new, and has prompted considerable interest among DuPont and Polaroid photopolymer researchers, accompanied by requests to determine the monomeric diffusion coefficients for their compositions.

7.   An explanation for the "spatial bandpass" characteristic of photopolymer recording media. In this model, low spatial frequencies cannot be recorded because the diffusion necessary for grating formation cannot take place in a reasonable time. At high spatial frequencies, diffusion of light-excited dye from light to dark fringes will limit the phase contrast of the finished grating.

8.   The novel aspects of the single-wavelength grating measurement techniques developed in this research are protected, by the Patent and Trademark office, as a statutory invention registration [138].

The results of this research suggest several lines of investigation that could further the understanding of diffusive mechanisms in photopolymer hologram formation. These include:

1. Performing a similar series of experiments using a dry photopolymer composition, such as the DuPont holographic photopolymer. The maintenance of constant humidity for the DMP-128 exposures was a vexing experimental problem, and a possible source of variability for the results presented here. A dry composition would avoid this problem and would present a "cleaner" system, since in DMP-128, water is one of the most important components.

2. Characterizing the grating evolution of a photopolymer using the phase modulated holography technique of Gehrtz et. al. [136]. This technique is capable, it is claimed, of measuring simultaneously and separately the sign and amplitude of both phase and absorption gratings recorded in a sample, as well as increasing the sensitivity of real-time holographic measurements. This technique would allow the effects of a bleached dye absorption grating to be separated from the response due to a mass density or molar refractivity phase grating. Some of the difficulty in the current research came from the numerically ill-conditioned problem of fitting data to a dual exponential decay. If diffusion causes uncoupled exponential decays of both the phase and amplitude gratings, the separate results would be much simpler to analyze.

3. An analytic or a partially analytic solution of the photopolymer diffusion Equation 4-27 may be possible, and would offer more insight than the Mathieu function solution, which was limited to a special case. The equation

$$\frac{\partial u(x,t)}{\partial t} - D\frac{\partial^2 u(x,t)}{\partial x^2} = - k_L\left[I_0 + I_s \cos\left(\frac{2\pi x}{\Lambda}\right)\right]^{1/2} u(x,t) \qquad (4\text{-}27)$$

reduces by separation of variables to a special case of Hill's equation [148], a second-order differential equation with general periodic coefficients. Even if a complete analytic solution is not feasible, theorems exist on the nature of the eigenvalues and the properties of solutions that may offer insight into the behavior of holographic photopolymers.

4.   The development of a revised model to account for the effects of dye diffusion on the dynamics of photopolymer grating formation. The current research has indicated that the dye diffusion in DMP-128 is considerably slower than the monomer diffusion, and may only be

significant if the diffusion time of the dye over one fringe spacing is less than the duration of the holographic exposure. This implies either very small fringe spacing, or a very weak exposure. Since a diffusion of the excited dye species tends to equalize polymerization rates in bright and dark fringes, the dye diffusion mechanism may limit the maximum spatial frequency that can be recorded in a holographic photopolymer medium.

REFERENCES

[1]   C.E.K. Mees, Theory of the Photographic Process, MacMillan and Co.,1954, Third Edition, pp.101-242.

[2]   J. Scheiner, "Application de la photographie a la determination des grandeurs stellaires," Bull. du comite permanent international pour l'execution photographique carte du ciel, 1889, 1:227.

[3]   W. Abney, "The Failure in a Photographic Law with Very Intense Light,"Phot.J.,1894, 18:302.

[4]   R.W. Gurney, N.F. Mott, "The Theory of the Photolysis of Silver Bromide and the Photographic Latent Image," Proc. Roy. Soc., 1938, 164A:151.

[5]   J.W. Mitchell, "Lattice Defects in Latent Image Formation," in Fundamental Mechanisms of Photographic Sensitivity, Butterworth, London,1951,242.

[6]   T. Tani, "Physics of the Photographic Latent Image," Physics Today, Sept. 1989, pp.36-41.

[7]   W.F. Berg, "The Reciprocity, Intermittency, Clayden, and Villard Effects," in The Theory of the Photographic Process, MacMillan and Co., Third Edition, 1954.

[8]   J.H. Webb, "The Relationship Between Reciprocity Law Failure and the Intermittency Effect in Photographic Exposure," JOSA, Vol. 23, No.5, May 1933, p.157.

[9]   J.H. Webb, "Low Intensity Reciprocity Failure in Photographic Exposure: Energy Depth of Electron Traps in Latent-Image Formation; Number of Quanta Required to Form the Stable Sublatent Image," JOSA, Vol. 40, No.1, Jan.1950, p. 3.

[10]   K.Johnson, Holographic Reciprocity Law Failure, with Applications to the 3-D Display of Medical Data, Ph.D. Dissertation, Stanford University Electrical Engineering Dept.,October 1983.

[11]   E.N. Leith and J.Upatnieks, JOSA, 54:1295 (1964).

[12]   K. Biedermann, "Attempts to Increase the Holographic Exposure Index of Photographic Materials," Applied Optics, Vol. 10, No. 3, March 1971, p.584.

[13]   R.L. Kurtz and R.B. Owen, "Holographic Recording Materials - A Review," Optical Engineering, Vol. 14, No. 5, September/October 1975, p. 393.

[14]   K. Biedermann, "Information storage materials for holography and optical data processing," Optica Acta, 1975, Vol. 22, No. 2, pp. 103-124.

[15]   A.B. Cohen, "Photopolymer Images for Electronics and Printing," Industrial Research, December 1976, p. 39.

REFERENCES (cont'd)

[16] R.T. Ingwall and H.L. Fielding, "Hologram recording with a new Polaroid photopolymer system," SPIE Proceedings Vol. 523:43.

[17] R.T. Ingwall and H.L. Fielding, "Hologram recording with a new photopolymer system," Optical Engineering, September/October 1985, Vol. 24, No. 5, p.808.

[18] D.J. Lanteigne, T.D. Hudson, and D.A. Gregory, "Matched spatial filtering using a new photopolymer," Applied Optics, Vol.26, No.2, January 15, 1987, p.184.

[19] J.C. Kirsch, D.J. Lanteigne, D.L. Marsh, and D.A. Gregory, "Optical information processing using a new photopolymer," Optical and Digital Pattern Recognition, Proceedings of the SPIE, Vol.754, 1987, p.326.

[20] T.D. Hudson, D.J. Lanteigne, D.A. Gregory, J.C. Kirsch, Joint Transform Optical Correlation, US Army MICOM Technical Report RD-RE-87-5.

[21] J.C. Kirsch, D.A. Gregory, T.D. Hudson, D.J. Lanteigne, "Design of photopolymer holograms for optical interconnect applications," Optical Engineering, Vol. 27, No. 4, p. 301.

[22] W. Hay, Analysis of a holographic photopolymer, Master's Thesis in the University of North Carolina Physics Dept., 1986.

[23] W.J. Tomlinson and E.A. Chandross, "Organic photochemical refractive-index image recording systems," in Advances in Photochemistry Vol.12, John Wiley and Sons, 1980.

[24] W.S. Colburn and K.A. Haines, "Volume hologram formation in photopolymer materials," Applied Optics, Vol. 10, No. 7, July 1971, p. 1636.

[25] J.A. Jenney, "Holographic recording with photopolymers," JOSA Vol. 60, No. 9, Sept. 1970, p.1155.

[26] H. Kogelnik, "Reconstructing response and efficiency of hologram gratings," Proc. Symp. Modern Optics, Polytechnic Institute of Brooklyn, March 1967, pp. 605-617

[27] J.D. Jackson, Classical Electrodynamics, 2nd. Edition, John Wiley and Sons, 1975, p. 155.

[28] R.T. Ingwall, A. Stuck, and W.T. Vetterling, "Diffraction properties of holograms recorded in DMP-128," Practical Holography, SPIE Proceedings, Vol. 615 (1986), p.81.

[29] R.S. Potember et. al., "Conducting organics and polymers for electronic and optical devices," Polymer, Vol 28, April 1987, p. 57.

131

REFERENCES (cont'd)

[30] C. Brauchle and D. M. Burland, "Holographic methods for the investigation of photochemical and photophysical properties of molecules," Angew. Chem. Int. Ed. Engl. 22 (1983) pp. 582-598.

[31] G.C. Bjorklund, D.M. Burland, and D.C. Alvarez, "A holographic technique for investigating photochemical reactions," J. Chem. Phys. 73(9), 1 November 1980, p.4321.

[32] D.M. Burland and C. Brauchle, "The use of holography to investigate complex photochemical reactions," J. Chem. Phys, 76(9),1 May 1982, p.4502.

[33] Arnost Reiser, Photoreactive polymers: The science and technology of resists, a Wiley-Interscience publication, John Wiley and Sons, 1989.

[34] E.R. Blout and H. Mark (editors), Monomers: A collection of data and procedures on the basic materials for the synthesis of fibers, plastics, and rubbers, Interscience Publishers, 1951.

[35] Kiichi Takemoto, Yoshiaki Inaki, and Raphael M. Ottenbrite (editors), Functional monomers and polymers: Procedures,synthesis, and applications, Marcel Dekker Inc., 1987.

[36] Fred W. Billmeyer, Jr., Textbook of Polymer Science, Third Edition, A Wiley Interscience Publication, 1984.

[37] Stanley R. Sandler and Wolf Karo, Polymer Syntheses Vol II, Academic Press, 1977.

[38] Gerald Oster, "Dye-Sensitized Photopolymerization," Nature, Volume 173, pp.300-301, February 13, 1954.

[39] David F. Eaton, "Dye-Sensitized Photopolymerization," Advances in Photochemistry, Volume 14, Interscience Publication, John Wiley and Sons, 1982.

[40] Raymond B. Seymour and Charles E. Carraher, Jr., Polymer Chemistry: An Introduction, Marcel Dekker,1981.

[41] Elizabeth M. Frith and R.F. Tuckett, Linear Polymers, Longman,Green, and Co., 1951.

[42] James Guillet, Polymer photophysics and photochemistry: an introduction to the study of photoprocesses in macromolecules, Cambridge University Press, 1985.

[43] J.C. Bevington, Radical polymerization, Academic Press, 1961.

[44] C.H. Bamford, W.G. Barb, A.D. Jenkins, and P.F. Onyon, The Kinetics of Vinyl Polymerization by Radical Mechanisms, Academic Press, New York, Butterworth Scientific Publications, London, 1958.

REFERENCES (cont'd)

[45]   A.M. North and D. Postlethwaite, "The Termination Mechanism in Radical Polymerization," from Structure and Mechanism in Vinyl Polymerization, edited by Teji Tsurata and Kenneth F. O'Driscoll. Marcel Dekker, Inc., New York, 1969.

[46]   J.G. Kloosterboer, G.M.M. van de Hei, R.G. Gossink and G.C.M. Dortant, "The effects of volume relaxation and thermal mobilization of trapped radicals on the final conversion of photopolymerized diacrylates," Polymer Communications, Vol. 25, November 1984, pp. 322-325.

[47]   J.G. Kloosterboer and G.J.M. Lippitts, "Replication of Video Discs Using Photopolymerization: Process Design and Study of Network Formation," Journal of Imaging Science, Vol. 30, No. 4, July/August 1986, pp.177-183.

[48]   J.G. Kloosterboer and G.F.C.M. Lijten, "Chain Cross-Linking Photopolymerization of Tetraethyleneglycol Diacrylate," in Cross-Linked Polymers: Chemistry, Properties, and Applications, American Chemical Society, Washington, D.C., 1988.

[49]   J.B. Rust, L.J. Miller, and J.D. Margerum, "Photopolymerization Studies: I. Polymers from new Photoredox Catalyst System," Polymer Engineering and Science, January 1969, Vol. 9, No.1, pp.40-48.

[50]   J. David Margerum, Leroy J. Miller, and John B. Rust, "Photopolymerization Studies: II. Imaging and Optical Fixing," Photographic Science and Engineering, Vol. 12, 1968, pp.177-184.

[51]   D.H. Close, A.D. Jacobsen, J.D. Margerum, R.G. Brault, and F.J. McClung, "Hologram Recording on Photopolymer Materials," Applied Physics Letters, Volume 14, No. 5, 1 March 1969, pp. 159-160.

[52]   J.A. Jenney, "Holographic Recording with Photopolymers," Journal of the Optical Society of America, Vol. 60, No.9, September 1970, pp.1155-1161.

[53]   Hughes Research Laboratories (prepared by J. David Margerum), "Chemistry of Photopolymer Light Sensitive Systems Relevant to Radar and other Displays," Prepared for Air Force Office of Scientific Research, distributed by the National Technical Information Service, AFOSR-TR-73-1365, Contract #F44620-68-C-0043, July 1973.

[54]   J.B. Rust, J.D. Margerum, and L.J. Miller, "Light-Scattering Imaging by Photopolymerization," Novel Imaging Systems, R.D. Murray, editor, Society of Photographic Scientists and Engineers (SPSE), Washington D.C., April 1969, pp.173-186.

[55]   J.A. Jenney, "Fixing of Photopolymer Holograms," Journal of the Optical Society of America, Vol. 61, No. 8, August 1971, pp.1116-1117.

REFERENCES (cont'd)

[56]   J.A. Jenney, "Nonlinearities of Photopolymer Holographic Recording Materials," Applied Optics, Vol. 11, No. 6, June 1972, pp.1371-1381.

[57]   R.G. Brault et al., "Photopolymerization holography studies", Image Technology 13, p. 13, (1971).

[58]   U.S. Patent #3,658,526, Hologram recording in photopolymerizable layers, invented by Eugene Frederick Haugh, assigned to E.I. du Pont de Nemours and Company, April 25, 1972.

[59]   U.S. Patent #3,479,185, Photopolymerizable compositions and layers containing 2,4,5-triphenylimidazoyl dimers, invented by Vaughan Crandall Chambers Jr., assigned to E.I. du Pont de Nemours and Company, November 18, 1969.

[60]   William K. Smothers, Bruce M. Monroe, Andrew M. Weber, and Dalen E. Keys, "Photopolymers for holography," Practical Holography IV, SPIE Vol. 1212, 1990, pp. 20-29.

[61]   Andrew M. Weber, William K. Smothers, T. John Trout, and Daniel J. Mickish, "Hologram recording in Du Pont's new photopolymer materials," Practical Holography IV, SPIE Vol. 1212, 1990, pp. 30-39.

[62]   U.S. Patent #4,588,665, Photopolymerizable compositions used in holograms, invented by Herbert L. Fielding and Richard T. Ingwall, assigned to Polaroid Corp., May 13, 1986.

[63]   U.S. Patent #4,535,041, Stabilization of Holograms, invented by Herbert L. Fielding and Richard T. Ingwall, assigned to Polaroid, August 13, 1986.

[64]   U.S. Patent #3,925,082, Multicolor screen element containing a hydrophilic colloid treated with a basic dye and zirconium acetate, invented by Herbert L. Fielding and Samuel H. Liggero, assigned to Polaroid Corp., December 29, 1972.

[65]   Richard D. Rallison and Stephen E. Bialkowski, "Survey of Properties of Volume Holographic Materials," SPIE Proceedings Vol. 1057.

[66]   R.T. Ingwall and Mark Troll, "Mechanism of hologram formation in DMP-128 photopolymer," Optical Engineering, Vol 28, No. 6, June 1989, pp. 586-591.

[67]   W. Driemeier, M. Kopietz, and M.D. Lechner, "Multiple storage of holograms in blocks of PMMA/MMA/Titanocenechloride," Colloid and Polymer Science, Vol. 264, No. 12, 1986, m .1024-1029.

[68]   J. Marotz, "Holographic Storage in Sensitized Polymethyl Methacrylate Blocks," Applied Physics B 37, pp.181-187 (1985).

REFERENCES (cont'd)

[69]   T. Luckemeyer and H. Franke, "Profiles in Volume Phase Holograms in Cp_2TiCl_2:PMMA," Applied Physics B 46, pp.157-164(1988).

[70]   W.J. Tomlinson, E.A. Chandross, H.P. Weber, and G.D. Aumiller, "Multicomponent photopolymer systems for volume phase holograms and grating devices," Applied Optics, Vol. 15, No. 2, February 1976, pp. 534-541.

[71]   E.A. Chandross, W.J. Tomlinson, and G.D. Aumiller, "Latent-imaging photopolymer systems," Applied Optics, Vol.17, No. 4, 15 February 1978, pp. 566-573.

[72]   Shungo Sugawara, Kei Murase, and Toyoki Kitayama, "Holographic Recording by Dye-Sensitized Photopolymerization of Acrylamide," Applied Optics, Vol. 14, No.2, February 1975, pp.378-382.

[73]   M.J. Jeudy and J.J. Robillard, "Spectral photosensitization of a variable index material for recording phase holograms with high efficiency," Optics Communications, January 1975, Volume 13, No.1, pp. 25-28.

[74]   C. Carre, D. Ritzenthaler, D.J. Lougnot, and J.P. Fouassier, "Biphotonic process for recording holograms," Optics Letters, Vol. 12, No. 9, September 1987, pp. 646-647.

[75]   Eugene Hecht and Alfred Zajac, Optics, Addison-Wesley Publishing Company, 1974, Chapter 3.3.1 and following.

[76]   Max Born and Emil Wolf, Principles of Optics, Sixth (Corrected) Edition, Pergamon Press, 1986, Chapter 2.2.

[77]   Ibid., Chapter 2.3.3.

[78]   G.H. Meeten, "Refraction and extinction of polymers," in Optical Properties of Polymers, edited by G.H. Meeten, Elsevier Applied Science Publishers, 1986.

[79]   D.W. Van Krevelen, Properties of Polymers: Their Estimation and Correlation with Chemical Structure, Chapter 10, "Optical Properties," Elsevier Scientific Publishing Company, 1976.

[80]   Zhong-he Lu and Sonja Krause, "Properties of Low Molecular Weight Block Copolymers. 2. Refractive Index-Temperature Measurements of Sytrene-Dimethylsiloxane Diblock Copolymers," Macromolecules, Vol. 15, 1982, pp. 112-114.

[81]   Sonja Krause and Zhong-he Lu, "Refractive Index Temperature Measurements on Anionically Polymerized Polystyrene," Journal of Polymer Science, Polymer Physics Edition, Vol. 19, p. 1925,1981.

REFERENCES (cont'd)

[82] Roy M. Waxler, Deane Horowitz, and Albert Feldman, "Optical and physical parameters of Plexiglass 55 and Lexan," Applied Optics, Vol. 18, No. 1, 1 January 1979, pp.101-104.

[83] Max Born and Emil Wolf, Principles of Optics, Sixth (Corrected) Edition, Pergamon Press,1986, Chapter 2.3.4.

[84] K.G. Denbigh, "The polarisabilities of bonds-I.," Transactions of the Faraday Society, Vol. 36, 1940, pp. 936-948.

[85] T.K. Foreman, "Planar photopolymer optical waveguides," Imaging Science and Technology (IS&T) 44th Annual Conference, May 1991, Advance Printing of Paper Summaries, p.558.

[86] L. Solymar and D.J. Cooke, Volume Holography and Volume Gratings, Academic Press, 1981, Chapter 5.6.

[87] C.V. Raman and N.S. Nagendra Nath, "The diffraction of light by high frequency sound waves, Part 5," Proceedings of the Indian Academy of Science, Volume A3, pp.459-465, (1936).

[88] P. Debye and F.W. Sears, "On the scattering of light by supersonic waves," Proceedings of the National Academy of Science, Vol. 18, pp. 409-414, (1932)

[89] J.W. Goodman, Introduction to Fourier Optics, McGraw-Hill, 1968, Chapter 4-2, pp. 69-70.

[90] G. Arfken, Mathematical Methods for Physicists, Chapter 11.1, p.584, Academic Press, Third International Edition.

[91] W.H. Beyer and S.M. Selby, Editors, CRC Standard Mathematical Tables, 24th Edition, CRC Press, 1976, p.445.

[92] H. Kogelnik, "Coupled Wave Theory for Thick Hologram Gratings", The Bell System Technical Journal, Volume 48, No. 9, November 1969, pp. 2909-2947.

[93] L. Solymar and D.J. Cooke, Volume Holography and Volume Gratings, Academic Press, 1981, Chapter 2.3.

[94] Ibid, Chapter 2.7.

[95] T.K. Gaylord and M.G. Moharam, 'Analysis and Applications of Optical Diffraction by Gratings," Proceedings of the IEEE, Vol. 73, No. 5, May 1985, pp. 894-937.

[96] M.G. Moharam and T.K. Gaylord, "Rigorous coupled-wave analysis of planar-grating diffraction," JOSA , Vol. 71, July 1981, pp. 811-818.

REFERENCES (cont'd)

[97]   T.W. Stone, <u>Holographic Optical Elements</u>, Doctoral Thesis at The Institute of Optics, University of Rochester, New York, 1986.

[98]   M.G. Moharam and T.K. Gaylord, "Diffraction analysis of dielectric surface-relief gratings," JOSA, Vol. 72, October 1982, pp. 1385-1392.

[99]   J. Crank, <u>The Mathematics of Diffusion: Second Edition</u>, Oxford University Press, 1975.

[100]   J. Crank, G.S. Park (editors), <u>Diffusion in Polymers</u>, Academic Press, 1968.

[101]   R. Ghez, <u>A Primer of Diffusion Problems</u>, John Wiley and Sons, 1988, Chapter 1.1 and 1.2.

[102]   J. Fourier, <u>The Analytical Theory of Heat</u>, translated by Alexander Freeman with notes, Dover Publications Inc., 1955.

[103]   H. Carslaw and J. Jaeger, <u>Conduction of Heat in Solids</u>, Second Edition, Oxford University Press, 1959.

[104]   W.H. Press, B.P. Flannery, S.A. Teukolsky, and W.T. Vetterling, <u>Numerical Recipes: The Art of Scientific Computing</u>, Chapter 17.2, Cambridge University Press, 1986.

[105]   C.E. Rogers, "Solubility and Diffusivity," Chapter 6 in <u>Physics and chemistry of the organic solid state, Volume II</u>, edited by D. Fox, M. Labes, and A. Weissberger, Wiley Interscience, 1965.

[106]   W. Jost, <u>Diffusion in solids, liquids, gases</u>, Chapter I, Section IV, pp. 16-25 Third printing, Academic Press, 1960.

[107]   R. Ghez, A Primer of Diffusion Problems, John Wiley and Sons, 1988, Chapter 1.3.

[108]   F. Reif, <u>Fundamentals of statistical and thermal physics</u>, McGraw-Hill Book Co., 1965, Section 10.2, p.415.

[109]   CRC Press, <u>Handbook of Chemistry and Physics</u>, 65th Edition, pp. F-44 to F-51.

[110]   D.D. Joseph, Luigi Preziozi, "Heat waves," Reviews of Modern Physics, Vol. 61, No. 1, January 1989, pp.41-73.

[111]   J. Crank and G.S. Park, "Methods of Measurement," in <u>Diffusion in Polymers</u>, J. Crank and G.S. Park (editors), Academic Press, 1968.

[112]   E. Wallace, Jr.(E.I Du Pont de Nemours and Company, Towanda, Pa.), et. al. "Compatibility and diffusion studies of components in peel-apart films," Paper Summaries of the IS&T (Imaging Science and Technology) 44th Annual Conference, May 1991.

137

REFERENCES (cont'd)

[113] V. Stannett, "Simple Gases," in <u>Diffusion in Polymers,</u> J. Crank and G.S. Park (editors), Academic Press, 1968.

[114] H. Fujita, "Organic vapors above the glass transition temperature," ibid.

[115] G.S. Park, "The glassy state and slow process anomalies," ibid.

[116] T. Alfrey, E.F. Gurnee, and W.G. Lloyd, "Diffusion in Glassy Polymers," Journal of Polymer Science: Part C, No. 12, pp. 249-261, (1966)

[117] R.T. Ingwall, A. Stuck, and W.T. Vetterling, "Diffraction properties of holograms recorded in DMP-128," <u>Practical Holography,</u> SPIE Vol. 615 (1986).

[118] J.A. Barrie, "Water in Polymers," in <u>Diffusion in Polymers,</u> J. Crank and G.S. Park (editors), Academic Press, 1968.

[119] L.J. Thompson Hughes and D.B. Fordyce, "Sorption of water vapor by water-soluble polymers: Kinetic, equilibrium, and glass temperature data," Journal of Polymer Science, Vol.XXII, pp. 509-526 (1956).

[120] W.M. Franklin, "Classical and quantum theory of diffusion in solids," in <u>Diffusion in Solids: Recent Developments,</u> edited by A.S. Nowick and J.J. Burton, Academic Press, 1975.

[121] B.L. Booth, "Photopolymer Material for Holography," Applied Optics, Vol. 14, No. 3, March 1975, pp. 593-601.

[122] R.H. Wopschall and T.R. Pampalone, "Dry photopolymer film for recording holograms," Applied Optics, Vol. 11, No. 9, September 1972, pp. 2096-2097

[123] B.L. Booth, "Photopolymer Laser Recording Materials," Journal of Applied Photographic Engineering, Volume 3, No. 1, Winter 1977, pp. 24-30.

[124] R.I. MacDonald and K.O. Hill, "Evaluation of a new photopolymer hologram recording medium," Communications Research Centre of Canada, CRC-659, September 1973, Report # 73N32395.

[125] H. Franke, "Refractive-index patterns in doped PMMA films, recorded with a HeNe laser," Polymer, April 1987 (Conference Issue), Vol. 28, pp.659-662.

[126] M.J. Bowden, E.A. Chandross, and I.P. Kaminow, "Mechanism of the photoinduced refractive index increase in polymethyl methacrylate," Applied Optics, Vol. 13, No. 1, January 1974, pp. 112-117.

REFERENCES (cont'd)

[127] T. Todorov, P. Markovski, N. Tomova, V. Dragostinova, and K. Stoyanova, "Photopolymers - Holographic investigations, mechanism of recording and applications," Optical and Quantum Electronics, Vol. 16 (1984), pp. 471-476.

[128] T. Stone, N. George, "Sensitometry and scattering characteristics of a holographic photopolymer," Presented at the 1989 annual meeting of the Optical Society of America.

[129] G. Odian and R.L. Kruse, "Diffusional effects in radiation-induced graft polymerization," Journal of Polymer Science:Part C, No. 22, pp.691-712 (1969).

[130] P.J. Flory, Principles of Polymer Chemistry, Chapter IV, "Polymerization of unsaturated monomers by free radical polymerization," Cornell University Press, 1953.

[131] H. Jeffreys and B.S. Jeffreys, Methods of Mathematical Physics, Third Edition, Cambridge University Press, 1966, Chapter 16.09, p.487.

[132] G. Blanch, "Mathieu Functions," Chapter 20 in Handbook of Mathematical Functions, edited by M. Abramowitz and I.A. Stegun, Dover ninth printing, 1965.

[133] J. Zhang, C.H. Wang, and D. Ehlick, "Investigation of the mass diffusion of camphorquinone in amorphous poly(methyl methacrylate) and poly(tert-butyl methacrylate) hosts by the induced holographic grating relaxation technique," Macromolecules, Volume 19, No. 5, pp.1390-1394, (1986)

[134] C.H. Wang and J.L. Xia, "Holographic grating studies of the diffusion process of camphorquinone in polycarbonate above and below T_g," Macromolecules, Volume 21, No. 12, pp. 3519-3523, (1988)

[135] J.L. Xia, C.H. Wang, and B.Y. Li, "Studies of the diffusion process of camphorquinone in poly(aryl ether ether ketone) by the holographic grating technique," Macromolecules, Vol. 23, No. 10, pp. 2739-2742,(1990)

[136] M. Gehrtz, J. Pinsl, and C. Brauchle, "Sensitive detection of phase and absorption gratings: Phase-modulated, homodyne detected holography," Applied Physics B, Vol. 43, pp.61-77.

[137] R.J. List, editor, Smithsonian meteorological tables, Sixth revised edition, Smithsonian press, 1958, Table 107.

[138] D.J. Lanteigne, Single Laser Exposure and Monitoring of Holograms, United States Statutory Invention Registration, Reg. Number H841, Assigned to the U.S. Army, Nov.6, 1990.

[139] W.H. Press and S.A. Teukolsky, "Numerical Calculation of Derivatives," Computers in Physics, Jan/Feb 1991, pp. 68-69.

REFERENCES (cont'd)

[140] G. Friedlander, J.W. Kennedy, E.S. Macias, and J.M. Miller, <u>Nuclear and Radiochemistry</u>, Third Edition, John Wiley and Sons, 1981, p. 191 and following.

[141] F.S. Acton, <u>Numerical Methods that Work</u>, Harper and Row, 1970, p. 253.

[142] W.H. Press, B.P. Flannery, S.A. Teukolsky, and W.T. Vetterling, <u>Numerical Recipes: The Art of Scientific Computing</u>, Chapter 14, Cambridge University Press, 1986.

[143] Ibid., Chapter 14.

[144] Ibid., Chapter 10.4.

[145] P.R. Bevington, <u>Data Reduction and Error Analysis for the Physical Sciences</u>, McGraw-Hill, 1969, Chapter 11, especially pp.235-236.

[146] J.A. Nelder and R. Mead, "A simplex method for function minimization," The Computer Journal of the British Computer Society, Vol. 7, 1964-65, pp. 308-313.

[147] J. Formosa, Polaroid photopolymer chemist, private communication.

[148] H. Hochstadt, <u>The Functions of Mathematical Physics</u>, Dover, 1986, Chapter 9.

[149] R.H. Adhami, D.J. Lanteigne, and D.A. Gregory, "Photopolymer hologram formation theory," Microwave and Optical Technology Letters, Vol.4, No. 3, February 1991, pp. 106-109.

[150] R.H. Adhami, D.J. Lanteigne, and D.A. Gregory, "An algorithm for decomposing a class of matrices into lower and upper triangular matrices," Journal of the Franklin Institute, June 1989.

[151] H.L. Penman, <u>Humidity</u>, Institute of Physics Series, published by Unwin Brothers Limited, London, 1955.

[152] M.J. Hickman, <u>Measurement of Humidity</u>, Notes on Applied Science, published by Her Majesty's Stationery Office, London, 1970.

APPENDIX A

NUMERICAL SOLUTIONS OF THE HOLOGRAPHIC DIFFUSION EQUATION

APPENDIX A. NUMERICAL SOLUTIONS OF THE HOLOGRAPHIC DIFFUSION EQUATION

The holographic diffusion equation developed as a model of photopolymer grating formation (Equations 4-27 and 4-28) can be expressed as

$$\frac{\partial u(x,t)}{\partial t} - D\frac{\partial^2 u(x,t)}{\partial x^2} = - L(x)\, u\,(x,t) \tag{A-1}$$

where L is a loss function related to the intensity of the holographic interference pattern. As shown in Chapter Four, approximate analytic solutions in terms of the orthogonal Mathieu functions are possible, but only for very restricted values of the parameters. In general, the solution of this equation demands the use of numerical methods. Fortunately, a variety of methods are known for the numerical solution of diffusion equations [99]. Diffusion equations are formulated as initial value problems, and are classified as parabolic differential equations.

In choosing a numerical algorithm for the solution of Equation 4-27, the chief factors are stability, speed, and storage requirements. One of the simplest numerical algorithms is known as the forward time, centered space (FTCS) technique [104]. In this technique, a finite difference formula is written that allows the concentration $u(x,t+\Delta t)$ to be calculated explicitly from the known values of $u(x-\Delta x, t)$, $u(x,t)$, and $u(x+\Delta x,t)$, where Δt and Δx are the time and space increments of the difference equation. The difference equation can be written

$$\frac{u_j^{n+1} - u_j^n}{\Delta t} = D\left[\frac{u_{j+1}^n - 2u_j^n + u_{j-1}^n}{(\Delta x)^2}\right] - L_j^n\, u_j^n \tag{A-2}$$

where the superscripts indicate the discrete time, $t = n\Delta x$, and the subscripts indicate discrete position, $x=j\Delta x$. The value of $u(j\Delta x,(n+1)\Delta t)$ can be solved for explicitly. Because of this, the differencing algorithm is also known as the fully explicit or forward time method. (Note also the similarity of the difference scheme to Equation 4-6, which expresses the diffusion of discrete particles hopping on a lattice.)

Unfortunately, the FTCS method is only conditionally stable. The condition for stability is

$$\frac{2D\Delta t}{(\Delta x)^2} \leq 1 \tag{A-3}$$

When the differential equation A-1 is interpreted as a diffusion equation, the meaning of the FTCS stability condition is clear. The numerical time step must be no larger than the

characteristic diffusion time across the spatial increment Δx. The practical implication of this stability limit is that doubling the spatial resolution of the numerical solution requires that the temporal resolution quadruple; in general, the calculational load increases as the cube of the spatial resolution, making this method quite slow.

A more useful method is known as the fully implicit or backward time algorithm. The differencing scheme is

$$\frac{u_j^{n+1} - u_j^n}{\Delta t} = D \left[\frac{u_{j+1}^{n+1} - 2u_j^{n+1} + u_{j-1}^{n+1}}{(\Delta x)^2} \right] - L_j^{n+1} \, u_j^{n+1} \qquad \text{(A-4)}$$

This equation has three unknowns: $u(x-\Delta x, t+\Delta t)$, $u(x, t+\Delta t)$, and $u(x+\Delta x, t+\Delta t)$. However, such an equation may be written for each point on the spatial grid, yielding a system of linear equations whose solutions give the values of u at the next time step. The algorithm is unconditionally stable. Stability does not guarantee accuracy, it only guarantees that the solution will not diverge to infinity in an unphysical fashion. When Dirichlet or Neuman boundary conditions are applied, this method yields a tri-diagonal set of equations, which can be solved by a well-known, efficient algorithm. The tri-diagonal matrix is very sparse, so computer memory requirements are small.

Unfortunately, the periodic boundary conditions required by the holographic diffusion equation, as discussed in Chapter Four, yield a set of equations that are not tri-diagonal. Storage of the complete sparse matrix, and solution by Gauss-Jordan techniques requires a good deal of memory and time. However, in the course of this investigation a technique was developed for solution of the holographic diffusion equation by means of the fully implicit, backward time algorithm, in which the matrix representing the set of linear equations was decomposed into lower and upper triangular matrices. Efficient techniques exist for the solution of such triangular matrices, which contain non-zero values only above (or below) the diagonal.

The use of numerical calculations makes it possible to solve forms of the holographic diffusion equation that are analytically intractable, such as systems where the diffusion coefficient is non-constant. Although it was later found to be not directly applicable in this investigation, a simulation was performed where polymerization is assumed to cause the diffusion coefficient to increase exponentially with both light intensity and exposure time. The diffusion coefficient is given by

$$D(x,t) = D_0 \exp\left[-K\left(\cos\left(\frac{2\pi x}{\Lambda}\right) + 1 \right) t \right] \qquad \text{(A-5)}$$

where K is an arbitrary constant, and the loss function L(x) is

$$L(x) = \cos\left(\frac{2\pi x}{\Lambda}\right) + 1 \qquad (A\text{-}6)$$

The units were chosen to be dimensionless, such that $\Lambda = 1$. Choosing D_0 to be 0.025, and K = 0.0125, numerical simulation yielded values for the monomer concentration $u(x,t)$, the polymerization $P(x,t,)$, and the total diffusive flux for each value of x. The non-sinusoidal character of the solution is more pronounced than for the analytical solutions with constant diffusion coefficients presented in Chapter 4.
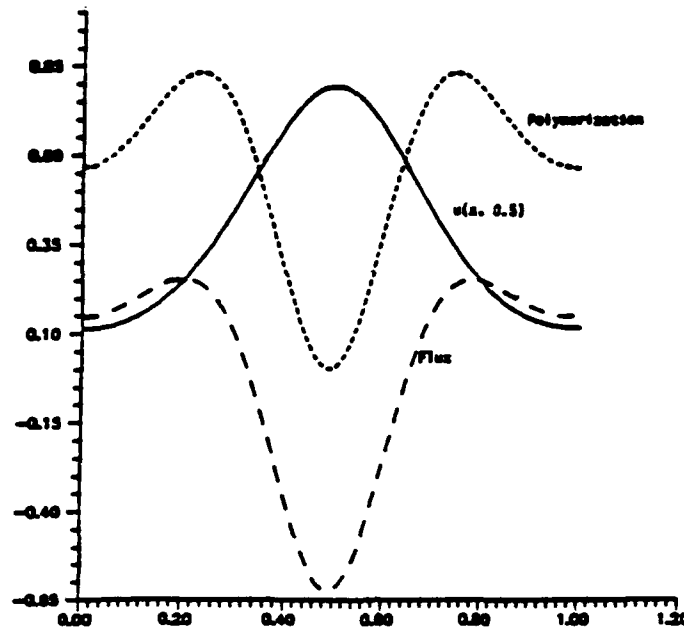

Figure A-1: Numerical solution of one cycle of photopolymer hologram with variable D.

A-3/(A-4 blank)

APPENDIX B

THE MEASURE OF RELATIVE HUMIDITY

APPENDIX B. THE MEASUREMENT OF RELATIVE HUMIDITY

A crucial aspect of this investigation was the measurement and control of relative humidity, since the DMP-128 photopolymer film absorbs moisture from the air. This moisture is necessary to promote the photochemical reactions and diffusion that are responsible for grating formation. Research has shown [118,119] that sodium acrylate absorbs 40% of its own weight in water from air that has a relative humidity of 50%. This is roughly in agreement with the Polaroid suggestion that DMP-128, consisting largely of lithium acrylate monomer, is best activated by 1 mg of water absorbed per micron of film thickness on a 2" by 2" plate.

The absorption of moisture from the air can be explained by the fact that the vapor pressure in equilibrium with liquid water depends upon the curvature of the vapor-liquid interface [151]. This surprising fact can be derived from an examination of the balance of forces acting on a column of liquid in a capillary tube, including the surface tension. If the radius of curvature r of the interface is taken to be taken as positive for a concave surface (such as a meniscus) and negative for a convex surface (a water droplet), then an expression can be written for the relative humidity h that is in equilibrium with a certain interface radius. The relative humidity h is the ratio between the actual vapor pressure of water and the saturation vapor pressure of water at the given temperature. The relationship between humidity and interface curvature is

$$\ln h = - \frac{2\sigma}{r} \frac{M}{RT\rho} \qquad (B-1)$$

where σ is the surface tension in dynes/cm, M the molecular weight, R the gas constant, T the temperature, and ρ the mass density. If $h = 0.5$, that is, 50% relative humidity, then r is on the order of 15 angstroms, and all voids of that size or smaller will fill with liquid water. At 80% relative humidity, all voids of 49 angstroms or less will be able to condense liquid water from the air. The actual amount of water taken up at a given level of humidity will thus depend upon the distribution of void sizes within the material. Another interesting consequence is that liquid droplets of pure water are only in equilibrium when the humidity is greater than 100%, that is to say, the air is supersaturated.

Several kinds of instruments have been designed to measure relative humidity [152]. The most common uses a porous fiber under spring tension to move an indicator dial. Most of the commercially available instruments of this type have only enough resolution to distinguish the humidity of the oven from the humidity of the sauna. A better device, that gives good accuracy and is reasonably rugged, is the psychrometer. The psychrometer consists of two thermometers mounted side-by-side in brackets. One thermometer, called the wet bulb, wears a little cotton sock or wick on the bulb which is kept moist with distilled water. The other thermometer is unadorned, and is called the dry bulb. A small electric fan circulates ambient air past the two at a speed in excess of several meters per second. The temperature of the two bulbs are read; the wet bulb is cooler, of course, due to evaporative cooling.

In order to reduce the psychrometric readings the saturation vapor pressure at the wet bulb and dry bulb temperatures must be calculated. The standard formula for the saturation pressure of water vapor at a given temperature is the Goff-Gratch formula [137]

$$\log_{10} e_w = -7.90298(T_s/T -1) + 5.02808 \ \log_{10}(T_s/T)$$
$$-1.3816*10^{-7}\left(10^{-11.344(1-T/T_s)}-1\right) \quad\quad\quad (B-2)$$
$$+ 8.1328*10^{-3}\left(10^{-3.49149(T_s/T-1)}-1\right)+ \log_{10} e_{ws}$$

where e_w is the saturation vapor pressure (in millibars) over a plane surface of liquid water at temperature T (kelvins), T_s is the steam point temperature 373.16 kelvins, and e_{ws} is the saturation pressure of pure ordinary liquid water at the steam point temperature (1013.246 millibars).

The saturation vapor pressure calculated for the wet bulb, e_{wb} must be corrected with the empirical formula

$$e' = e_{wb} - .00066* P_A*(1 + .00115 * T_{wb})(T_{db} - T_{wb}) \quad\quad\quad (B-3)$$

where e' is the corrected ambient water vapor pressure in millibars. P_A is the ambient air pressure (average value of 992 millibars in Huntsville, AL), and T_{db} and T_{wb} are the dry and wet bulb temperature readings in degrees Centigrade. After this correction, the relative humidity h is just

$$h = \frac{e'}{e_{db}} \quad\quad\quad (B-4)$$

where e' is the corrected vapor pressure corresponding to the wet bulb reading, and e_{db} is the vapor pressure calculated using the dry bulb reading.

The thermometers used in the psychrometer in this investigation were calibrated in the Fahrenheit scale. Nominal conditions were considered to be wet and dry bulb temperatures of 63 and 75 degrees Fahrenheit, corresponding to 50% relative humidity. An assumed measurement error of 0.5 degrees Fahrenheit in reading both thermometers implies that the humidity was accurately known to within plus or minus 3%.

INITIAL DISTRIBUTION

	Copies
Director U.S. Army Research Office ATTN: SLCRO-PH P.O. Box 12211 Research Triangle Park, NC 27709-2211	1
Headquarters Department of the Army ATTN: DAMA-ARR Washington, DC 20310-0623	1
Headquarters OUSDR&E ATTN: Ted Berlincourt The Pentagon Washington, DC 20310-0623	1
IIT Research Institute ATTN: GACIAC 10 W. 35th Street Chicago, IL 60616	1
U.S. Army Materiel System Analysis Activity ATTN: AMXSY-MP (Herbert Cohen) Aberdeen Proving Ground, MD 21005	1
AMSMI-RD	1
AMSMI-RD-CS-R	5
AMSMI-RD-CS-T	1
AMSMI-RD-WS, W. Wharton	1
S. Troglen	1
AMSMI-RD-WS-PO, David J. Lanteigne	30
AMSMI-GC-IP, Fred Bush	1